

SOLVENT-BASED DEVELOPMENT OF PHOTORESISTS FOR
NEXT-GENERATION LITHOGRAPHY

A Dissertation

Presented to the Faculty of the Graduate School

of Cornell University

In Partial Fulfillment of the Requirements for the Degree of

Doctor of Philosophy

by

Christine Y Ouyang

August 2013

© 2013 Christine Y Ouyang

SOLVENT-BASED DEVELOPMENT OF PHOTORESISTS FOR NEXT-GENERATION LITHOGRAPHY

Christine Y Ouyang, Ph.D.

Cornell University 2013

As feature sizes continue to shrink, the need for new materials and new processes for next-generation lithography becomes more urgent. Although aqueous base development has been the industry standard for over twenty years, there are still several issues that need to be overcome. First, the high surface tension of aqueous base developers can lead to pattern collapse of high aspect ratio patterns and limit resolution. The toxicity of aqueous base developers has also raised concerns about the environment. In order to reduce the problems related to aqueous development, solvents or materials with desirable properties must be used. Recently, there has also been growing interest in solvent-based negative-tone development (NTD) due to its better performance in printing certain feature types. Therefore, solvent-based development of photoresists was investigated in this study.

One approach to reduce the pattern collapse problem and environmental issues of the lithographic process is through the use of environmentally friendly solvents with low surface tension. Supercritical carbon dioxide (scCO₂) and linear methyl siloxanes (LMS) are green solvents that have low toxicity, low surface tension, low viscosity and can be recycled. Solvent-based development of both polymeric and molecular glass resists with positive- and negative-tone images have been successfully demonstrated in both solvents. High-resolution and high aspect ratio patterns were obtained with no pattern collapse observed using both solvents. As there is little

understanding about the solvent power of linear methyl siloxanes, the dissolution behavior of polymers and molecular glasses in linear methyl siloxanes was also studied.

Besides using low surface tension developers to mitigate pattern collapse problem, another approach is by using materials with high etch resistance that eliminates the use of thick films. Also, because of the low intensity of current EUV light source, the next-generation resists need to demonstrate high sensitivity and optimum absorbance. Inorganic metal oxide nanoparticles based on zirconium oxide (ZrO_2) and hafnium oxide (HfO_2) with organic ligands have been synthesized for EUV lithography. These nanoparticle resists can be developed as negative-tone patterns using an organic solvent and high-resolution patterns were achieved. The patterning performance of these nanoparticles in different organic solvents was also evaluated.

BIOGRAPHICAL SKETCH

Christine Ouyang was born in Orange County, CA and spent part of her childhood in Taipei, Taiwan. Born to an architect and a computer engineer, arts and math were her favorite subjects from the start of elementary school. With curiosity and creativity, she enjoyed turning many of her ideas into art at an early age. Science was never appealing until high school. After her first physics class, she was fascinated by the many physical phenomena present in nature and became enthralled with physics. Besides school activities, she spent a lot of her time chasing after her physics teacher asking questions. Her childhood dream of being an artist and her interest in physics led to her decision to major in Materials Science and Engineering because of the many possible fields she could work in as a materials scientist.

She enrolled at National Taiwan University in Fall 2004 and was soon attracted to polymer science after her introductory materials science class. As an undergraduate researcher, she had the opportunity to learn the synthesis of conducting polymers for solar cell applications at Professor Wei-Fung Su's lab. In the 2006-2007 academic year, she studied as an exchange student at the University of California in Berkeley. She received her Bachelor of Science degree in June 2008, and after spending most of her life in warm and sunny cities, she decided to move to the East Coast and started the Ph.D. program in Materials Science and Engineering at Cornell University.

At Cornell University, she joined Professor Christopher Ober's research group and worked on various projects related to lithography. Although the winter in Ithaca was unbearably cold, she loved the colorful trees in the fall, the cherry blossoms in the spring and the waterfalls in the summer. She also enjoyed baking and hanging out with friends during her free time. Besides doing research in Ithaca, she was also provided with many opportunities to travel (which earned her a Star Alliance Gold

status) and work in different labs around the world, as well as presenting at national and international conferences. She was awarded a GRC/Applied Materials Fellowship in 2010 and received her Master of Science Degree in February 2011. Although she had a great time on the East Coast, she was still a California girl at heart. Upon completion of her Ph.D. in June 2013, she moved back to the West Coast and began employment with Applied Materials in Santa Clara, CA.

To my family, for their unconditional love and support

ACKNOWLEDGMENTS

First, I want to thank God for His unceasing love and patience for me no matter how many times I failed. I am thankful for the opportunity to study and work with some of the world's most intelligent people at Cornell. I am also grateful for the people He placed around me in Ithaca and for the friendships and encouragements I received.

I would like to thank my advisor, Professor Christopher Ober for his guidance and support for the past five years, especially for his patience and advice in training me to overcome my fear of public speaking. I am also thankful for the opportunities to attend many national and international conferences. I want to thank my committee members, Professor Emmanuel Giannelis and Professor Robert Jarrow for their help during my graduate work and for reviewing my thesis, as well as Professor R. Bruce van Dover for serving as a proxy for Professor Giannelis at my B-exam. The staff at CNF, CCMR and NBTC are gratefully acknowledged for their assistance and helpful discussions. Dr. Hsin-Wei Tseng from the Physics department, Jack Chen at TSMC, Professor Juan de Pablo and his group at the University of Chicago, Che-Chen Hsu and Yan-Chun Lee at National Taiwan University, and the staff at LBNL are thanked for their help during various collaborations.

I would also like to express my appreciation to the Ober group members, past and present, for their help and support. Professor Jin-Kyun Lee and Dr. Jing Sha are acknowledged for assisting me to start my research and training me during my first year at Cornell. Dr. Marie Krysak, my former conference buddy and office neighbor, thank you for always keeping me company, I miss all the fun moments and laughter we had together. Dr. Yeon Sook Chung, thank you for your insightful advice and help, I really enjoyed working with you and I miss having tea with you in the office. Dr. Christian Ohm, my fellow Apple lover, I miss all the adventures we took together.

Dr. Zhaoli Zhou, thank you for always encouraging me and for planning fun activities. Jing Jiang, thank you for bringing so much laughter into my life during my last year here. Professor Claudio dos Santos, thank you for giving me confidence when I had none. I would also like to thank Dr. Alwin Wan, Dr. Yosuke Hoshi, Dr. Rina Maeda and Carol Newby for helping me during my A-exam preparation.

I would like to acknowledge my collaborators and friends in the department. Dr. Markos Trikeriotis, thank you for your guidance in nanoparticle synthesis and for the helpful discussions. Dr. Teeraporn (Aey) Suteewong, thank you for being so caring and for being the person I could look up to. Zihui (Cathy) Li, you are the big sister I always wanted, thank you for being the friend I could always turn to for help. Yibei Gu, thank you for always showing me different perspectives of things. Dr. Hiroaki Sai and Dr. Kahyun Hur, whom I could count on whenever I had research questions, thank you for your patience and willingness to help.

I would also like to give my appreciation to the financial support I received for my research and graduate study. I am grateful for a GRC Graduate Fellowship provided by the Semiconductor Research Corporation (SRC) and Applied Materials. I would also like to thank the SRC Engineering Research Center for Environmentally Benign Semiconductor Manufacturing and SEMATCH for funding my research projects.

To the friends I made in Ithaca, thank you for making my stay in Ithaca more enjoyable than it could have been. Tiffany Ho, thank you for always praying for me, supporting me and reassuring me when I felt discouraged. Jessie Luk and Victor Liu, my favorite couple from Cornell, thank you for keeping me company my first two years here. Randa Chiang and Eugene Cha, thank you for cheering me up during my most stressful time at Cornell. Thank you also to Grace Chen, Paul and Hildy Epp, Jefferson Wu, Van-Kim Bui, Kathleen Chang, KK Yu, Jyying Kan, Michael Chin,

Cynthia Kwong, Charles Lai, Wei-Tsui Leong, Luke McDermott, Justin Sun, Ellen Chuang, and Lemuel Kumarga for praying for me and being my brothers and sisters here at Cornell.

I would also like to thank my friends and family in Taiwan and California. Hsao Hsih, thank you for being my biggest cheerleader and for always having faith in me. Jo-Ann Lieu, my number one fan, thank you for listening to me, praying for me and for providing me a place to stay whenever I visited NorCal. Chosen Lee, the little brother I always wanted, thank you for all the phone calls and encouragements. Janet Chyan, thank you for loving me as your own daughter and for calling me and praying with me all the time. Stephanie Jung, Jeremy Lin, Dr. Katrina Chang and Samuel Lee, thank you for believing in me when I wanted to give up and thanks for all the prayers. Last but not least, I would like to acknowledge my family for their everlasting love and support, especially my mother, Debbie Shih-Chin Lai, for never giving up on me and constantly praying for me. Thank you for providing me a place that I can always call home and for loving me unconditionally.

TABLE OF CONTENTS

BIOGRAPHICAL SKETCH.....	v
DEDICATION	vii
ACKNOWLEDGEMENTS.....	viii
TABLE OF CONTENTS	xi
LIST OF FIGURES	xv
LIST OF TABLES	xix
CHAPTER 1: SOLVENT-BASED DEVELOPMENT OF PHOTORESISTS	
<i>Abstract</i>	1
<i>1.1 Introduction to the Development Process</i>	2
1.1.1 Development Methods.....	2
1.1.2 Aqueous Base Development Process	4
1.1.3 Solvent-Based Development Process	5
1.1.3.1 Traditional Solvent-Based Development Process	5
1.1.3.2 Chemical Amplification and Solvent-Based Development.....	8
<i>1.2 Common Development Problems</i>	9
1.2.1 Pattern Collapse.....	12
1.2.2 Resist Pattern Deformation.....	12
1.2.3 Micro-Bridging.....	14
1.2.4 Line-Width Control	14
<i>1.3 Environmentally Friendly Solvent-Based Developers</i>	14
1.3.1 Supercritical Carbon Dioxide	15
1.3.2 Linear Methyl Siloxanes.....	23
<i>1.4 Recent Interest in Solvent-Based Negative-Tone Development</i>	25

1.5 Summary	27
<i>References</i>	30

CHAPTER 2: PATTERNING NON-FLUORINATED POLYMERIC AND
MOLECULAR GLASS MATERIALS IN SUPERCRITICAL CARBON DIOXIDE

Abstract	36
2.1 Introduction	37
2.2 Experimental	40
2.2.1 Materials.....	40
2.2.2 Partially <i>t</i> -boc Protected (ca. 80%) Poly (4-hydroxystyrene) (PBOCST).....	40
2.2.3 Lithographic Evaluation.....	40
2.2.4 Development in ScCO ₂	42
2.2.5 Metrology.....	42
2.3 Results and Discussion	42
2.3.1 Development of Conventional Photoresists.....	42
2.3.2 Molecular Glass Photoresists for ScCO ₂ Development.....	48
2.3.3 Computational Simulations.....	51
2.4 Conclusions	56
<i>References</i>	58

CHAPTER 3: ENVIRONMENTALLY FRIENDLY PATTERNING OF THIN
FILMS IN LINEAR METHYL SILOXANES

Abstract	63
3.1 Introduction	64
3.2 Experimental	67
3.2.1 Materials.....	67

3.2.2 Lithographic Evaluation	68
3.2.3 Metrology	69
3.3 Results and Discussion.....	69
3.4 Conclusions.....	77
<i>References.....</i>	<i>79</i>
<i>Appendix A: X-Ray Photoelectron Spectroscopic Study of Residual Solvents.....</i>	<i>81</i>

CHAPTER 4: DISSOLUTION BEHAVIOR OF MOLECULAR GLASSES IN
LINEAR METHYL SILOXANES

<i>Abstract</i>	<i>84</i>
<i>4.1 Introduction</i>	<i>85</i>
<i>4.2 Experimental.....</i>	<i>87</i>
4.2.1 Materials	87
4.2.2 Lithographic Evaluation	87
4.2.3 Metrology	89
<i>4.3 Results and Discussion.....</i>	<i>89</i>
4.3.1 Hansen Solubility Parameters of Molecular Glasses.....	89
4.3.2 Dissolution Behavior of Molecular Glasses	97
4.3.3 Patterning of Molecular Glasses in Linear Methyl Siloxanes	101
<i>4.4 Conclusions.....</i>	<i>103</i>
<i>References.....</i>	<i>106</i>
<i>Appendix B: Calculations of Hansen Solubility Parameters</i>	<i>109</i>

CHAPTER 5: THE ROLE OF ADDITIVES AND SOLVENTS IN PATTERNING
INORGANIC METAL OXIDE NANOPARTICLES

<i>Abstract</i>	<i>115</i>
------------------------------	-------------------

5.1 Introduction	116
5.2 Experimental	119
5.2.1 Materials	119
5.2.2 Nanoparticle Synthesis	119
5.2.3 Nanoparticle Characterization	119
5.2.4 Lithographic Evaluation	119
5.2.5 Metrology	120
5.3 Results and Discussion	120
5.3.1 Zirconium Oxide Nanoparticle Characterization	120
5.3.2 Etch Resistance Study	123
5.3.2.1 Effect of Oxygen Plasma Cleaning Time	123
5.3.2.2 Pattern Transfer	125
5.3.3 Solvent-Based Negative-Tone Development	129
5.3.3.1 Patterning Mechanism	129
5.3.3.2 Effect of Different Additives on Patterning Inorganic Nanoparticles	135
5.3.3.2.1 Effect of Photoactive Compounds	135
5.3.3.2.2 Effect of Cross-Linkable Additives	141
5.3.3.3 Effect of Different Developing Solvents	146
5.4 Conclusions	155
<i>References</i>	<i>159</i>
<i>Appendix C: EUV Exposure Data for ZrO₂-MAA</i>	<i>164</i>

LIST OF FIGURES

1.1.	The development process	3
1.2.	Chemical structures of a bisarylazide-rubber resist and bisazide sensitizer	7
1.3.	Pinacol rearrangement of polymeric <i>vic</i> -diol for reverse polarity switch	10
1.4.	Intramolecular dehydration resulting in polarity change.....	11
1.5.	Schematic illustration of the rinse liquid remaining between resist patterns	13
1.6.	Phase diagram of supercritical carbon dioxide.....	16
1.7.	Lithographic patterning mechanism of P(THPMA- <i>b</i> -F7MA)	19
1.8.	Solubility switching mechanism of polysilane.....	20
1.9.	Solubility switching mechanism of hexa(hydroxyphenyl) benzene molecular glass	22
1.10.	Chemical structures of linear methyl siloxanes.....	24
1.11.	Chemical structures of epoxide-based molecular resists for solvent development	26
2.1.	Chemical structures of ESCAP, PBOCST and calix[4]resorcinarene.....	41
2.2.	Deprotection reaction of ESCAP upon exposure	43
2.3.	Chemical structures of silylating reagents.....	45
2.4.	Silylation of ESCAP after exposure	46
2.5.	E-beam patterns of ESCAP developed in scCO ₂ at 6000 psi, 50°C for 40 minutes (dose: 40μC/cm ²)	47
2.6.	Deprotection reaction of PBOCST upon exposure	49
2.7.	Deprotection reaction of CHPB after exposure.....	50
2.8.	E-beam patterns of CHPB (dose: 32μC/cm ²) developed in scCO ₂ at 40°C, 2000 psi for 5 minutes	52
2.9.	Interactions of DMTS with (a) ESCAP, (b) PBOCST in scCO ₂	53
2.10.	Free energy curve of ESCAP and PBOCST using DMTS as an additive in scCO ₂	54
2.11.	Computational simulations of CHPB in scCO ₂	55

3.1.	Chemical structures of (a) linear methyl siloxanes [hexamethyldisiloxane (HDS), octamethyltrisiloxane (OTS), and decamethyltetrasiloxane (DTS)], (b) silylating agent [(<i>N,N</i> -dimethylamino)trimethylsilane (DMTS)], and (c) polymeric or molecular resist materials investigated in this study	66
3.2.	(a) Probable chemical reactions of PBOCST, (b) film thickness changes of PBOCST films in OTS and DMTS mixture at 40 °C with and without UV exposure, (c) Probable chemical reactions of ESCAP, (d) film thickness changes of ESCAP films in OTS and DMTS mixture at 40 °C with and without UV exposure	70
3.3.	Grazing angle FT-IR spectrum of PBOCST exposed to 243 mJ cm ⁻² at 365 nm followed by development in OTS-DMTS mixture at 40°C for 3 minutes	73
3.4.	Chemical contrast curves of PBOCST after PEB and silylation (OH: 3400 cm ⁻¹ , Si-O: 925 cm ⁻¹ , using C=C aromatic stretch at 1500 cm ⁻¹ as reference peak)	74
3.5.	(a) PBOCST patterned using 365 nm light (dose: 50 mJ cm ⁻²) and developed in an OTS-DMTS mixture, (b) DHP-BOC patterned using e-beam(dose: 40 μC/cm ²) and developed in OTS-DMTS mixture, (c) ESCAP patterned using 365 nm light (dose: 50 mJ/cm ²) and developed in an OTS-DMTS mixture, (d) CHPB-BOC patterned using e-beam (dose: 32 μC/cm ²) and developed in OTS	76
A.1.	(a) Au spectrum and (b) Si Spectrum of Sample A	82
A.2.	(a) Au spectrum and (b) Si Spectrum of Sample B	82
A.3.	(a) Au spectrum and (b) Si Spectrum of Sample C	83
A.4.	(a) Au spectrum and (b) Si Spectrum of Sample D	83
4.1.	Chemical structures of (a) linear methyl siloxanes, (b) C-4-hydroxyphenylcalix[4]resorcinarene (CHPB), (c) hexa-(3 or 4-hydroxyphenyl)benzene (HHPB), and (d) 1,3,5-tri(1,1-di(4-hydroxyphenyl) ethyl)benzene (CR15) (R=H or <i>tert</i> -butoxycarbonyl)	88
4.2.	(a) Chemical reactions of CHPB upon exposure, (b) FT-IR of CHPB before and after exposure	90
4.3.	Hansen solubility parameter map of each molecular glass relative to linear methyl siloxanes	96
4.4.	QCM study of (a) CHPB in hexamethyldisiloxane, (b) CR-15 in octamethyltrisiloxane, (c) HHPB in octamethyltrisiloxane.....	98
4.5.	Dissolution rate of <i>t</i> -boc protected (a) CR-15, (b) HHPB in three linear	

methyl siloxanes	100
4.6. Chemical and dissolution contrast curves of CHPB in octamethyltrisiloxane	102
4.7. E-beam patterns of (a) CHPB (dose: 32 $\mu\text{C}/\text{cm}^2$) developed in octamethyltrisiloxane, (b) CR-15 (dose: 50 $\mu\text{C}/\text{cm}^2$) developed in octamethyltrisiloxane, (c) HHPB (dose: 30 $\mu\text{C}/\text{cm}^2$, 60 nm lines) developed in hexamethyldisiloxane and developed in octamethyltrisiloxane (dose: 70 $\mu\text{C}/\text{cm}^2$)	104
5.1. Nanoparticle resist platform	121
5.2. (a) TGA data of ZrO_2 -MAA nanoparticles, (b) Size distribution of ZrO_2 -MAA, (c) FT-IR of ZrMAA.....	122
5.3. Etch rate comparison of ZrO_2 -MAA and PHOST (a) CF_4 etching, (b) SF_6/O_2 etching.....	124
5.4. Etch rate comparison with different oxygen plasma cleaning time for ZrO_2 -MAA	126
5.5. Pattern transfer of ZrO_2 -MAA (a) CF_4 etching, (b) SF_6/O_2 etching with 30s O_2 cleaning, (c) SF_6/O_2 etching with 7 min O_2 cleaning.....	128
5.6. Chemical structures of photoactive compounds used in this study (a) dimethoxy phenyl acetophenone (DPAP), (b) N-hydroxynaphthalimide (NI-Tf), (c) triphenylsulfonium perfluoro-1-butane sulfonate (TPS-nf), (d) triphenylsulfonium triflate (TPS-tf).....	130
5.7. Photochemical reactions of (a) DPAP, (b) NI-Tf, (c) TPS-tf upon exposure.....	131
5.8. Negative-tone patterns of ZrO_2 -MAA with (a) DPAP (dose: 200 mJ/cm^2 , 50 wt% MAA), (b) NI-Tf (dose: 150 mJ/cm^2 , 50 wt % MAA)	132
5.9. Proposed negative-tone patterning mechanism	133
5.10. QCM of unexposed and exposed ZrO_2 -MAA in 4-methyl-2-pentanol	134
5.11. E-beam patterns of ZrO_2 -MAA with different amounts of DPAP (a) 0.5 wt % (dose: 20 $\mu\text{C}/\text{cm}^2$), (b) 1 wt % (dose: 20 $\mu\text{C}/\text{cm}^2$), (c) 2 wt % (dose: 18 $\mu\text{C}/\text{cm}^2$).....	136
5.12. Cross-sectional SEM images of ZrO_2 -MAA with different DPAP amounts.....	138
5.13. (a) QCM of unexposed ZrO_2 -MAA with 1 wt% of each PAG in 4-methyl-2-pentanol; E-beam patterns of ZrO_2 -MAA with 1 wt% of (b) NI-Tf (dose:15 $\mu\text{C}/\text{cm}^2$), (c) TPS-tf (dose:10 $\mu\text{C}/\text{cm}^2$), (d)TPS-nf (15 $\mu\text{C}/\text{cm}^2$)	139

5.14.	E-beam patterning of ZrO ₂ -MAA with 1 wt% of (a) NI-Tf, (b) DPAP (dose: 15μC/cm ²).....	140
5.15.	Effect of PAG content on dissolution rate in 4-methyl-2-pentanol.....	142
5.16.	(top) HfO ₂ -MAA with different weight percentages of DPAP (bottom) HfO ₂ -MAA with 1 wt % of DPAP and different amounts of MAA	143
5.17.	ZrO ₂ -MAA with different amounts of PAG (NI-Tf) showing that increasing PAG content has no detrimental effect on film quality	144
5.18.	(a) Chemical structure of dipentaerythritol penta-/hexa-acrylate; E-beam patterning of ZrO ₂ -MAA with 1 wt% NI-Tf and, (b) 55 % of multifunctional acrylate, (c) 45 % of multifunctional acrylate (dose: 10μC/cm ²).....	145
5.19.	Developing solvents used in this study	148
5.20.	QCM of unexposed ZrO ₂ -MAA in (a) 4-methyl-2-pentanol, (b) o-xylene	151
5.21.	Patterning results of ZrO ₂ -MAA with 1 wt % PAG in different NTD developers.....	152
5.22.	Patterning results of ZrO ₂ -MAA with 5 wt % PAG in different NTD developers.....	154
5.23.	Contrast curves of different developers for ZrO ₂ -MAA at EUV wavelength.....	156
5.24.	EUV patterning of ZrO ₂ -MAA (a) 21.5 nm line/space (7 wt% PAG, dose: 4.2 mJ/cm ² , LER:5.6 nm) and (b) 72.1 nm contact holes (5 wt % PAG, dose: 3 mJ/cm ² , LER: 6.5 nm).....	157
C.1.	Proposed positive-tone patterning mechanism with a non-ionic PAG.....	166

LIST OF TABLES

1.1.	Physical properties of gas, liquid, and supercritical fluid of typical organic fluid.....	17
A.1.	Details of each sample.....	81
4.1.	Physical properties of linear methyl siloxanes used in this study	92
4.2.	Hansen solubility parameters of each linear methyl siloxanes.....	93
4.3.	Estimated Hansen solubility parameters of each molecular glass.....	95
B.1.	First-order group approximation for the prediction of the dispersion partial solubility parameter.....	110
B.2.	Second-order group approximation for the prediction of the dispersion partial solubility parameter.....	110
B.3.	First-order group approximation for the prediction of the polar partial solubility parameter	110
B.4.	Second-order group approximation for the prediction of the polar partial solubility parameter.....	111
B.5.	First-order group approximation for the prediction of the hydrogen-bonding partial solubility parameter.....	111
B.6.	Second-order group approximation for the prediction of the hydrogen-bonding partial solubility parameter.....	111
B.7.	First-order group approximation for the prediction of the dispersion partial solubility parameter.....	112
B.8.	Second-order group approximation for the prediction of the dispersion partial solubility parameter.....	112
B.9.	First-order group approximation for the prediction of the polar partial solubility parameter	113
B.10.	Second-order group approximation for the prediction of the polar partial solubility parameter.....	113
B.11.	First-order group approximation for the prediction of the hydrogen-bonding partial solubility parameter.....	114
5.1.	Organic and inorganic content of ZrO ₂ -MAA with different oxygen plasma cleaning time	127
5.2.	Surface tension of the NTD solvents.....	147

5.3.	Dissolution rate of unexposed (R_{\max}) and exposed (R_{\min}) ZrO_2 -MAA in different developing solvents	150
C.1.	Exposure data for ZrO_2 -MAA (EUV lithography).....	164
C.2.	LER trade-off for ZrO_2 -MAA (EUV lithography).....	165
C.3.	Exposure data for ZrO_2 -MAA, developer: 0.28 N TMAH (EUV lithography)	167

CHAPTER 1

SOLVENT-BASED DEVELOPMENT OF PHOTORESISTS

Abstract

The resist development process in lithography is critical for achieving high-resolution patterns. Traditional solvent-based development has poor lithographic performance for high-resolution patterning due to the cross-linking nature of the resist materials. Although conventional aqueous base developers have achieved excellent patterning results, its toxicity has always been a concern. In addition, several problems related to the development process such as pattern collapse, swelling and micro-bridging can affect the following processing steps. In order to reduce these problems, alternative solvents and resist materials must be studied. This chapter discusses the different development methods, processes and their related issues. Properties and recent work of alternative environmentally friendly developers such as supercritical CO₂ and linear methyl siloxanes are discussed. Recent trends in negative-tone solvent-based development and inorganic resists are described later in this chapter.

1.1 Introduction to the Development Process

Lithography is the process of patterning small features in a photosensitive material (photoresist), where a photoresist is coated on a substrate and irradiated using UV light or electron-beam sources. After exposure, in a development process the soluble part of the photoresist must be removed either in a solvent or through other dry development techniques to generate a pattern. The wet development process requires a developing solvent (developer) to selectively dissolve either the exposed or unexposed photoresist. Photoresist images are classified into two different imaging systems, depending on the developing solvent that is being used. If the exposed region is more soluble than the unexposed area, it is called positive-tone development (PTD) and the opposite is called negative-tone development (NTD) (Figure 1.1). The development step is critical in lithographic processes as the resist-developer interactions determine the resist profile and other factors such as contrast and line-width control. Besides wet development methods, dry development methods which eliminate the use of a developing solvent such as top-surface imaging (TSI)¹ were also studied and are not discussed here. The development methods and different types of the wet development process are introduced in the following sections.

1.1.1 Development Methods

The most common and convenient way of developing photoresists is through static immersion; other methods include spin development, continuous spray and puddle development. During spin development, the developing solvent is poured onto the photoresist while the resist is spun using equipment similar to a spin-coater. The resist is also rinsed and dried during spinning. Spray development requires one or more nozzles to disperse the developer onto the spinning photoresists. This process reduces the amount of developer usage and the development uniformity is closely related to the spinning speed.² For puddle development, the developer is poured onto a

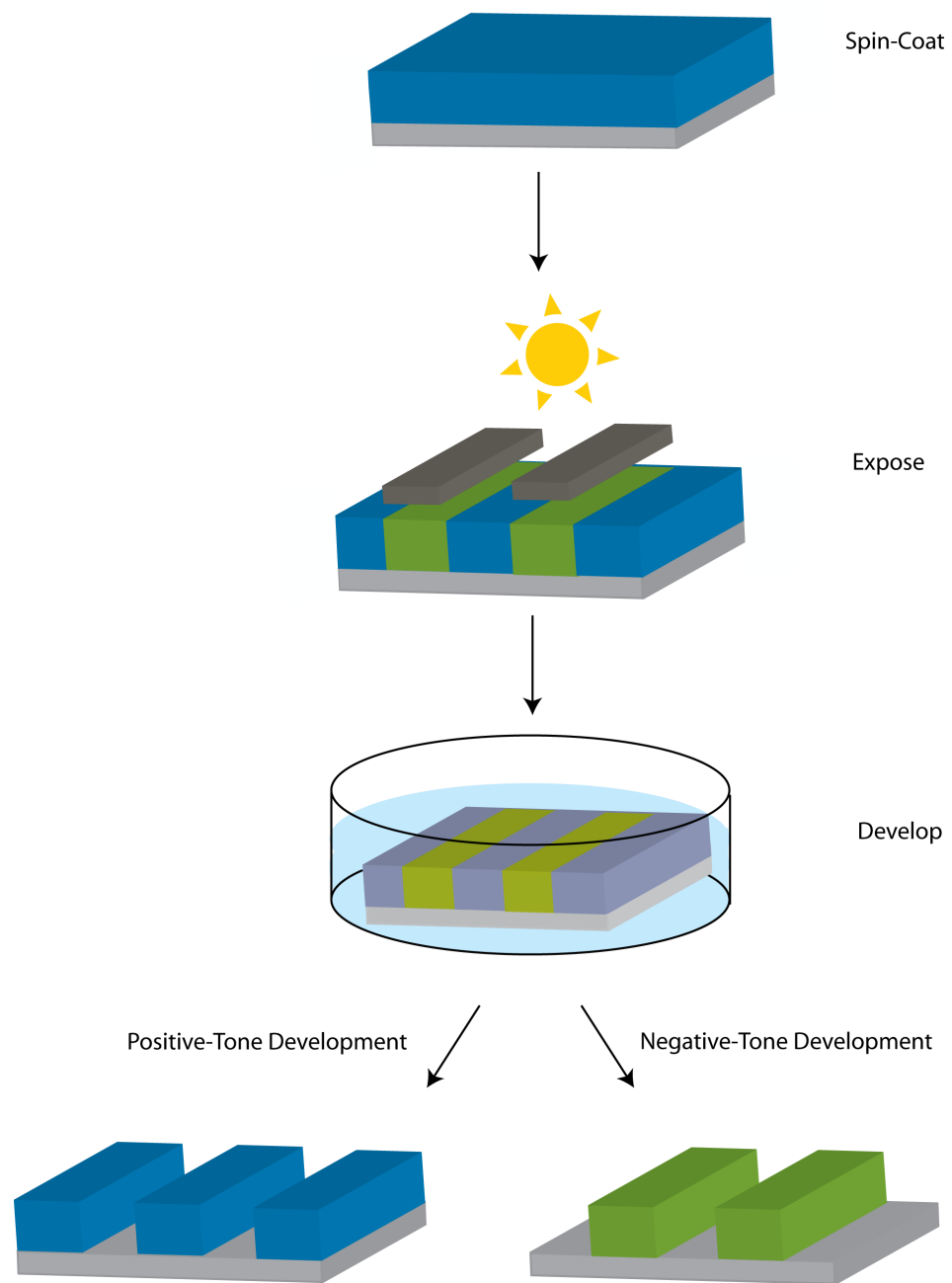


Figure 1.1. The development process.

slowly spinning photoresist and then stopped and allowed to sit during the development time. The developing solvent is then spin rinsed and dried.

1.1.2 Aqueous Base Development Process

Typical developers used in today's semiconductor industry are aqueous base solvents. Early developers include aqueous alkaline solutions such as sodium hydroxide (NaOH) or potassium hydroxide (KOH).³ However, this class of developer has been abandoned due to possible metal ion contamination of devices and the focus was switched to metal ion-free tetramethylammonium hydroxide (TMAH). TMAH developer concentrations in the range of 0.2-0.3 N can provide sufficient sensitivity with high contrast and 0.26 N TMAH has become the standard developer for today's microelectronic fabrication process. After development, a rinsing step using ultra pure water is required to remove any remaining developers and the resist film is dried after rinsing.

Although the development strength of 0.26 N TMAH was first selected for DNQ/Novolac resists, most photoresists used in today's microfabrication process are engineered for 0.26 N TMAH and are based on chemical amplification where acid-catalyzed deprotection can occur upon exposure to change its chemical property.^{4, 5} The high development contrast of chemically amplified resists in aqueous developers can be attributed to the development mechanism. Because polymers can dissociate into polyelectrolytes in aqueous developers, as the deprotection reaction progresses, more sites along the photoresists become available for charging in aqueous base developers. The repulsion of charges can be strong enough to force the poorly soluble polymer chain to uncoil. Charges build along the polymer in locations that minimizes the charge density and leads to charged and uncharged regions. The polymer backbone in the charged regions can extend while the uncharged regions remain coiled.^{6, 7} The repulsion of like charges is a potent thermodynamic term in comparison to the

chemical term that causes a poorly soluble polymer to remain coiled in the solvent. The difference in terms is sufficient enough that a resist may change from a coiled and undeveloped form to an extended and developed form with the addition of only one charge. As a single charge can result in developed and undeveloped resists, chemical amplification photoresists generally exhibit high development contrast.

1.1.3 Solvent-based development process

According to the Flory-Huggins theory,⁸ the Gibbs free energy for dissolving an uncharged polymer in a solvent can be described as

$$\frac{\Delta G}{RT} = \phi_1 \ln \phi_1 + \frac{\phi_2}{x} \ln \phi_2 + \chi \phi_1 \phi_2 \quad (1.1)$$

where ϕ_1 and ϕ_2 are the volume fractions of the solvent and polymer, respectively, x is the number of lattice sites occupied by a polymer molecule (degree of polymerization assuming one solvent molecule/monomer occupies one lattice), and χ is a measure of the interaction between the solvent and the polymer. From Flory-Huggins theory, there are two driving forces for the formation of a polymer solution, one is the entropic force (first two terms) and the other is related to the enthalpy (last term). In the following sections, solvent-based development related to each forces are discussed.

1.1.3.1 Traditional Solvent-Based Development Process

Before aqueous base became the standard developing solvent, most photoresists were developed using organic solvents. Traditionally, cross-linkable or chain-scission resists have been used for solvent-based development. As described by the Flory-Huggins theory, the change in size (x) can lead to change in driving force for solution formation and lead to a solubility difference between the exposed and unexposed areas in the developer. Poly(methyl methacrylate) (PMMA) and its derivatives are the most widely used and studied positive-tone resists for solvent-based developers. These resists undergo chain scission upon exposure and can be developed

in solvents such as 2-ethoxyethanol, ethanol, isopropanol and methyl isobutyl ketone (MIBK).⁹ Although PMMA has shown good patterning capabilities, its low sensitivity and poor plasma-etch stability are two main drawbacks for its practical use. Besides positive-tone patterning, most solvent-based development has been focused on negative-tone patterning and are discussed below.

The most commonly used two-component, negative-tone resists are bis-arylazide/rubber resists as shown in Figure 1.2.¹⁰ The matrix resin material is a synthetic rubber that is obtained by a Ziegler-Natta polymerization of isoprene which forms *cis*-poly(isoprene), an elastomeric material with a low glass transition temperature (T_g). It is then subsequently treated with a reagent which leads to partial cyclization of the polymer to obtain a material with a higher T_g and greater structural integrity than its precursor. The cyclized rubber matrix materials are extremely soluble in non-polar, organic solvents such as toluene, xylene, or halogenated aliphatic hydrocarbons. Upon photolysis, bis-arylazide sensitizers lose nitrogen and generate a highly reactive nitrene. The nitrene intermediate undergoes a series of reactions that leads to cross-linking of the resin and renders the resist insoluble in the organic developer.

Several e-beam resists with a polystyrene backbone have also been studied for solvent-based development.^{11, 12} The proposed mechanism for this type of resists is that radiation-induced homolysis of the carbon-halogen bond can generate a radical which undergoes rearrangement, abstraction, or recombination reactions that leads to network formation. Solvents such as 2-methyl-cyclohexanone, 2-propanol, 1,4-dioxane and isoamyl acetate have been used as developing solvents for these resists. Although there have been successful patterning results with these solvent-developed resists; however, there are several problems related to this process. First, the cross-linking reactions start from the top of the resist film and overexposure is required for

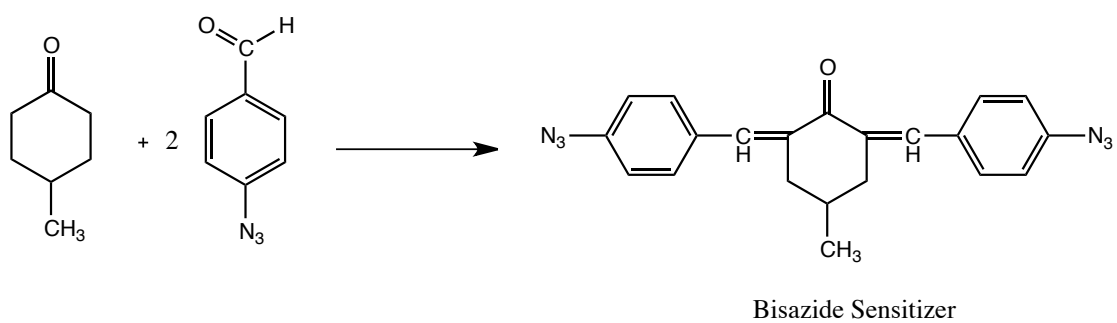
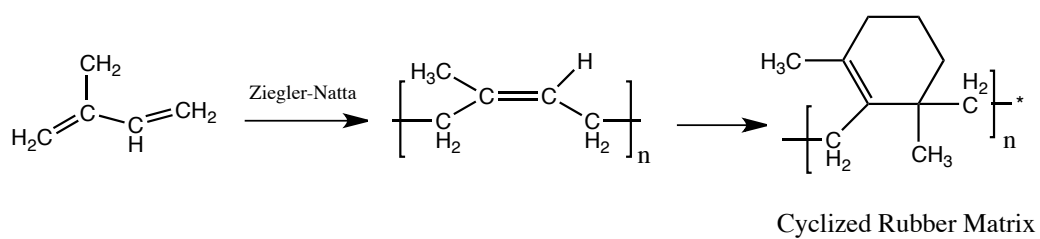


Figure 1.2. Chemical structures of a bisarylazide-rubber resist and bisazide sensitizer.

the resist to become insoluble at the substrate interface. The thicker the resist film is, the greater the over-dose is needed and the larger the scattered radiation. Scattered radiation at the resist/substrate interface can result in low resolution. In addition, the large volume of solvent absorbed by the cross-linked area during the development process can increase the volume of the cross-linked resist and lead to swelling and image distortion. Closely spaced lines may swell to an extent that adjacent networks can join and lead to “bridging” between the lines upon the removal of the solvent. Another common problem related to swelling is the formation of snake-like distortions of long, narrow images. It is possible for these regions to expand in the vertical direction during development. However, the adhesion force between the resist/substrate interface limits the resist to expand freely in the plane of the substrate. In order to relieve this stress, these lines must increase their length and lose adhesion to the substrate. Both “snaking” and “bridging” can limit the final resolution and are undesirable.

1.1.3.2 Chemical Amplification and Solvent-Based Development

The poor performance of traditional solvent-based development can be explained by Eq. (1.1). When the polymer is large (larger x), the entropic driving force is much smaller compared to the enthalpic term. When there is little change of the enthalpic term, the solvent can still dissolve the exposed area and lead to large amount of swelling. Therefore, in order to improve the solvent-based development process, it is more important to have an enthalpic change. Most resists used in today’s microelectronic fabrication process are chemically-amplified resists⁵ based on radiation-induced polarity changes. As these resists can create a chemical difference between the exposed and unexposed area, there is a more dramatic solubility difference for the two areas which can lead to a better development contrast. Chemically amplified resists that undergo a pinacol-pinacolone rearrangement

reaction involving the polarity switch of a polar to a non-polar group has been studied for solvent-based development.¹³ Poly[3-methyl-2-(4-vinylphenyl)-2,3-butanediol], as shown in Figure 1.3, can convert to a non-conjugated ketone upon exposure and be developed in an alcohol developer such as isopropanol to wash away the unexposed film. Another example is poly[4-(2-hydroxy-2-propyl)styrene]⁸ as shown in Figure 1.4, an acid-catalyzed dehydration can take place to generate a stable tertiary benzylic carbocation and subsequently eliminates a β -proton to form a pendant olefinic structure. This intramolecular dehydration reaction converts the hydrophilic alcohol to a lipophilic olefin. Depending on the developing solvent, this resist can be developed as positive-tone patterns using a non-polar solvent like xylene and as negative-tone patterns using a polar alcohol. Although these types of resists have shown promising patterning results, their potential was not fully exploited as there were more interests in developing resists for the standard aqueous developer at that time.

Chemically amplified resists based on acid-catalyzed deprotection have become the main workhorse for today's lithographic processes due to their high performance and high development contrast in aqueous base developers. Therefore, recent solvent-based development process work has been focused on using this type of chemically amplified resist which is reviewed later in this chapter.

1.2 Common Development Problems

The development process is a critical step for lithography as the resulting resist profile can affect subsequent processing steps. Common development problems including pattern collapse, micro-bridging, and resist deformation can lead to undesirable line-edge roughness (LER), line-width roughness (LWR) and limited resolution.

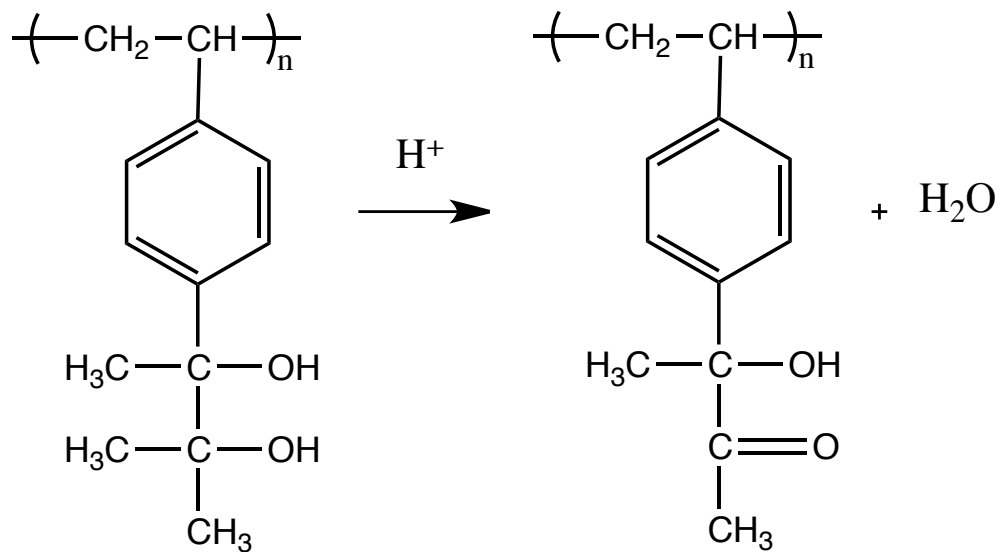


Figure 1.3. Pinacol rearrangement of polymeric *vic*-diol for reverse polarity switch.

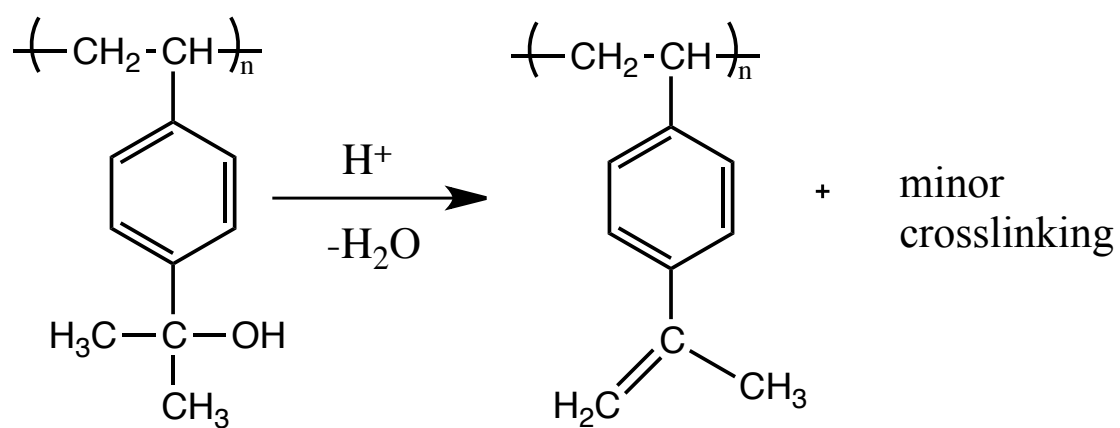


Figure 1.4. Intramolecular dehydration resulting in polarity change.

1.2.1 Pattern Collapse

Pattern collapse is generally seen in ultra-fine and high aspect ratio patterns. This phenomenon is related to the surface tension of the rinse liquid used after development and its mechanism has been studied by Tanaka.¹⁴ A simplified model without the consideration of resist bending is shown in Figure 1.5 where the surface tension of the rinse liquid can create forces on the resist sidewalls and lead to pattern collapse. The pressure produced from the surface tension can be expressed by the Young-Laplace equation as

$$P = \frac{\sigma}{R} \quad (1.2)$$

the radius R is given by $R=d/(2 \cos\theta)$, where θ is the contact angle of the rinse liquid at the resist surface. The resist peeling force F is proportional to the resist pattern aspect ratio according to the lever principle, $F=P \times A$, where A is the aspect ratio of the resist pattern. The resist peeling force can be accordingly calculated as

$$F = \frac{2\sigma \cos\theta}{d} A \quad (1.3)$$

where the force is proportional to both the surface tension and aspect ratio but inversely proportional to the distance between the resist sidewalls and is therefore more important for ultra-fine and dense patterns. A more complex model considering the bending of resist sidewalls as the capillary forces increases has shown that pattern collapse is more pronounced for symmetric structures and more hydrophobic resists in addition to the factors shown by Eq. (1.3).¹⁴ As the semiconductor industry is striving to achieve smaller and smaller features, pattern collapse can become a serious issue and limit device dimensions.

1.2.2 Resist Pattern Deformation

Resist pattern deformation such as swelling during the development process can affect critical dimension (CD) control and accurate pattern dimension that needs to be achieved. For resist systems based on solvent development, some degree of

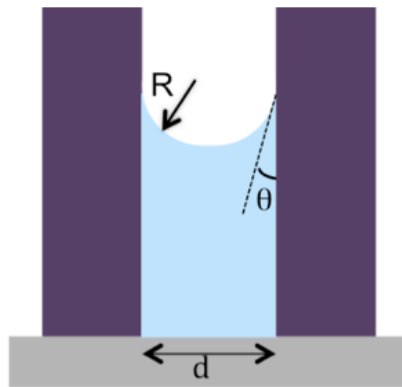


Figure 1.5. Schematic illustration of the rinse liquid remaining between resist patterns.

swelling is required to allow removal of soluble chains or fragments. However, excessive swelling can result in limited resolution. Swelling typically occurs in gel-formation-type resists such as cyclized-rubber-based negative-tone resists¹⁵ and is also seen in other resists such as poly(methyl methacrylate) (PMMA).¹⁶ As the feature sizes decrease, it is important to minimize the swelling effect by choosing the optimal resist-developer pair to achieve better resolution.

1.2.3 Micro-Bridging

In the over- and under-dosed region of photoresists, micro-bridging can occur during development. Micro-bridging are defects that can influence CD control and affect the subsequent etching step. For negative-tone systems, over cross-linking in the unexposed region can lead to residual resists between pattern sidewalls and result in bridging. It was shown that bridging was related to the molecular weight of photoresists and the defect can be reduced by using resists with smaller molecular weights.¹⁷ It was also reported that micro-bridging was closely related to CD and LWR, as larger CD and larger LWR accelerate bridging effect.¹⁸

1.2.4 Line-Width Control

As the dissolution characteristics of a photoresists can be determined by the developer concentration, development temperature and development time,^{19, 20} it is important to control these parameters carefully. Optimal conditions are important for line-width control as both over- and underdevelopment of photoresists can have adverse effect on resolution.

1.3 Environmentally Friendly Solvent-Based Developers

The toxicity of chemical solvents used in the lithographic process has prompted the need to use more environmentally friendly solvents such as water or other solvents to reduce volatile organic compound (VOC) emission.²¹ There have been many reports on developing water-castable and developable photoresists. The

development mechanism is based on cross-linking²²⁻²⁵ or polarity change through pinacol rearrangement²⁶⁻²⁸ after exposure. A new approach using temperature-triggered development of water-soluble resists for biological applications has also been recently reported.²⁹ However, most of the images can suffer from low contrast and low resolution due to swelling. It is also undesirable to develop photoresists in a high surface tension solvent like water as the image may collapse after development and limit the resolution. Pure water was therefore replaced with standard TMAH solution for better image quality.³⁰ To reduce environmental impact without sacrificing the image quality, two environmentally friendly solvents, supercritical carbon dioxide and linear methyl siloxanes, have been considered and are discussed in detail.

1.3.1 Supercritical Carbon Dioxide

Supercritical carbon dioxide (scCO₂) as shown in Figure 1.6, is the supercritical state ($T_c=31.1^\circ\text{C}$, $P_c=73.8$ bar) of carbon dioxide. It is non-toxic, non-flammable and inert under most conditions. Because it is a homogenous phase in-between gas and liquid, it possesses liquid-like density which provides good solvent capability and gas-like diffusivity, as shown in Table 1.1. The solvent power of scCO₂ can be easily tuned by varying the pressure and temperature without introducing a phase interface because of the high compressibility of near-critical CO₂ and the dependence of solubility and other properties on density. Besides its tunable solvent power, scCO₂ also has zero surface tension that can eliminate pattern collapse problems and can be easily recycled after usage. Because of its unique physical properties, scCO₂ have been widely used in many applications including polymerization, cleaning, coating, pharmaceutical applications and food extractions.³¹⁻

35

ScCO₂ is generally a good solvent for small, non-polar molecules but a poor

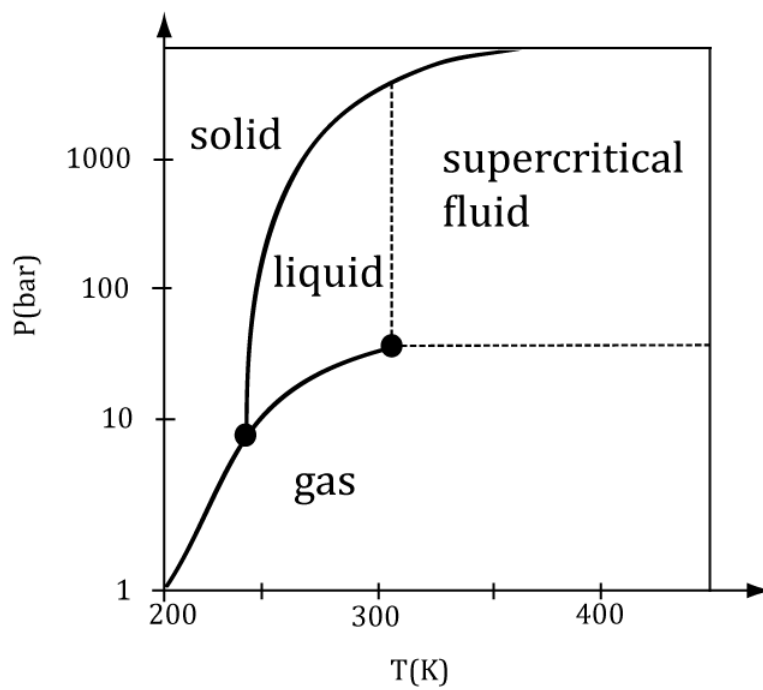


Figure 1.6. Phase diagram of supercritical carbon dioxide.

Table 1.1. Physical properties of gas, liquid, and supercritical fluid of typical organic fluid⁴⁴

	Density (g/ml)	Diffusivity (cm ² /s)	Dynamic viscosity (g/cm s)
Gas	1×10^{-3}	1×10^{-1}	1×10^{-4}
Liquid	1.0	5×10^{-6}	1×10^{-2}
Supercritical fluid	3×10^{-1}	1×10^{-3}	1×10^{-4}

solvent for polymers. It was shown that flexible molecules with large free volumes had higher solubility in scCO_2 ³⁶ and certain functional groups such as fluorine and silicon were incorporated to increase the solubility of polymers in scCO_2 . The first example of using scCO_2 to develop a polymethacrylates resist containing an acid-labile group and fluorine or siloxane esters was shown by Allen and Wallraff.³⁷ Ober et al. have reported the scCO_2 development of a block polymer of tetrahydropyranyl methacrylate and fluorinated methacrylate (P(THPMA-*b*-F7MA)) with negative-tone images as small as $0.1\ \mu\text{m}$,³⁸ as shown in Figure 1.7. Positive-tone images were also demonstrated by using vapor hexamethyldisilazane (HMDS) and tetramethyldisilazane (TMDS) to silylate the resists prior to development,^{39,40} features as small as $500\ \text{nm}$ were obtained through this method. Fluorinated polymers with alicyclic backbones such as norbornyl have also been reported and features as small as $3\ \mu\text{m}$ were achieved.⁴¹ The weak interactions between fluorinated polymers can contribute to their solubility in scCO_2 . In partially fluorinated polymer systems, the fluorine atom acts as a Lewis base towards electron deficient carbon atom of CO_2 and the hydrogen atoms, being positively charged because of the neighboring fluorine atoms, act as Lewis acids toward the electron rich oxygen atoms of CO_2 .⁴² Besides fluorine, it is also known that silicon can increase the solubility of polymers in scCO_2 as well as improve the etch resistance of photoresists. The increased solubility can be related to their flexible nature that provides them a larger free volume compared to other polymers. One early example of using silicon-containing photoresists is to convert polysilanes to polysiloxanes by the photoinduced insertion of oxygen,⁴³ as shown in Figure 1.8.

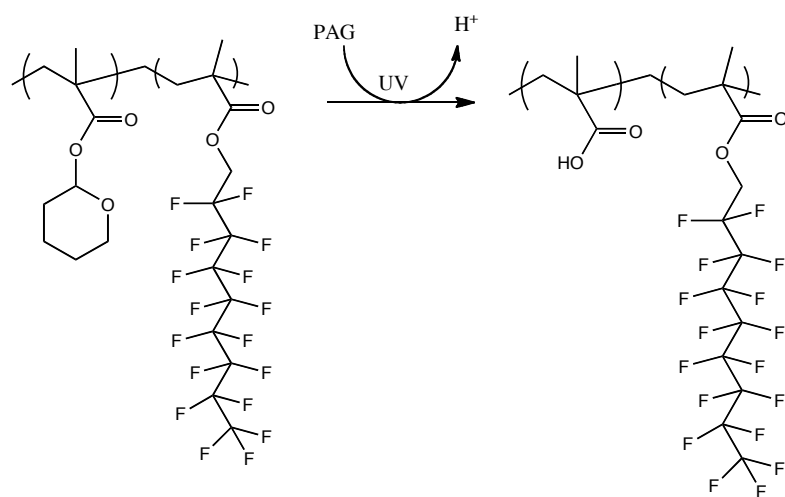


Figure 1.7. Lithographic patterning mechanism of P(THPMA-*b*-F7MA).

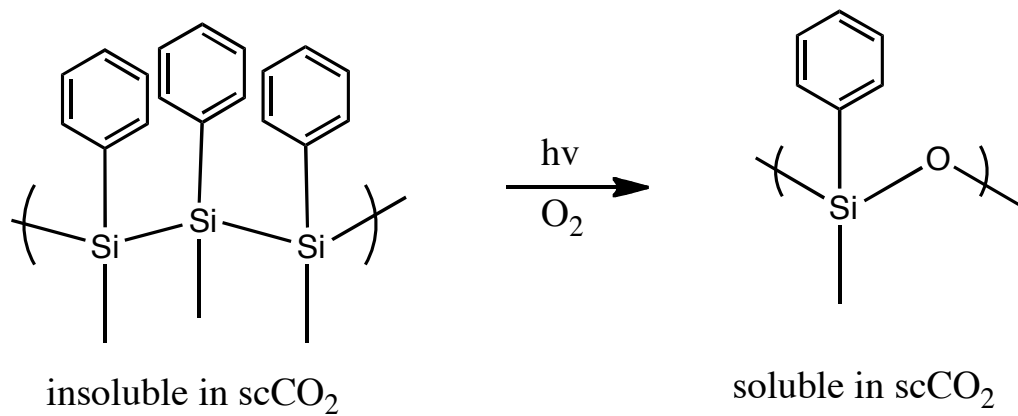


Figure 1.8. Solubility switching mechanism of polysilane.

In addition to designing new fluorinated or silicon-containing photoresist materials, another approach is to develop conventional photoresists in scCO₂ by adding co-solvents or additives.⁴⁵ Wagner and Tanaka both showed the development of conventional non-fluorinated photoresists in scCO₂ by using a class of fluorinated additives called quaternary ammonium salts (QAS).⁴⁶⁻⁴⁹ The ammonium center was able to interact with the resists and the fluorinated chain can provide scCO₂-solubility, the resist-QAS pair therefore formed a micelle that can dissolve in scCO₂, negative-tone images as small as 100 nm were achieved.

Although fluoropolymers and fluorinated additives showed good patterning results in scCO₂, the incorporation of fluorine into photoresists can have adverse effects on the etch resistance and fluorinated materials are undesirably expensive. The persistent nature of fluorinated compounds can also affect the environment.⁵⁰ Another class of photoresist materials, molecular glasses have the advantage of being intrinsically soluble in scCO₂ without the incorporation of fluorine. It is also believed that resolution limits and LER are related to the molecular size of photoresists⁵¹ which leads to increasing interest in developing small molecular glass photoresists.^{52, 53} Molecular glass photoresists that are based on phenolic structures or calix[4]resorcinarene derivatives have been both successfully developed in scCO₂, patterns as small as 50 nm with 3:1 aspect ratio have been achieved.⁵³⁻⁵⁵ It was shown that by removing just a few protecting groups of molecular glass resists can dramatically decrease their solubility in scCO₂ and led to high development contrast,⁵⁵ with the solubility switching mechanism shown in Figure 1.9. Higher molecular weight molecular glass, so called “Noria-boc,” were also developed in scCO₂ with sub-100 nm resolution.⁵⁶ Molecular glass resists that are based on natural materials such as cyclodextrin were also investigated for scCO₂ development.^{57, 58}

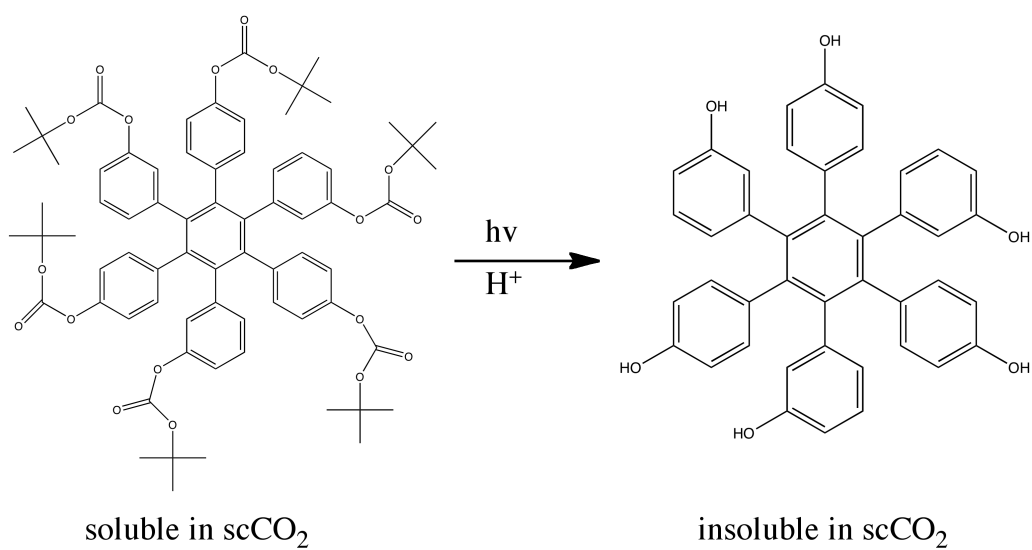
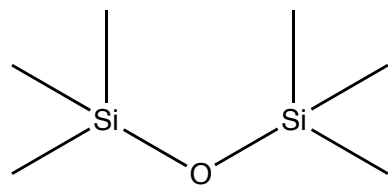


Figure 1.9. Solubility switching mechanism of hexa(hydroxyphenyl)benzene molecular glass.

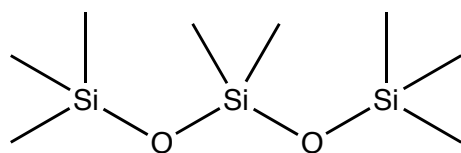
1.3.2 Linear Methyl Siloxanes

Linear methyl siloxanes are a class of non-polar solvents with low molecular weights that are based on silicon, oxygen, carbon and hydrogen, with some examples shown in Figure 1.10. Their solvent strength is weaker than saturated hydrocarbons but stronger than hydrofluorocarbons.⁵⁹

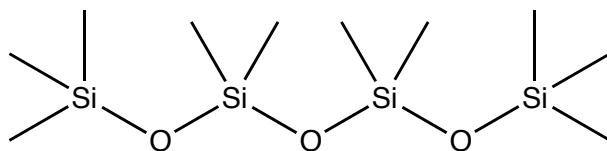
They are low in toxicity, not ozone-depleting,⁶⁰ contribute little to global warming and are exempt from federal regulations of VOC.⁵⁹ Instead of accumulating in the atmosphere, they are rapidly transformed to naturally occurring species and can be recycled.⁶¹⁻⁶³ They have been previously used in applications including personal formulations, cleaning, lubrication and precision water removal in microelectronic processing.⁵⁹ Similar to scCO₂, linear methyl siloxanes possess low surface tensions and their solvent power can be tuned by adding additives. Recent research has shown the successful development of conventional polymeric photoresists, poly(hydroxystyrene-co-styrene-co-*t*-butylacrylate (ESCAP) and poly(4-*t*-butoxycarbonyloxystyrene) (PBOCST) in linear methyl siloxanes by using a silylating agent,^{64, 65} with images in the sub-100 nm resolution. High resolution patterns of 30 nm lines with approximately 5:1 aspect ratio were also developed in linear methyl siloxanes using a phenolic molecular glass resist.⁶⁶



hexamethyldisiloxane



octamethyltrisiloxane



decamethyltetrasiloxane

Figure 1.10. Chemical structures of linear methyl siloxanes.

1.4 Recent Interest in Solvent-Based Negative-Tone Development

Recently, there has been growing interest in negative-tone development (NTD) due to its improved lithographic performance compared to positive-tone development (PTD). The reason for better performance can be related to the ease of mask design and better optical contrast provided by a bright-field mask for NTD.^{1, 67, 68} It has been demonstrated that NTD provides better performance when printing contact holes and narrow trenches, which are generally challenging for the PTD process.^{66, 69, 70} Unlike traditional solvent-based development that uses cross-linkable photoresists, the recent trend in solvent-based development has been focused on the use of chemically amplified photoresists with acid-labile protecting groups.^{69, 70} Instead of altering the solubility through changes in molecular weight, a chemically amplified resist creates a chemical difference between the exposed and unexposed areas to provide better contrast and eliminates the swelling problems occurring in cross-linkable photoresists. In addition, because most resists used in the microfabrication process are chemically amplified resists, studying the NTD process using these resists eliminates the need for designing new resist materials. As most chemically amplified resists are designed for aqueous development and PTD, it has been found that the choice of NTD solvents can dramatically affect the NTD performance.⁶⁹ The effect of ketone- and acetate- based solvents on 193 nm resists for NTD process have been studied and it was shown that both the solvents and imaging materials are critical for NTD performance.

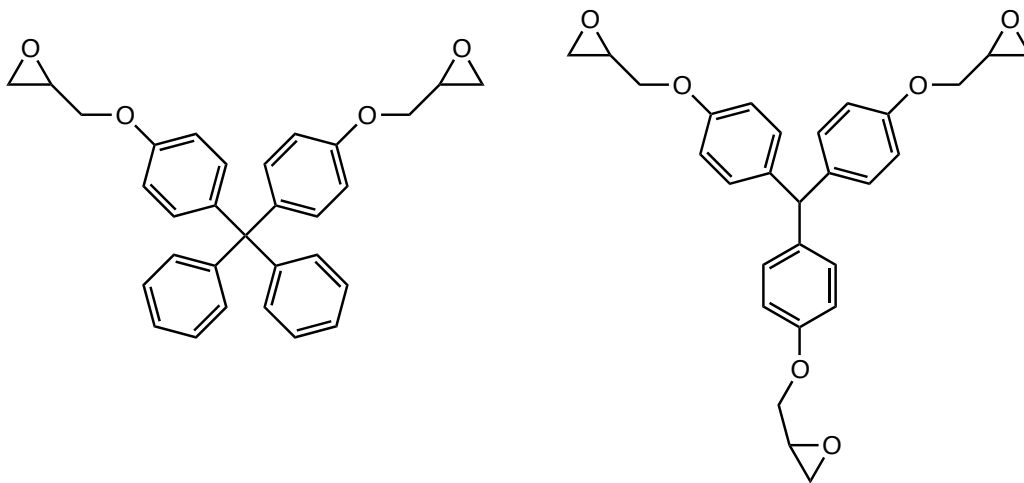


Figure 1.11. Chemical structures of epoxide-based molecular resists for solvent development.

Although chemically amplified resists have shown promising NTD results, they do suffer from post-NTD film loss. As mentioned earlier, traditional solvent-based development uses cross-linkable polymer resists which provides better resist integrity after development due to the network formation. In order to keep the advantage of traditional solvent-based resists while improving the dissolution behavior, resolution and LER, small molecular resists have drawn much attention for solvent-based development.^{71, 72} Calixarene-based e-beam resists have been widely studied. Solvents such as isopropanol, xylene and ethanol were used as developers and features as small as 10 nm have been demonstrated.^{9, 73} Besides calixarene-based resists, epoxide-based molecular resists (Figure 1.11) have been designed for solvent-based development.^{71, 72} A general characteristic of these resists is that they show reasonably significant cross-linking at very low dose which provides high sensitivity. Development was carried out using methyl isobutyl ketone (MIBK) and features as small as 25 nm with a sensitivity of 50 $\mu\text{C}/\text{cm}^2$ were shown. Besides cross-linkable small molecules, the increasing interests in inorganic resists due to their better etch resistance and high-resolution patterning capability¹³ have also led to research on solvent-based development of inorganic nanoparticle resists. Using a ligand-exchange reaction upon exposure which changes the solubility in the developing solvent, hafnium and zirconium oxide nanoparticles have been synthesized and developed in organic solvents, high EUV sensitivity (4.2 mJ/cm^2) and high resolution patterns down to 21.5 nm have been achieved.⁷⁴⁻⁷⁶

1.5 Summary

As the feature sizes continue to shrink, new processes and new materials are required for better lithographic performance. The development process is a critical step as the development results affect the subsequent etching step and

pattern transfer. Because of the emerging concerns about the environmental impact of the lithographic process, environmentally friendly solvents have been considered as alternative developers for the process. However, the main challenge lies in the solubility of the resist materials in these developers since conventional resists are designed for aqueous base developers. In addition to environmental issues, performance issues such as pattern collapse can become more serious as the feature size decreases and the aspect ratio increases. There are two solutions to this problem: one is through the use of low surface tension fluids to reduce the capillary forces during the development and rinsing step; the other solution is to improve the etch resistance of the resist materials and thus eliminates the need for high aspect ratio patterns. Chapter 2 presents the development of conventional photoresists in $scCO_2$ with the use of non-fluorinated additives. Previous work has shown successful patterning results of conventional photoresists with fluorinated additives, however, fluorinated materials are expensive and toxic. By using a silylating reagent, the environmental impact of the process was further reduced and the resolution was improved. Besides conventional polymeric resists, a molecular glass resist was synthesized and improved patterning results in $scCO_2$ were shown.

Chapters 3 and 4 focus on the development of photoresists using linear methyl siloxanes. Although linear methyl siloxanes have been used in many applications, Chapter 3 demonstrates the first application of linear methyl siloxanes for photoresist development. Both polymeric resists and molecular glass resists were developed in linear methyl siloxanes with high-resolution patterns down to 30 nm. The low surface tension of linear methyl siloxanes also proved to eliminate pattern collapse issues for high aspect ratio patterns. Chapter 4 further discusses the dissolution behavior of molecular glasses in linear methyl siloxanes

that provides useful information for improving development results. It was shown that both the polarity and molecular weight of the molecular glasses play important roles in terms of their solubility in linear methyl siloxanes.

Chapter 5 provides another approach to reduce pattern collapse problem. High etch-resistant inorganic metal oxide nanoparticles which eliminate the need for thick films have been synthesized for EUV and e-beam lithography. Previous studies have shown high-resolution patterning results, however, little was known about its development process. In this chapter, the effect of different components in the resist on patterning results and the development results with different negative-tone developers was studied. It was shown that photoactive compounds and developer strength are important for patterning inorganic nanoparticle resists.

REFERENCES

1. V. Marriot, *Proceedings of SPIE*, 1983, p. 144.
2. J. M. Shaw, M. Hatzakis, J. Paraszczak, J. Liutkus and E. Babich, *Polymer Engineering & Science*, 1983, **23**, 1058.
3. H. J. Levinson, *Principles of Lithography: Third Edition*, SPIE, 2010.
4. H. Ito, in *Microlithography-Molecular Imprinting*, Springer, 2005, pp.37-205
5. A. V. Dobrynin, M. Rubinstein and S. P. Obukhov, *Macromolecules*, 1996, **29**, 2974-2979.
6. Y. Kentor and M. Kardar, *Physical Review E: Statistical Physics, Plasmas, Fluids, and Related Interdisciplinary Topics*, 1995, **51**, 1229-1312.
7. H. Ito, Y. Maekawa, R. Sooriyakumaran and E. A. Mash, in *Polymers for Microelectronics*, American Chemical Society, 1993, pp. 64-87.
8. K. Harada, T. T. and K. O., *Journal of Electrochemical Society*, 1982, **129**, 2576-2580.
9. L. F. Thompson, C. G. Wilson and M. J. Bowden, *Introduction to Microlithography*, American Chemical Society, 1983.
10. H. Shiraishi, Y. Taniguchi, S. Horigome and S. Nonogaki, *Polymer Engineering & Science*, 1980, **20**, 1054-1057.
11. E. D. Feit and L. E. Stillwagon, *Polymer Engineering & Science*, 1980, **20**, 1058-1063.
12. H. Ito, in *Microlithography - Molecular Imprinting*, Springer-Verlag Berlin, Berlin, 2005, pp. 37-245.
13. R. Sooriyakumaran, H. Ito and E. A. Mash, *Proceedings of SPIE*, 1991, 419-428.
14. T. Tanaka, M. Morigami and N. Atoda, *Japanese Journal of Applied*

- Physics Part 1-Regular Papers Short Notes & Review Papers*, 1993, **32**, 6059-6064.
15. H. Ito and C. G. Willson, *Applications of photoinitiators to the design of resists for semiconductor manufacturing*, 1984.
 16. W. D. Hinsberg, F. A. Houle, M. I. Sanchez, J. A. Hoffnagle, G. M. Wallraff, D. R. Medeiros, G. M. Gallatin and J. L. Cobb, *Proceedings of SPIE*, 2003, pp. 1-14.
 17. J. W. Thackeray, T. Adams, M. F. Cronin, M. Denison, T. H. Fedynyshyn, J. Georger, M. Mori, G. W. Orsula and R. Sinta, *Journal of Photopolymer Science and Technology*, 1994, **7**, 619-630.
 18. S. Miyoshi, Y. Kobayashi, S. Tanaka, K. Kawano, K. Hashimoto and S. Inoue, *Journal of Micro/Nanolithography, MEMS, and MOEMS*, 2009, **8**, 013004.
 19. C. Mack, *Fundamental Principles of Optical Lithography*, Wiley, West Sussex, England, 2007.
 20. J. M. Shaw and M. Hatzakis, *Journal of The Electrochemical Society* 1979, **126**, 2026-2031.
 21. T. Saito and S. Takeichi, *Clinical Toxicology*, 1995, **33**, 343-348.
 22. J. M. Havard, S.-Y. Shim, J. M. J. Fréchet, Q. Lin, D. R. Medeiros, C. G. Willson and J. D. Byers, *Chemistry of Materials*, 1999, **11**, 719.
 23. J. M. Havard, D. Pasini, J. M. J. Fréchet, D. R. Medeiros, K. Patterson, S. Yamada and C. G. Willson, *Proceedings of SPIE*, 1998, p. 111.
 24. J. M. Havard, Vladimirov. N, J. M. J. Fréchet, S. Yamada, C. G. Willson and J. D. Byers, *Macromolecules*, 1999, **32**, 86.
 25. Q. H. Lin, T. Steinhausler, L. Simpson, M. Wilder, D. R. Medeiros, C. G. Willson, J. Havard and J. M. J. Fréchet, *Chemistry of Materials*, 1997, **9**,

- 1725-1730.
26. R. Sooriyakumaran, H. Ito and E. A. Mash, *Proceedings of SPIE*, 1991, p. 419.
 27. H. Ito, R. Sooriyakumaran and E. A. Mash, *Journal of Photopolymer Science and Technology*, 1991, **4**, 319.
 28. H. Ito and Y. Maekawa, ACS Symposium Series 579, Washington, D.C., 1994.
 29. L. Ionov and S. Diez, *Journal of the American Chemical Society*, 2009, **131**, 13315-13319.
 30. S. Yamada, O. J., T. Rager, M. Nielsen, J. D. Byers and C. G. Willson, *Proceedings of SPIE*, 2000, p. 569.
 31. J. L. Kendall, D. A. Canelas, J. L. Young and J. M. DeSimone, *Chemical Reviews*, 1999, **99**, 543-563.
 32. U. B. Kompella and K. Koushik, *Critical Reviews in Therapeutic Drug Carrier Systems*, 2001, **18**, 173-199.
 33. K. Johns and G. Stead, eds., *Supercritical Fluids for Coating-From Analysis to Xenon. A Brief Overview*, Kluwer Academic/Plenum Publishers, New York, NY, 1999.
 34. M. Sihvonen, E. Jarvenpaa, V. Hietaniemi and R. Huopalahti, *Trends Food Science and Technology*, 1999, **10**, 217-222.
 35. J. McHardy and S. P. Sawan, *Supercritical Fluid Cleaning Fundamentals*, Noyes, Westwood, NJ, 1998.
 36. J. Eastoe, A. Paul, S. Nave, D. C. Steytler, B. H. Robinson, E. Rumsey, M. Thorpe and R. K. Heenan, *Journal of American Chemical Society*, 2001, **123**, 988.
 37. R. D. Allen and G. M. Wallraff, ed. U. Patent, 1997, p. 527.

38. N. Sundararajan, S. Yang, K. Ogino, S. Valiyaveetil, J. G. Wang, X. Y. Zhou, C. K. Ober, S. K. Obendorf and R. D. Allen, *Chemistry of Materials*, 2000, **12**, 41-48.
39. V. Q. Pham, G. L. Weibel, P. T. Nguyen, R. J. Ferris and C. K. Ober, *Abstracts of Papers of the American Chemical Society*, 2002, **224**, 658-POLY.
40. V. Q. Pham, G. L. Weibel, A. H. Hamad and C. K. Ober, *Abstracts of Papers of the American Chemical Society*, 2001, **221**, 27-PMSE.
41. M. K. Boggiano, D. Vellenga, R. Carbonell, V. S. Ashby and J. M. DeSimone, *Polymer*, 2006, **47**.
42. P. Raveendran and S. L. Wallen, *Journal of Physical Chemistry B*, 2003, **107**, 1473.
43. P. M. Gallagher-Wetmore, G. M. Wallraff and R. D. Allen, *Proceedings of SPIE*, 1995, p. 694.
44. Y. Mao, N. M. Felix, P. T. Nguyen, C. K. Ober and K. K. Gleason, *Journal of Vacuum Science and Technology B*, 2004, **22**, 2473-2478.
45. J. DeYoung, M. Wagner, C. Harbinson, M. Miles, A. E. Zweber and R. G. Carbonell, *Proceedings of SPIE*, 2006, pp. 615345-615341.
46. A. E. Zweber, M. Wagner and R. G. Carbonell, *Journal of Physical Chemistry B*, 2009, **113**, 9687-9693.
47. M. Tanaka, A. Rastogi, G. N. Toepperwein, R. A. Riggleman, N. M. Felix, J. J. de Pablo and C. K. Ober, *Chemistry of Materials*, 2009, **21**, 3125-3135.
48. A. E. Zweber, M. Wagner, J. DeYoung and R. G. Carbonell, *Langmuir*, 2009, **25**, 6176-6190.
49. J. P. Giesy and K. Kannan, *Environmental Science and Technology*, 2001,

- 35**, 1339-1342.
50. A. De Silva, N. M. Felix and C. K. Ober, *Advanced Materials*, 2008, **20**, 3355-3361.
 51. S. W. Chang, R. Ayothi, D. Bratton, D. Yang, N. Felix, H. B. Cao, H. Deng and C. K. Ober, *Journal of Materials Chemistry*, 2006, **16**, 1470-1474.
 52. N. M. Felix, A. De Silva and C. K. Ober, *Advanced Materials*, 2008, **20**, 1303.
 53. N. M. Felix, A. De Silva, C. M. Y. Luk and C. K. Ober, *Journal of Materials Chemistry*, 2007, **17**, 4598-4604.
 54. N. M. Felix, K. Tsuchiya and C. K. Ober, *Advanced Materials*, 2006, **18**, 442-446.
 55. M. Tanaka, A. Rastogi, H. Kudo, D. Watanabe, T. Nishikubo and C. K. Ober, *Journal of Materials Chemistry*, 2009, **19**, 4622-4626.
 56. M. Kryszak, A. De Silva, J. Sha, J.-K. Lee and C. K. Ober, *Proceedings of SPIE*, 2009, p. 72732N.
 57. J. Sha, J.-K. Lee and C. K. Ober, *Proceedings of SPIE*, 2009, p. 72732T.
 58. S. P. Manivannan, *Supercritical Fluid Cleaning: Fundamentals, Technology and Applications*, Noyes Publications, Westwood, NJ, 1998.
 59. D. E. Williams, ACS symposium 2000.
 60. R. Atkinson, *Environmental Science & Technology*, 1991, **25**, 863-866.
 61. D. W. Hairston, *Chemical Engineering*, 1996, **103**, 69-&.
 62. J. Sherman, B. Chin, P. D. T. Huibers, R. Garcia-Valls and T. A. Hatton, *Environmental Health Perspectives*, 1998, **106**, 253-271.
 63. W. J. Chatterton, in *IEEE International Symposium on Electrical Insulation*, 2000, pp. 412-416.

64. C. Y. Ouyang, J.-K. Lee, J. Sha and C. K. Ober, *Proceedings of SPIE*, 2010.
65. C. K. Ober, C. Y. Ouyang, J.-K. Lee and J. Sha, *PMSE Preprints*, 2010.
66. C. Y. Ouyang, J.-K. Lee, M. E. Krysak, J. Sha and C. K. Ober, *Journal of Materials Chemistry*, 2012, **22**, 5746-5750.
67. T. A. Brunner and C. A. Fonseca, *Proceedings of SPIE*, 2001, 30-36.
68. C. A. Mack and J. E. Connors, *Proceedings of SPIE*, 1992, 328-338.
69. Y. C. Bae, S.-H. Lee, R. Bell, L. Joesten and G. G. Barclay, *Proceedings of SPIE*, 2011, 797207.
70. A. E. Grigorescu, M. C. van der Krogt, C. W. Hagen and P. Kruit, *Microelectronic Engineering*, 2007, **84**, 822-824.
71. R. A. Lawson, J. Cheng, D. E. Noga, T. R. Younkin, L. M. Tolbert and C. L. Henderson, *Proceedings of SPIE*, 2010, 76390O.
72. R. A. Lawson, D. E. Noga, J. Cheng, L. M. Tolbert and C. L. Henderson, *Proceedings of SPIE*, 2010, 76392F.
73. J. M. Shaw, J. D. Gelorme, N. C. LaBianca, W. E. Conley and S. J. Holmes, *IBM Journal of Research*, 1997, **41**, 94.
74. M. Krysak, M. Trikeriotis, E. Schwartz, N. Lafferty, P. Xie, B. Smith, P. Zimmerman, W. Montgomery, E. Giannelis and C. K. Ober, *Proceedings of SPIE*, 2011, **7972**, 79721C/79721-79721C/79726.
75. M. Trikeriotis, W. J. Bae, E. Schwartz, M. Krysak, N. Lafferty, P. Xie, B. Smith, P. A. Zimmerman, C. K. Ober and E. P. Giannelis, *Proceedings of SPIE*, 2010, **7639**, 76390E/76391-76390E/76310.
76. M. Trikeriotis, M. Krysak, Y. S. Chung, C. Ouyang, B. Cardineau, R. Brainard, C. K. Ober, E. P. Giannelis and K. Cho, *Journal of Photopolymer Science and Technology*, 2012, **25**, 583-586.

CHAPTER 2

PATTERNING NON-FLUORINATED POLYMERIC AND MOLECULAR GLASS MATERIALS IN SUPERCRITICAL CARBON DIOXIDE

Abstract

Supercritical carbon dioxide (scCO₂) has drawn much attention due to its unique physical properties that can benefit many applications. The large amount of organic solvents used in many chemical processes has also led to the need for more environmentally friendly alternatives. ScCO₂ is non-toxic, non-flammable, inert under most conditions, inexpensive and can be recycled. However, in order to take full advantage of the unique properties of scCO₂, more understanding of its solvent power is required. Because of the zero surface tension and high diffusivity of scCO₂, it is a promising candidate for patterning thin films and here we seek to understand the dissolution behavior of non-fluorinated materials through high-resolution patterning using lithography. Previous work has shown scCO₂ development of conventional photoresists using fluorinated additives. In this study, we demonstrated the development of a conventional photoresist in scCO₂ using non-fluorinated additives. Because of the high solubility of non-polar and small molecules in scCO₂, a molecular glass was synthesized for high-resolution patterning using scCO₂. Features as small as 50 nm were obtained with no pattern collapse observed.

* Part of this chapter was adapted from Christine Y. Ouyang, Jin-Kyun Lee, Jing Sha, Christopher K. Ober, "Environmentally Friendly Processing of Photoresists in scCO₂ and decamethyltetrasiloxane," *Proceedings of SPIE*, 2010, 7639, 763912

2.1 Introduction

Supercritical carbon dioxide (scCO₂) is a single-phase fluid¹ that exists above the critical state (T=31°C, P=7.4 MPa) of carbon dioxide. Because it exists in a homogenous phase between a gas and a liquid, it possesses gas-like diffusivity and liquid-like density. Unlike conventional solvents, the density of scCO₂ changes under different operating pressures and temperatures which leads to differences in solvent power under selected processing conditions.^{2, 3} Besides tuning its solvent power by changing the processing conditions, its solvent power can also be further increased by adding co-solvents or additives.^{4, 5} In addition to its adjustable solvent power, scCO₂ also has many unique physical properties such as low viscosity and zero surface tension that can be advantageous for many applications. It is also non-toxic, non-flammable, inert under most conditions and can be recycled after use. As the large amount of organic solvent used in many chemical processes has raised many concerns about the environment, scCO₂ is an ideal candidate to replace these toxic solvents due to its environmental friendliness,^{6, 7} and it has been widely used in applications such as polymer synthesis, cleaning, and drying.^{2, 8, 9}

Although there are many appealing benefits of using scCO₂ as processing solvent, there is still little understanding of its solvent power which is a major obstacle for its practical use. One topic of interest for using scCO₂ as a processing solvent is to pattern thin films because of its unique physical properties. It has high diffusivity that can aid in effective dissolution and it possesses zero surface tension, which prevents pattern collapse for high aspect ratio patterns.¹⁰⁻¹² However, in order to pattern thin films, scCO₂-soluble molecules need to be designed which requires more understanding of the dissolution behavior of materials in scCO₂. Due to its non-polar nature, scCO₂ is generally a good solvent

for non-polar and small molecules but a poor solvent for polymers. Many research groups have focused on the design on CO₂-philic molecules in order to take full advantage of the unique properties of CO₂ as a solvent. DeSimone and co-workers have studied the synthesis of fluoropolymers and the miscibility of fluorinated polymers in scCO₂.^{9, 13-17} Besides fluorinated polymers, Beckman has examined the effect of increasing the flexibility of polymer side-chains and incorporating non-fluorinated groups into the polymer backbones on scCO₂-solubility.¹⁸⁻²⁴ McHugh and co-workers have also showed the solubility of polymers and copolymers in scCO₂ can be affected by the polymer free volume.^{3, 25-27} The high solubility of fluorinated materials can be attributed to the polar-quadrupole interactions between CO₂ and fluorinated polymer.²⁷ It was also found that a high level of fluorination decreases miscibility due to the stronger dipole-dipole interactions between the fluorinated polymer chains.²⁵ Other reasons for miscibility in scCO₂ can be related to the increase of flexibility and free volume of the functional groups²⁸ or the weak self-interactions of the molecules.²⁹ Although fluorinated and silicon-containing polymers have shown high miscibility with scCO₂, the solubility of most polymers in scCO₂ is still poor³⁰ and generally requires co-solvents or additives.³¹ In this work, we seek to understand the solvent power of scCO₂ through high-resolution patterning of non-fluorinated materials.

A common process to pattern thin films is the use of a polymer (photoresist) with photo-switchable functional groups that can change a polymer's solubility after exposure.³² As the current lithographic process involves a large quantity of organic solvents, scCO₂ is also an ideal candidate to reduce the environmental impact of the whole process.³³ However, most conventional photoresists are not soluble as scCO₂ is a poor solvent for polymers and thus the solubility of photoresists in scCO₂ has become a limiting factor for its use for

patterning polymer thin films. Previously, polymers containing silicon and fluorine have been synthesized and patterned in scCO₂.³⁴⁻³⁷ Conventional polymeric photoresists lacking fluorine or silicon are not soluble in scCO₂ and instead may require a co-solvent to be developed in scCO₂.³⁸ Wagner and Ober^{31, 39-41} have also studied the use of fluorinated quaternary ammonium salts (QAS) to increase the solubility of conventional polymer photoresists in scCO₂. However, using fluoropolymers may decrease the plasma etch resistance and is expensive. In addition, fluorinated compounds are coming under increased scrutiny because of their persistent nature.⁴² In order to increase the environmental-friendliness of this process, we have selected several non-fluorinated additives to develop conventional photoresists in scCO₂ and have shown high-resolution patterns using e-beam lithography.

Besides structure modifications or the use of additives, another approach is to use low molecular weight molecules since scCO₂ is generally a good solvent for non-polar small molecules. Therefore, several molecular glass resists have been synthesized for this purpose.^{31, 43-47} Another advantage of using molecular glasses is that their small sizes may enable high-resolution patterning and reduce line edge roughness (LER). Because of the plasticizing nature of scCO₂, it is necessary that the molecular glass photoresists possess high glass transition temperature (T_g). Previously, a family of calix[4]resorcinarene derivatives has been studied in photoresist applications using scCO₂.⁴⁶ The ring architecture of calix[4]resorcinarene is important for its high glass transition temperature because it reduces molecular flexibility. We have also shown successful high-resolution patterning of a molecular glass in scCO₂ without any additives. In order to understand the dissolution behavior on a molecular level, computational

simulations were carried out to provide more understanding of the development mechanism.

2.2 Experimental

2.2.1 Materials

Poly(hydroxystyrene-co-styrene-co-*t*-butylacrylate) (ESCAP) was obtained from DuPont Electronic Polymers Inc. High Purity carbon dioxide was purchased from Airgas and used as received. Triphenylsulfonium nonaflate (TPS-nf), N-hydroxynaphthalimide triflate (NI-Tf), 1-(trimethylsilyl)imidazole (TMSI) and N,O-Bis-(trimethylsilyl)acetamide (BSA) were purchased from Sigma-Aldrich. (N,N-dimethylamino)trimethyl silane (DMTS) was obtained from Gelest. The calix[4]resorcinarene (CHPB) molecular glass was synthesized according to a procedure reported by literature.⁴⁸

2.2.2 Partially *t*-boc Protected (ca. 80%) Poly (4-hydroxystyrene) (PBOCST)

To a solution of poly(4-hydroxystyrene) ($M_n=8000 \text{ g mol}^{-1}$, 2.0 g, 0.25 mmol) in acetone (50 cm^3) was added 4-(dimethylamino) pyridine (DMAP) (2.4 mg, 0.02 mmol) and di-*tert*-butyl dicarbonate (1.45 g, 6.66 mmol) at ambient temperature.

The solution was stirred overnight and passed through a short plug of silica gel column with ethyl acetate wash. The solution was then concentrated in a rotary evaporator to obtain a yellow solid.

2.2.3 Lithographic Evaluation

For ESCAP and PBOCST, a 5 wt% solution of each photoresist in propylene glycol methyl ether acetate (PGMEA) with 5 wt% photoacid generator (PAG) was prepared. Each solution was spin-coated onto a 4-inch HMDS-primed silicon wafer at 2000 rpm for 60 seconds and was baked at 130°C for 60 seconds.

For the calix[4]resorcinarene molecular glass, a 10 wt% solution of calixarene in PGMEA with 5wt% PAG was prepared. It was then spin-coated onto a 4-inch

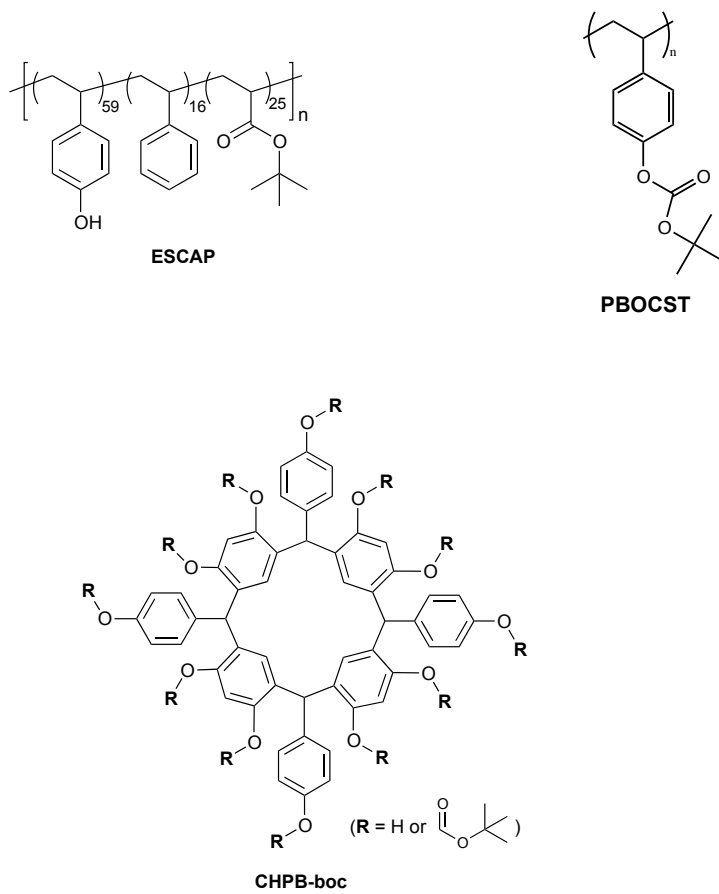


Figure 2.1. Chemical structures of ESCAP, PBOCST and calix[4]resorcinarene.

silicon wafer at 2000 rpm for 60 seconds and baked subsequently at 115°C for 60 seconds.

Dose testing was performed by using a GCA Autostep 200 DSW i-line Wafer stepper (500 mW/cm²) and an ABM contact aligner ($\lambda=254\text{nm}$, power= 8.6 mW/cm²). High-resolution patterning was done using a Leica VB6HR or a JEOL 9300 e-beam lithography system operating at 100 kV. Post-exposure bake was performed at 90°C (calix[4]resorcinarene, PBOCST), 115°C (ESCAP) for 60 seconds.

2.2.4 Development in scCO₂

Each resist film was developed in scCO₂ using a dissolution rate monitor with the setup described elsewhere.⁴⁹ For ESCAP and PBOCST, a silylating reagent (0.5-1.5ml) was added into the pre-chamber and mixed at 5000-6000 psi and 50°C for 15 minutes. It was then transferred into the main chamber for development at 4000-6000 psi and 50°C for different time lengths. For CHPB, it was developed in scCO₂ at 3500 psi and 40°C for 5 minutes.

2.2.5 Metrology

A Tencor P10 profilometer was used to measure the film thickness of each photoresist before and after development. The developed patterns were examined using the Nikon Digital Sight D5-5M-L1 optical microscope and the LEO 1550 FESEM scanning electron microscope.

2.3 Results and Discussion

2.3.1 Development of Conventional Photoresists in scCO₂

Because scCO₂ is a poor solvent for polar polymers, conventional photoresists are generally insoluble and require additives³¹ to increase their solubility in scCO₂. In this study, we examined two standard DUV resists, one is ESCAP and the other is PBOCST with their chemical structures shown in Figure

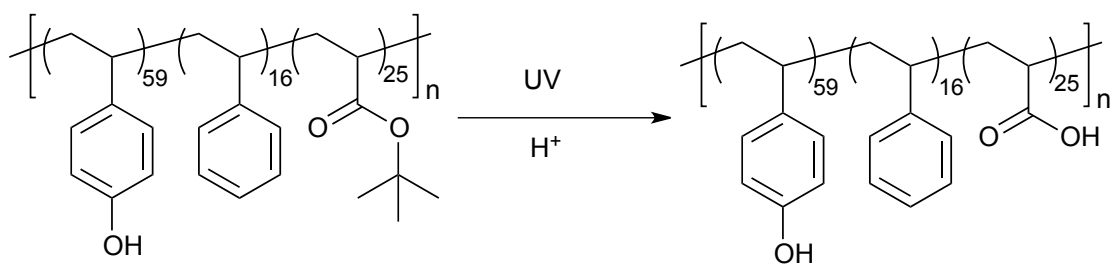
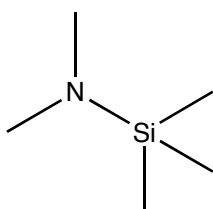
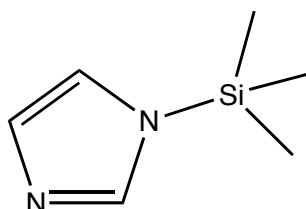


Figure 2.2. Deprotection reaction of ESCAP upon exposure.

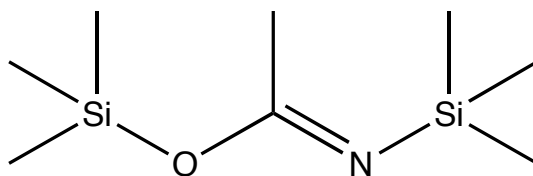
2.1. The acid-labile *t*-butyl groups in ESCAP can form carboxylic acids when the acid is generated from the PAG upon exposure as shown in Figure 2.2. The benzene ring provides high etch resistance and the phenol groups are important to increase the polarity and glass transition temperature (T_g) of the resist. Unexposed ESCAP showed almost no solubility in $scCO_2$ even when the pressure was increased to 5000 psi at 50°C. As the *tert*-butyl groups deprotected, the polarity of ESCAP increased and made it even less soluble in a non-polar solvent such as $scCO_2$. However, it is known that hydroxyl groups can be silylated and silicon-containing groups are generally less polar and are soluble in $scCO_2$.²⁴ Therefore, three silylating reagents were selected as additives to increase the solubility of ESCAP in $scCO_2$ (Figure 2.3). Because both exposed and unexposed ESCAP contains hydroxyl groups, both areas can react with the silylating reagent as shown in Figure 2.4. As the silylating reagent interacted with ESCAP and trimethylsilyl (TMS) groups being incorporated into the resist, the solubility of ESCAP in $scCO_2$ increased. When comparing the unexposed and exposed regions of ESCAP, although the exposed region had more TMS groups, the bulkier silicon atom made the TMS group more polar than *tert*-butyl group and therefore the exposed ESCAP was more polar than the unexposed region and was less soluble in $scCO_2$. Because of this polarity and solubility difference, we were able to develop ESCAP as a negative-tone resist in $scCO_2$. Both 1-(trimethylsilyl)imidazole (TMSI) and N,O-Bis-(trimethylsilyl)acetamide (BSA) are stronger silylating reagents compared to (N,N-dimethylamino)trimethyl silane (DMTS) and both exposed and unexposed ESCAP were dissolved in $scCO_2$ when silylated using TMSI and BSA. This shows that the silylating ratio and the silylating strength play an important role for the solubility change of ESCAP in $scCO_2$. Because DMTS showed the best solubility difference between the exposed



(N,N-dimethylamino)trimethyl silane



1-(trimethylsilyl)imidazole



N,O-Bis-(trimethylsilyl)-acetamide

Figure 2.3. Chemical structures of silylating reagents.

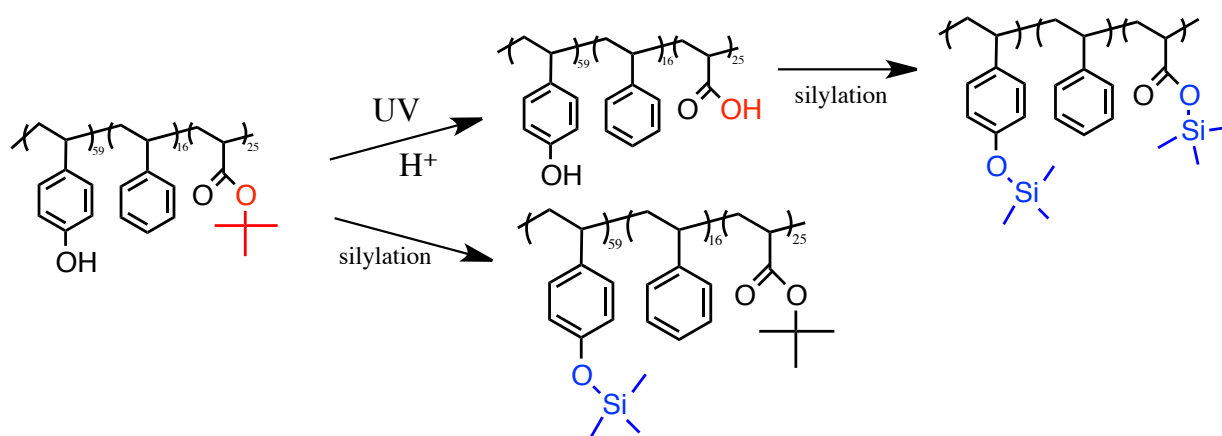


Figure 2.4. Silylation of ESCAP after exposure.

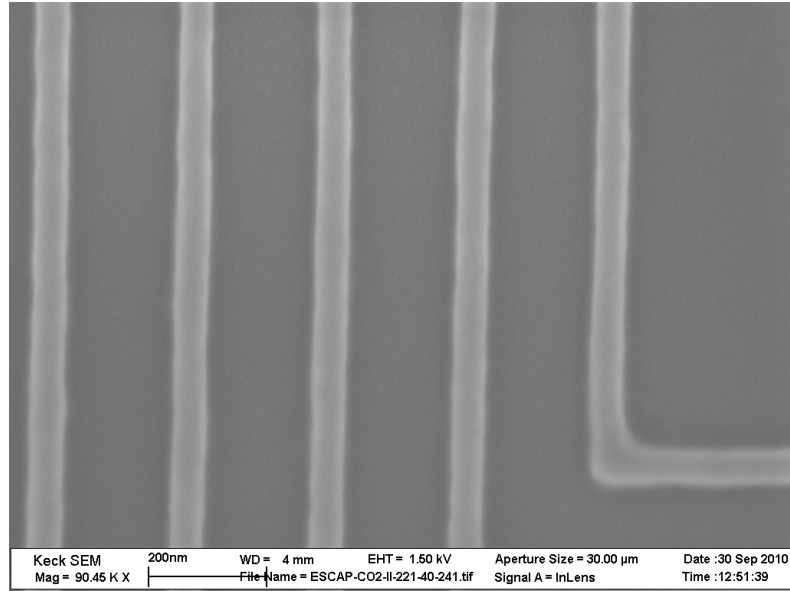


Figure 2.5. E-beam patterns of ESCAP developed in scCO₂ at 6000 psi, 50°C for 40 minutes (dose: 40μC/cm²).

and unexposed area of ESCAP, e-beam lithography was utilized to study the patternability of ESCAP in scCO₂. As shown in Figure 2.5, 0.5 ml of DMTS was added into the pre-chamber and dissolved in scCO₂ at 50°C and 6180 psi for 15 minutes and transferred into the main chamber where ESCAP was developed at 50°C and 6000 psi for 40 minutes, smooth and high-resolution 55 nm line/space patterns were successfully demonstrated. It has been previously shown that the resolution limit of ESCAP-type resists is about 50 nm experimentally and theoretically⁵⁰ and previous work with fluorinated additives has shown features down to sub-100 nm³¹ using conventional photoresists. We have been able to increase the resolution and demonstrate the capability of using scCO₂ to achieve high-resolution patterns with non-fluorinated additives, which further increased the environmental-friendliness of this development process.

PBOCST is protected by acid-labile *tert*-butoxycarbonyl (*t*-boc) groups (Figure 2.1), as the acid being generated upon exposure, the *t*-boc groups can be cleaved and hydroxyl groups are formed as seen in Figure 2.6. As DMTS showed the best result with ESCAP, it was also added into scCO₂ to dissolve PBOCST. However, it was observed that both exposed and unexposed PBOCST were soluble at 5500 psi and both areas were insoluble at lower pressures, which shows that the silylating ratio and the solvating power both play important roles when dissolving high molecular weight polymers in scCO₂. As the solubility difference for the unexposed and exposed regions of PBOCST was not as big as the difference for ESCAP, we were not able to pattern PBOCST in scCO₂ with this silylation process.

2.3.2 Molecular Glass Photoresists for ScCO₂ Development

A series of calix[4]resorcinarene have been previously synthesized as scCO₂-developable materials due to their smaller sizes.⁴⁶ As CHPB has previously

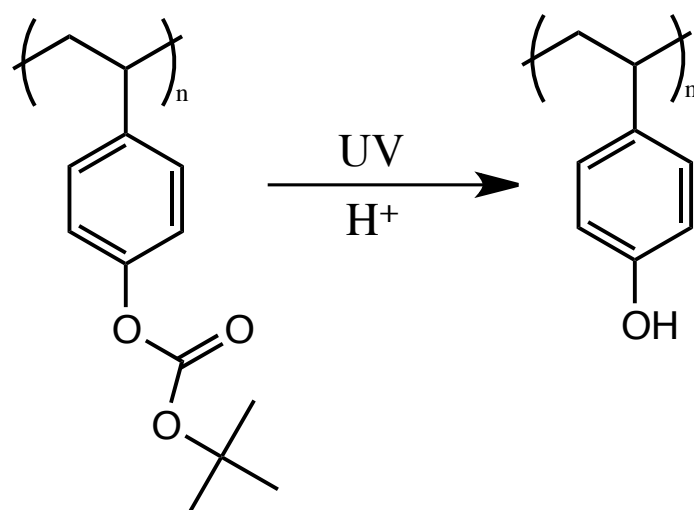


Figure 2.6. Deprotection reaction of PBOCST upon exposure.

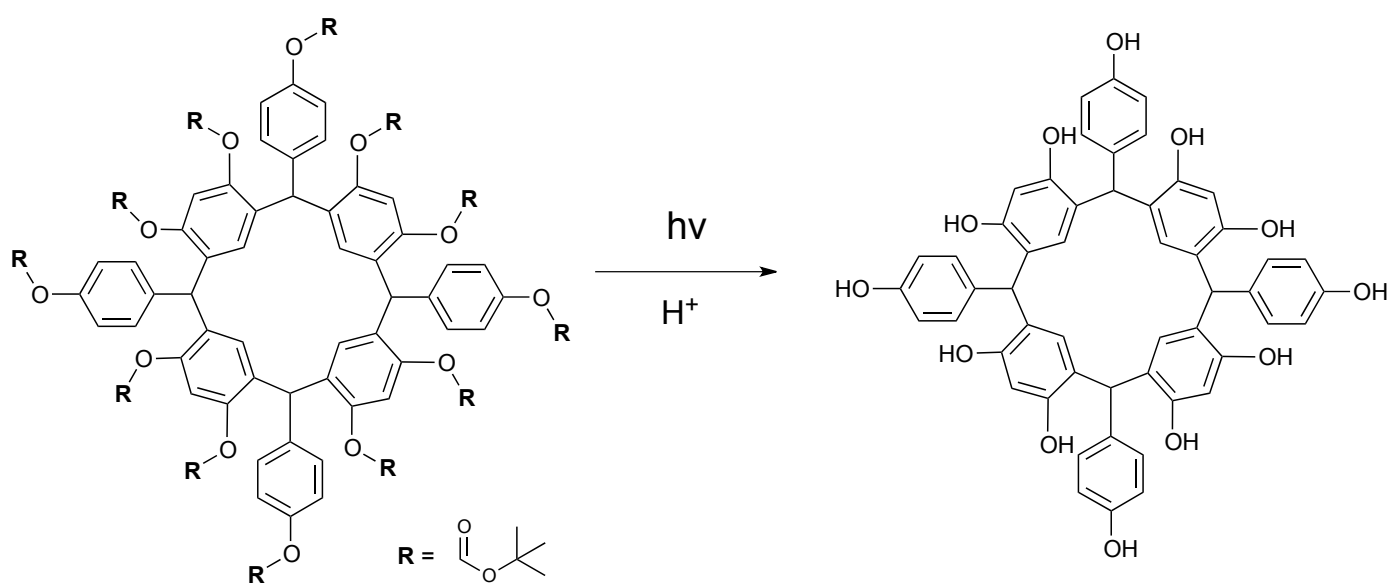


Figure 2.7. Deprotection reaction of CHPB after exposure.

shown excellent positive-tone patterning results at EUV using a conventional aqueous base developer, it was chosen here to achieve high-resolution patterns in scCO₂.⁴⁸ When CHPB is protected by *t*-boc groups, it is relatively soluble in scCO₂ due to its small size and non-polarity. When it is exposed to UV light or electron beam radiation, the acid generated from the photoacid generator deprotects the acid-labile *t*-boc groups and form hydroxyl groups (Figure 2.6). Since hydroxyl groups are more polar than *t*-boc groups, the molecule becomes less soluble and form negative-tone images in a non-polar solvent. Previous work with calix[4]resorcinarene derivatives was able to show feature sizes as small as 70 nm using a silicon-containing molecular glass.⁴⁶ However, the silicon-containing calix[4]resorcinarene was more expensive to synthesize compared to CHPB and the bulky silicon-containing groups can limit the resolution. With the small size of CHPB, high-resolution patterns as small as 50 nm were achieved (Figure 2.8) and no pattern collapse was observed. This verifies the ability of scCO₂ to mitigate pattern collapse problems commonly seen in high aspect ratio and high-resolution patterns.

2.3.3 Computational Simulations

In addition to the direct experiments, the dissolution of ESCAP, PBOCST and CHPB were studied through the use of molecular simulation. This work was performed using GROMACS as described in previous work.³¹ This approach includes quantum mechanical and statistical mechanical calculations of realistic molecules and the various aspects of the dissolution process in scCO₂. For the computational simulations, model parameters were used from the Optimized Potential for Liquid Simulation (OPLS) force field. Additional quantum calculations were performed to provide a more accurate charge model, necessary to accurately describe ionic species and aromatic ring interactions. Using this

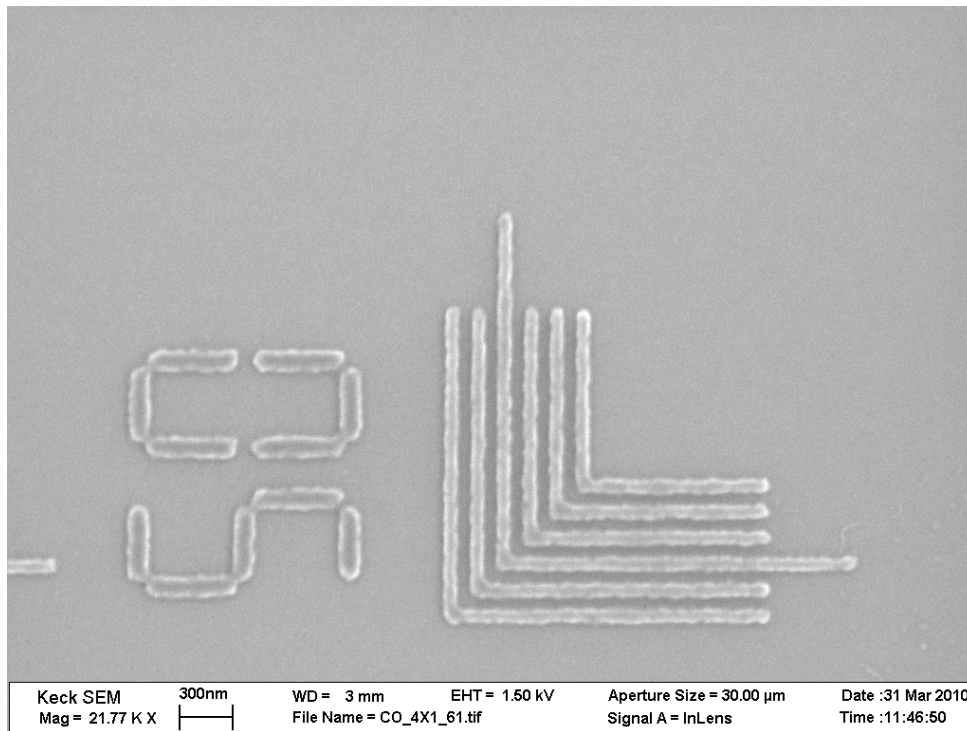
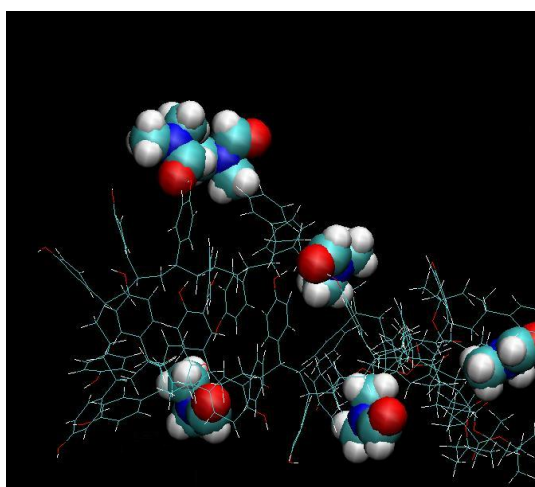
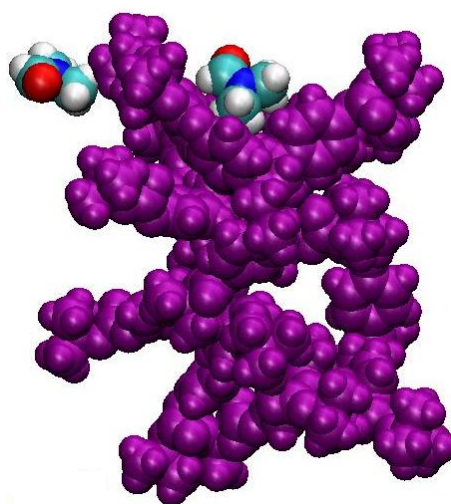


Figure 2.8. E-beam patterns of CHPB (dose: $32\mu\text{C}/\text{cm}^2$) developed in scCO_2 at 40°C , 2000 psi for 5 minutes.



(a)



(b)

Figure 2.9. Interactions of DMTS with (a) ESCAP, (b) PBOCST in scCO₂.

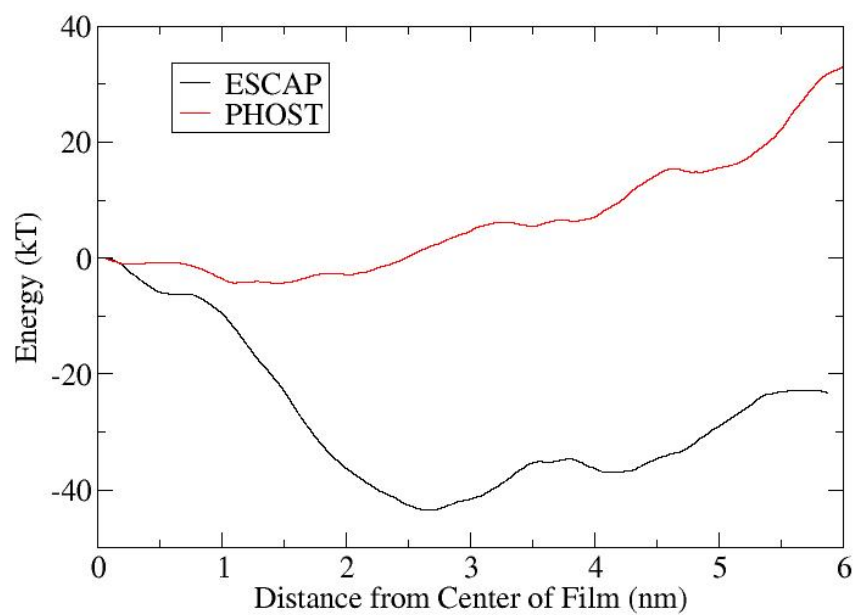


Figure 2.10. Free energy curves of ESCAP and PBOCST using DMTS as an additive in $scCO_2$.

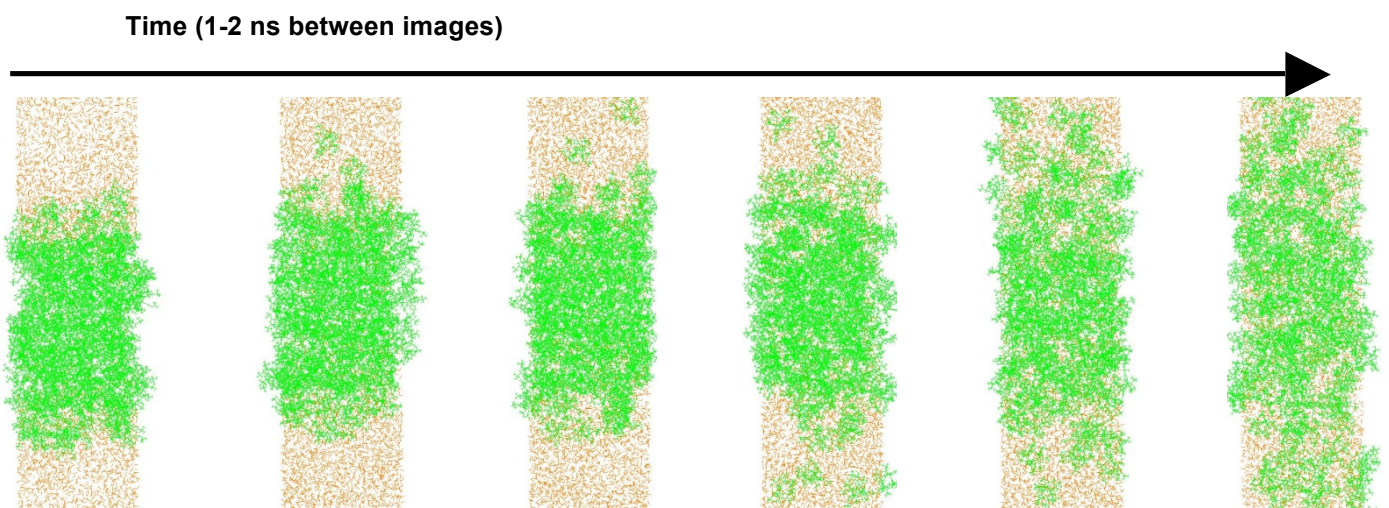


Figure 2.11. Computational simulations of CHPB in scCO₂.

model, thin films of resists were equilibrated in the presence of scCO₂. As shown in Figure 2.9, DMTS is able to interact with the hydroxyl groups in ESCAP and lead to solubility in scCO₂ as demonstrated by experiment. For PBOCST, the bulky *t*-boc groups can hinder the interaction and lead to ineffective silylation and poor solubility in scCO₂ which was observed experimentally when the pressure was not sufficiently high. Free energy curves (Figure 2.10) were produced by integrating the average force on each chain as a function of position throughout the film. Systems with lower free energy at the surface of the film are thermodynamically unstable and soluble, whereas those with lower free energy at the center are insoluble. As shown in Figure 2.10, the solubility of ESCAP in scCO₂ is increased in the presence of DMTS while PBOCST stays almost insoluble, which is consistent with the experimental results. For the molecular glass, CHPB, the resist film was first equilibrated in the bulk and exposed to scCO₂ as a thin film. After equilibration, production runs were performed for 2 ns to show the dissolution of unexposed CHPB in scCO₂ as shown in Figure 2.11. Figure 2.11 shows that CHPB dissolves more and more into scCO₂ as the time increases and we were also able to show negative-tone images experimentally.

2.4 Conclusions

In order to understand the dissolution behavior of non-fluorinated materials in scCO₂, thin film patterning was carried out to investigate the solvent power of scCO₂. ScCO₂ can be a promising candidate for patterning photoresists due to its unique properties such as zero surface tension which can eliminate the pattern collapse problem and its green characteristics that can reduce the environmental impact of the lithographic process. Two conventional photoresists, ESCAP and PBOCST, and one molecular glass, CHPB, were chosen to study the development process of photoresists in scCO₂. It was found that when using a

silylating reagent, both ESCAP and PBOCST were more soluble in scCO₂. However, depending on the silylation ratio and the pressure of scCO₂, different patterning results were obtained. Successful negative-tone patterns with features as small as 55 nm were achieved with ESCAP using e-beam lithography but no patterns were obtained with PBOCST. Because of the small size of CHPB, it can be developed in scCO₂ without any additives. When the non-polar *t*-boc groups were cleaved, it became less soluble and formed negative-tone images. We have shown high-resolution 50 nm line/space patterns with CHPB using e-beam lithography. Computational simulations were also carried out to provide an understanding of the dissolution mechanism at a molecular level and it was shown the interaction between the resist (ESCAP, CHPB) and scCO₂ provided increased solubility. Because of the bulky *t*-boc groups that hindered the interaction between the additive and PBOCST, it remained insoluble in scCO₂ at lower pressures.

REFERENCES

1. R. S. Oakes, A. A. Clifford and C. M. Rayner, *Journal of the Chemical Society, Perkin Transactions 1*, 2001, **9**, 917-941.
2. A. I. Cooper, *Journal of Materials Chemistry*, 2000, **10**, 207-234.
3. C. F. Kirby and M. A. McHugh, *Chemical Reviews*, 1999, **99**, 565-602.
4. B. De Gioannis, A. Vega-Gonzalez and P. Subra, *Journal of Supercritical Fluids*, 2004, **29**, 49-57.
5. X. G. Zhang, B. X. Han, Z. S. Hou, H. L. Zhang, Z. M. Liu, T. Jiang, J. He and H. P. Li, *Chemistry-A European Journal*, 2002, **8**, 5107-5111.
6. M. Poliakoff, J. M. Fitzpatrick, T. R. Farren and P. T. Anastas, *Science*, 2002, **297**, 807-810.
7. J. Sherman, B. Chin, P. D. T. Huibers, R. Garcia-Valls and T. A. Hatton, *Environmental Health Perspectives*, 1998, **106**, 253-271.
8. G. L. Weibel and C. K. Ober, *Microelectronic Engineering*, 2003, **65**, 145-152.
9. J. M. Desimone, Z. Guan and C. S. Elsbernd, *Science*, 1992, **257**, 945-947.
10. T. Tanaka, M. Morigami and N. Atoda, *Japanese Journal of Applied Physics Part 1-Regular Papers Short Notes & Review Papers*, 1993, **32**, 6059-6064.
11. D. L. Goldfarb, J. J. de Pablo, P. F. Nealey, J. P. Simons, W. M. Moreau and M. Angelopoulos, *Journal of Vacuum Science & Technology B*, 2000, **18**, 3313-3317.
12. D. L. Goldfarb, J. J. de Pablo, P. F. Nealey, J. P. Simons, W. M. Moreau and M. Angelopoulos, *Journal of Vacuum Science & Technology B*, 2001, **19**, 600-600.
13. J. Guo, P. Andre, M. Adam, S. Panyukov, M. Rubinstein and J. M.

- DeSimone, *Macromolecules*, 2006, **39**, 3427-3434.
14. M. K. Boggiano, D. Vellenga, R. Carbonell, V. S. Ashby and J. M. DeSimone, *Polymer*, 2006, **47**, 4012-4017.
 15. J. M. Desimone, E. E. Maury, Y. Z. Menciloglu, J. B. McClain, T. J. Romack and J. R. Combes, *Science*, 1994, **265**, 356-359.
 16. Y. L. Hsiao, E. E. Maury, J. M. Desimone, S. Mawson and K. P. Johnston, *Macromolecules*, 1995, **28**, 8159-8166.
 17. Z. B. Guan and J. M. Desimone, *Macromolecules*, 1994, **27**, 5527-5532.
 18. T. A. Hoefling, R. M. Enick and E. J. Beckman, *Journal of Physical Chemistry*, 1991, **95**, 7127-7129.
 19. T. Hoefling, D. Stofesky, M. Reid, E. Beckman and R. M. Enick, *J. Supercrit. Fluids*, 1992, **5**, 237-241.
 20. R. Fink, D. Hancu, R. Valentine and E. J. Beckman, *Journal of Physical Chemistry B*, 1999, **103**, 6441-6444.
 21. Y. Wang, L. Hong, D. Tapriyal, I. C. Kim, I.-H. Paik, J. M. Crosthwaite, A. D. Hamilton, M. C. Thies, E. J. Beckman, R. M. Enick and J. K. Johnson, *Journal of Physical Chemistry B*, 2009, **113**, 14971-14980.
 22. S. Kilic, S. Michalik, Y. Wang, J. K. Johnson, R. M. Enick and E. J. Beckman, *Macromolecules*, 2007, **40**, 1332-1341.
 23. P. Munshi, A. Ghosh, E. J. Beckman, Y. Patel, J. George, S. Z. Sullivan, S. Pulla, P. Ramidi and V. Malpani, *Green Chemistry Letters and Reviews*, 2010, **3**, 319-328.
 24. E. J. Beckman, *Chemical Communications*, 2004, 1885-1888.
 25. M. A. McHugh, I. H. Park, J. J. Reisinger, Y. Ren, T. P. Lodge and M. A. Hillmyer, *Macromolecules*, 2002, **35**, 4653-4657.
 26. W. H. Tuminello, G. T. Dee and M. A. McHugh, *Macromolecules*, 1995,

- 28**, 1506-1510.
27. F. Rindfleisch, T. P. DiNoia and M. A. McHugh, *Journal of Physical Chemistry*, 1996, **100**, 15581-15587.
 28. J. Eastoe, A. Paul, S. Nave, D. C. Steytler, B. H. Robinson, E. Rumsey, M. Thorpe and R. K. Heenan, *Journal of the American Chemical Society*, 2001, **123**, 988-989.
 29. M. L. O'Neill, Q. Cao, R. Fang, K. P. Johnston, S. P. Wilkinson, C. D. Smith, J. L. Kerschner and S. H. Jureller, *Industrial & Engineering Chemistry Research*, 1998, **37**, 3067-3079.
 30. D. K. Dandge, R. J. Card and L. G. Donaruma, 1985, 679-686.
 31. M. Tanaka, A. Rastogi, G. N. Toepperwein, R. A. Riggleman, N. M. Felix, J. J. de Pablo and C. K. Ober, *Chemistry of Materials*, 2009, **21**, 3125-3135.
 32. H. Ito, in *Microlithography - Molecular Imprinting*, Springer-Verlag Berlin, Berlin, 2005, pp. 37-245.
 33. E. D. Williams, R. U. Ayres and M. Heller, *Environmental Science & Technology*, 2002, **36**, 5504-5510.
 34. C. K. Ober, A. H. Gabor, P. GallagherWetmore and R. D. Allen, *Advanced Materials*, 1997, **9**, 1039.
 35. V. Q. Pham, G. L. Weibel, A. H. Hamad and C. K. Ober, *Abstracts of Papers of the American Chemical Society*, 2001, **221**, 27-PMSE.
 36. V. Q. Pham, G. L. Weibel, P. T. Nguyen, R. J. Ferris and C. K. Ober, *Abstracts of Papers of the American Chemical Society*, 2002, **224**, 658-POLY.
 37. N. Sundararajan, S. Yang, K. Ogino, S. Valiyaveetil, J. G. Wang, X. Y. Zhou, C. K. Ober, S. K. Obendorf and R. D. Allen, *Chemistry of*

- Materials*, 2000, **12**, 41-48.
38. Y. Mao, N. M. Felix, P. T. Nguyen, C. K. Ober and K. K. Gleason, *Journal of Vacuum Science & Technology B*, 2004, **22**, 2473-2478.
 39. J. DeYoung, M. Wagner, C. Harbinson, M. Miles, A. E. Zweber and R. G. Carbonell, *Proc. of SPIE*, 2006, **6153**, 615345-615341.
 40. A. E. Zweber, M. Wagner, J. DeYoung and R. G. Carbonell, *Langmuir*, 2009, **25**, 6176-6190.
 41. M. Tanaka, A. Rastogi, N. M. Felix and C. K. Ober, *Journal of Photopolymer Science and Technology*, 2008, **21**, 393-396.
 42. K. Kannan, J. C. Franson, W. W. Bowerman, K. J. Hansen, J. D. Jones and J. P. Giesy, *Environmental Science & Technology*, 2001, **35**, 3065-3070.
 43. A. De Silva, N. M. Felix and C. K. Ober, *Advanced Materials*, 2008, **20**, 3355-3361.
 44. N. Felix and C. K. Ober, *Chemistry of Materials*, 2008, **20**, 2932-2936.
 45. N. M. Felix, A. De Silva, C. M. Y. Luk and C. K. Ober, *Journal of Materials Chemistry*, 2007, **17**, 4598-4604.
 46. N. M. Felix, A. De Silva and C. K. Ober, *Advanced Materials*, 2008, **20**, 1303.
 47. A. De Silva, J. K. Lee, X. Andre, N. M. Felix, H. B. Cao, H. Deng and C. K. Ober, *Chemistry of Materials*, 2008, **20**, 1606-1613.
 48. S. W. Chang, R. Ayothi, D. Bratton, D. Yang, N. Felix, H. B. Cao, H. Deng and C. K. Ober, *Journal of Materials Chemistry*, 2006, **16**, 1470-1474.
 49. V. Q. Pham, N. Rao and C. K. Ober, *Journal of Supercritical Fluids*, 2004, **31**, 323-328.
 50. W. D. Hinsberg, F. A. Houle, M. I. Sanchez, J. A. Hoffnagle, G. M.

Wallraff, D. R. Medeiros, G. M. Gallatin and J. L. Cobb, *Proceedings of SPIE*, **5039**, 14.

CHAPTER 3

ENVIRONMENTALLY FRIENDLY PATTERNING OF THIN FILMS IN LINEAR METHYL SILOXANES

Abstract

A number of green solvents have been explored to reduce the environmental impact of many chemical processes. Among them, linear methyl siloxanes make up a class of solvents that are low in toxicity, VOC exempt and not ozone-depleting. In addition, their unique physical properties such as low surface tension and low viscosity can mitigate several issues encountered with conventional processing solvents. In order to understand the behavior of linear methyl siloxanes as processing solvents, the solubility of polymer and small molecular glass are studied in this work. Using lithography as a test of solubility differences, we have successfully shown patterning of thin films in linear methyl siloxanes thereby demonstrating their utility in processing organic systems.

* This chapter was adapted from Christine Y. Ouyang, Jin-Kyun Lee, Marie E. Krysak, Jing Sha, Christopher K. Ober, “Environmentally Friendly Patterning of Thin Films in Linear Methyl Siloxanes,” *Journal of Materials Chemistry*, 2012, 22, 5746-5750

3.1 Introduction

Green chemistry is an emerging topic due to the increasing awareness of the environmental impact of chemicals and organic solvents involved in many chemical processes. Instead of controlling the use, handling, treatment and disposal of chemicals to minimize the risk posed by chemical processes, green chemistry seeks to reduce hazard by careful design and selection of both chemicals with reduced toxicity and reaction pathways that eliminate by-products or ensure they are benign.¹ In order to improve and reduce the environmental impact of solvent-based processes, many green solvents, such as supercritical carbon dioxide (scCO₂)¹⁻⁴ and water⁵⁻¹¹, have been previously studied. However, both solvents have their limitations for practical applications. For example, high pressure is required to achieve the supercritical state of CO₂ and water possesses high surface tension that is undesirable in a number of circumstances.¹²

In the search for alternative green solvents, silicon-based solvents should be considered due to their well-established and benign organosilicon chemistry and the versatility of silicon-based materials. Frederic Stanley Kipping and his pioneering work in organosilicon chemistry contributed to the rapid growth of organosilicon chemistry between 1899-1936, when he used Grignard reaction to synthesize organosilicon compounds.¹³ Since the 1930s, with the initial applications as heat-resistant polymers in electrical industry, the unique and versatile character of silicon-based compounds were soon recognized and developed for various applications. Silicon-based materials can be tailored by varying molecular structure, molecular size, or functional composition. Currently, different forms and molecular weights of silicon-based materials are used in numerous applications depending on their physical and chemical properties.

Among silicon-based materials, linear methyl siloxanes (Figure 3.1) are a

class of non-polar solvents with low molecular weights. They are low in toxicity, contribute little to global warming, do not contribute to urban ozone depletion,¹⁴ and do not harm stratospheric ozone or form any urban ozone layer. Rather than accumulating in the atmosphere, they are rapidly transformed to naturally occurring chemical species and can be recycled.¹⁵⁻¹⁷ The solvent strength of linear methyl siloxanes is less than that of saturated hydrocarbons, but can be enhanced by the addition of suitable co-solvents.¹⁷ Because of their advantageous chemical and physical properties, they have been used as components of cosmetics and personal formulations.¹⁸ They have also been used for water removal in microelectronics processing, lubrication and cleaning applications.²⁰ However, little research has been done on linear methyl siloxanes as solvents for polymer materials.¹⁹

In the high resolution patterning of polymers, it is possible to detect subtle differences in solvent power. A common practice to pattern thin films is the use of a polymer (photoresist) with photo-switchable functional groups that can change the polymer's polarity after exposure. One can use these small changes in the exposed polymer to enable subtle discrimination of a solvent's characteristics. A thin film is developed in a solvent that selectively dissolves either the exposed or unexposed polymer. Thus we have elected to use photolithography to explore the solvent aspects of these green materials. In addition, linear methyl siloxanes are promising for patterning thin films because they possess low surface tension with the potential to eliminate pattern collapse for ultra dense patterns.

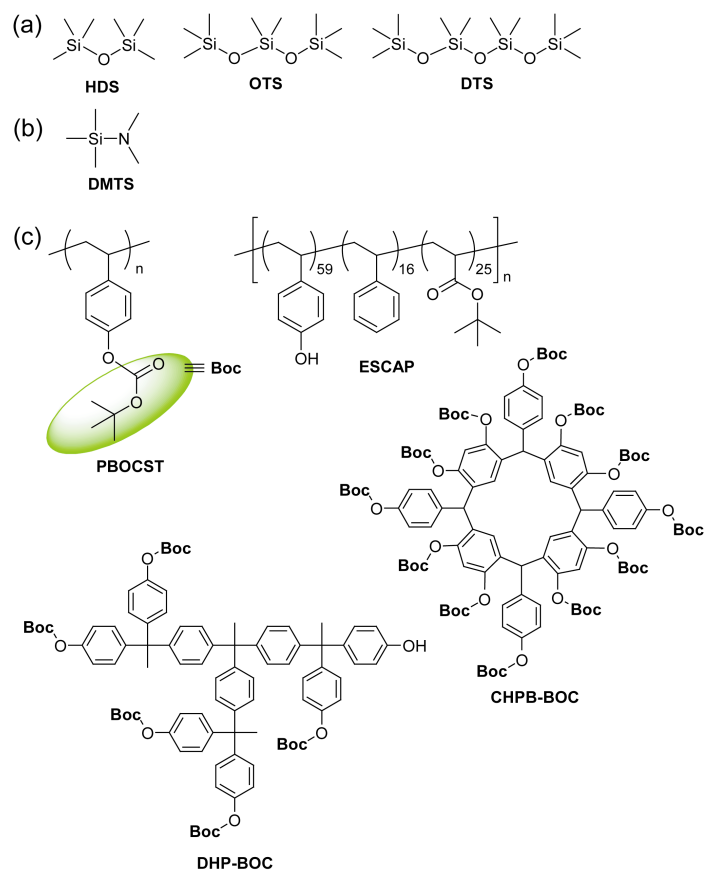


Figure 3.1. Chemical structures of (a) linear methyl siloxanes [hexamethyldisiloxane (HDS), octamethyltrisiloxane (OTS), and decamethyltetrasiloxane (DTS)], (b) silylating agent [(*N,N*-dimethylamino)trimethylsilane (DMTS)], and (c) polymeric or molecular resist materials investigated in this study.

Although small and non-polar materials are soluble in linear methyl siloxanes, it is still challenging to use such solvents to pattern polar polymers. Silylation is a common process for introducing silyl groups into molecules and it is widely used for surface modification²⁰ or introduction of silicon-containing protecting groups.²¹ A silylation method was therefore combined with linear methyl siloxane solvents in the patterning of these polymer thin films. Besides polymers, small and amorphous molecular glasses have also been studied for high-resolution patterning.²² Three linear methyl siloxanes, hexamethyldisiloxane (HDS, b.p.= 99-100 °C, viscosity=0.65 cSt, surface tension=18 dynes cm⁻¹), octamethyltrisiloxane (OTS, b.p. 152-3 °C, viscosity=1.04 cSt, surface tension=17.4 dynes cm⁻¹) and decamethyltetrasiloxane (DTS, b.p.=194-5 °C, viscosity=1.53 cSt, surface tension=18 dynes cm⁻¹) were chosen in this investigation and we have demonstrated a new patterning process with these solvents.

3.2 Experimental

3.2.1 Materials

Three linear methyl siloxanes and (*N,N*-dimethylamino)trimethylsilane (DMTS) were purchased from Gelest and used without further purification. Poly(hydroxystyrene-*co*-styrene-*co-tert*-butylacrylate) (ESCAP) was obtained from DuPont Electronic Polymers Inc. Photoacid generators (PAGs), *N*-hydroxynaphthalimide triflate (NI-Tf) and bis(4-*tert*-butylphenyl)iodonium perfluoro-1-butanesulfonate (Iod-Nf), were purchased from Sigma-Aldrich. *C*-4-Hydroxyphenyl calix[4]resorcinarene (CHPB) and its fully *tert*-butoxycarbonylated (Boc) molecular resist (CHPB-BOC) were synthesized according to procedures reported in literature.²²

Partially Boc-protected (ca. 80%) Poly(4-hydroxystyrene) (PBOCST): To a

solution of poly(4-hydroxystyrene) ($M_n=8,000 \text{ g mol}^{-1}$, 2.0 g, 0.25 mmol) in acetone (50 cm^3) was added 4-(dimethylamino)pyridine (DMAP) (2.4 mg, 0.02 mmol) and di-*tert*-butyl dicarbonate (1.45 g, 6.66 mmol) at ambient temperature. The solution was stirred overnight and passed through a short plug of silica gel column with ethyl acetate wash. The solution was then concentrated in a rotary evaporator to obtain a yellow solid.

Partially Boc-protected (ca. 80%) dendritic hexaphenol (DHP-BOC): To a magnetically stirred solution of DHP²³ (0.47 g, 0.53 mmol) and DMAP (0.013 g, 0.11 mmol) in tetrahydrofuran (THF) (10 cm^3) was added a solution of di-*tert*-butyl dicarbonate (0.516 g, 2.36 mmol) in THF (5 cm^3) at ambient temperature. The solution was then stirred for 4 h at ambient temperature and poured into water (150 cm^3). The precipitated solid was filtered, washed with water and dissolved in ethyl acetate (50 cm^3). The organic solution was dried over anhydrous MgSO_4 and passed through a short plug of silica gel with ethyl acetate wash. The solution was then concentrated under reduced pressure to give a pale-yellow foamy solid (DHP-BOC) (0.7 g, *ca.* 80% protection by $^1\text{H-NMR}$).

3.2.2 Lithographic Evaluation

5 wt% Solutions of each photoresist in propylene glycol methyl ether acetate (PGMEA) with NI-Tf or Iod-Nf (5 wt% with respect to photoresist) were prepared. The resist solutions were then spin-coated onto 4-inch 1,1,1,3,3,3-hexamethyldisilazane (HMDS)-primed Si wafers at 2000 rpm for 60 seconds yielding *ca.* 100 nm thick films. The films were subsequently baked at 130 °C (ESCAP, PBOCST, DHP-BOC) or 115 °C (CHPB-BOC) for 60 seconds. Dose testing was performed using a GCA Autostep 200 DSW i-line Wafer Stepper ($\lambda=365 \text{ nm}$, 500 mW cm^{-2}) with NI-Tf as a photoacid generator (PAG). High-resolution patterning was done using a JEOL JBX-9300FS e-beam lithography

system operating at 100 kV with Iod-Nf as a PAG. Post-exposure bake was performed at 90 °C (PBOCST, DHP-BOC) or 115 °C (ESCAP, CHPB-BOC) for 60 seconds.

The exposed films of CHPB-BOC were developed in each linear methyl siloxane for 60 seconds. The films of PBOCST, ESCAP and DHP-BOC were developed in mixed solvents (DMTS:linear siloxane=1:10 by vol.) at 40 °C for 5 minutes and rinsed with pure linear siloxanes before drying.

3.2.3 Metrology

A Tencor P10 surface profiler was used to measure the film thickness of each photoresist before and after pattern development. The developed images were examined using a Nikon Digital Sight D5-5M-L1 optical microscope and a Keck scanning electron microscope (SEM). Film dissolution studies were carried out by a quartz crystal microbalance (QCM) technique²⁴ with a piezoelectric quartz crystal oscillator. Infrared spectra of exposed and unexposed PBOCST films were collected using a Mattson Infinity Gold FT-IR. Thin-film samples are applied to a KBr plate manually. Grazing-angle FT-IR using a Vertex80v FT-IR instrument was utilized to monitor the silylation reaction of exposed PBOCST. A Mattson Infinity FT-IR instrument was used to study the silylation contrast of PBOCST.

3.3 Results and Discussion

To understand the solvent properties of linear methyl siloxanes and their ability to pattern polymer thin films, two polymeric photoresist materials were selected, one is poly(4-*tert*-butoxycarbonyloxystyrene) (PBOCST) and the other is poly(hydroxystyrene-*co*-styrene-*co*-*tert*-butylacrylate) (ESCAP) as shown in Figure 3.1. Both of these model photoresists undergo structural changes from

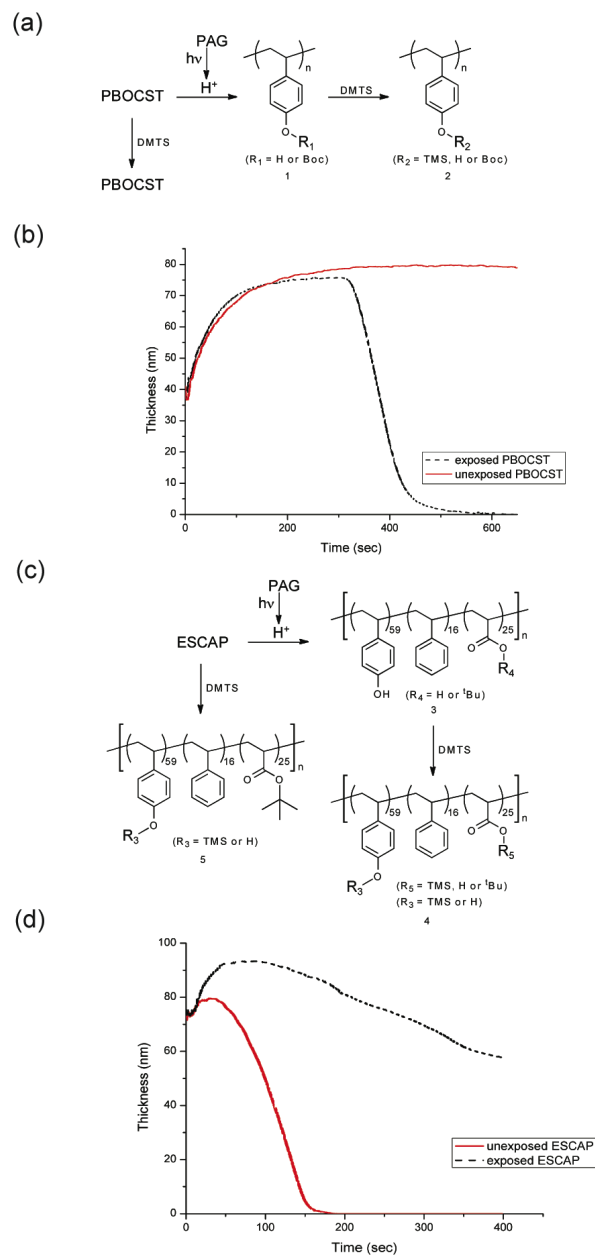


Figure 3.2. (a) Probable chemical reactions of PBOCST, (b) film thickness changes of PBOCST films in OTS and DMTS mixture at 40 °C with and without UV exposure, (c) Probable chemical reactions of ESCAP, (d) film thickness changes of ESCAP films in OTS and DMTS mixture at 40 °C with and without UV exposure.

the acidolysis of *tert*-butoxycarbonyl or *tert*-butyl groups when acids are generated from the photoacid generator (PAG) as shown in Figure 3.2 (a) and 3.2 (c). The dissolution behaviors of both polymers in linear methyl siloxanes were first studied because a solubility switch after exposure is required to pattern thin films. A quartz crystal microbalance (QCM) technique was used to monitor the film thickness changes to obtain dissolution information, as shown in Figure 3.2 (b) and 3.2 (d).²⁴

No dissolution of the exposed and unexposed PBOCST films was observed in linear methyl siloxanes even when the solvent temperature was raised to 40°C which showed that the solvent strength of linear methyl siloxanes was insufficient to dissolve the polymer films. The possibility of silylating the hydroxyl groups in exposed PBOCST to increase its solubility in linear methyl siloxanes was therefore considered. (N,N-dimethylamino)trimethyl silane (DMTS), as shown in Figure 3.1(b) was chosen as a silylating reagent because of its moderate boiling point, higher reactivity compared to that of hexamethyldisilazane (HMDS) and its easily removable by-product, dimethylamine.²¹ As shown in Figure 3.2 (a), the hydroxyl groups can be protected with trimethylsilyl (TMS) groups after reacting with DMTS, and the TMS groups can increase the solubility of exposed PBOCST in linear methyl siloxanes due to their lower polarity. The siloxanes can thus selectively dissolve exposed PBOCST while the unexposed region remains insoluble.

As shown in Figure 3.2 (b), it is found that the film did not dissolve at a constant rate but passed through a swelling stage before it completely dissolved. When the exposed films were immersed in the OTS and DMTS (1:10 by vol.) mixed solvent, the hydroxyl groups in PBOCST initially reacted with the DMTS, resulting in a TMS-rich layer. Film swelling was first observed when the

incorporated TMS moieties were not sufficient to dissolve the polymers in linear methyl siloxanes. As the TMS-protection ratio increased beyond a critical level, the exposed film began to dissolve and thus exposing the less TMS-protected layer underneath which led to dissolution. The swelling stage was also observed in unexposed PBOCST because it was not fully boc-protected and its free hydroxyl groups can still react with DMTS. However, the unexposed film went through a longer swelling stage before starting to show some solubility.

Grazing-angle FT-IR was carried out to monitor the silylation reaction as shown in Figure 3.3. The characteristic trimethylsilyloxy absorption peaks were observed at 1258 cm^{-1} (Si-CH₃) and 1015 cm^{-1} (Si-O). In order to understand how the silylation process can affect the chemical contrast of the polymer, FT-IR was conducted as shown in Figure 3.4. Each sample of PBOCST was exposed at different radiation doses and gas-phase silylation was carried out using DMTS at 90°C for 5 minutes. The changes in boc-protection and silylation ratio were monitored using FT-IR and plotted into Figure 3.4. The intensity change of each functional group was observed at their characteristic absorption peaks (OH: 3400 cm^{-1} and Si-O: 925 cm^{-1}) using C=C aromatic stretch at 1500 cm^{-1} as a reference peak. Comparing to the change of boc-deprotection (change of hydroxyl groups after PEB) ratios, the difference in the extent of silylation between each dose was much higher. Chemical amplification, where the polymer changes its polarity after exposure, is known to provide high chemical contrast which leads to high development contrast. Conventional processing is based on chemical amplification and uses aqueous base to dissolve away exposed PBOCST and is shown as the blue triangle line. From this study, it we see that we can further increase the chemical contrast by using a silylation process. A sharp contrast was also

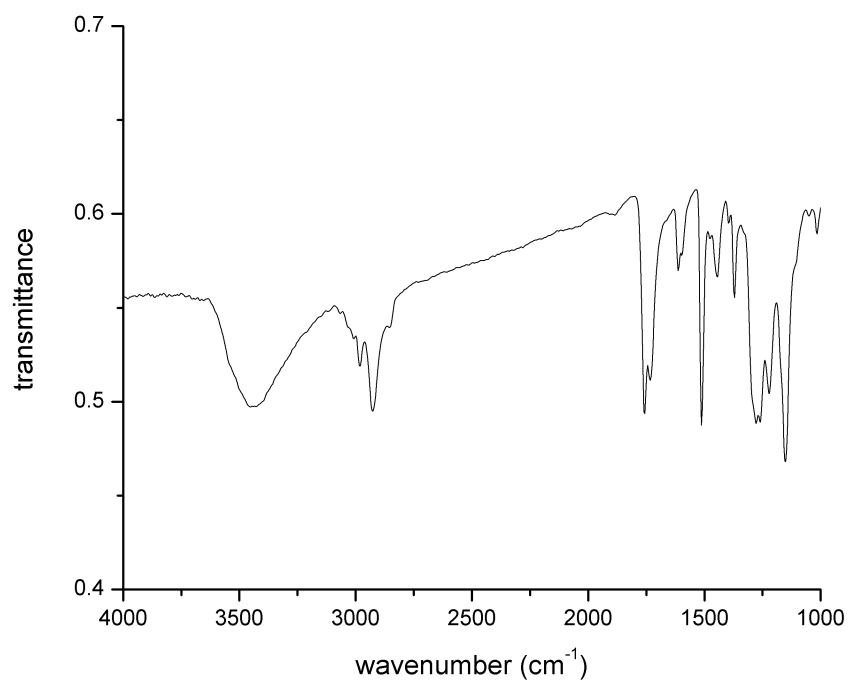


Figure 3.3. Grazing angle FT-IR spectrum of PBOCST exposed to 243 mJ cm^{-2} at 365 nm followed by development in OTS-DMTS mixture at 40°C for 3 minutes.

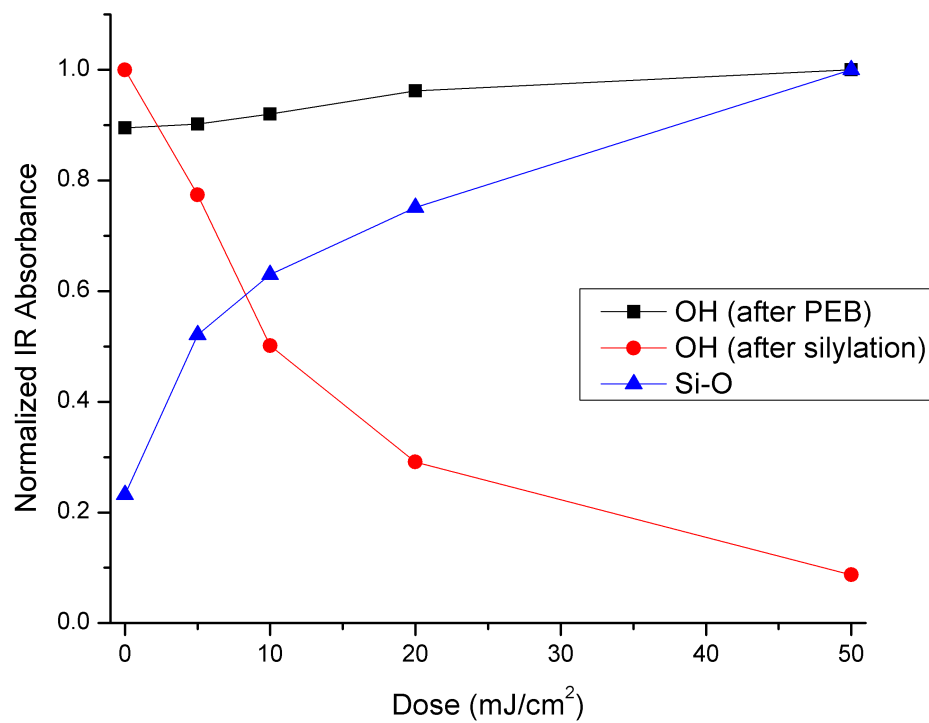


Figure 3.4. Chemical contrast curves of PBOCST after PEB and silylation (OH: 3400 cm^{-1} , Si-O: 925 cm^{-1} , using C=C aromatic stretch at 1500 cm^{-1} as reference peak).

observed with the decrease of hydroxyl groups after silylation. This shows that this process should increase the development contrast compared to the conventional water based process.

The dissolution behavior of ESCAP was also studied under similar conditions. As seen with PBOCST, the exposed and unexposed ESCAP films were not soluble in linear methyl siloxanes even at elevated temperatures. However, when the films were immersed in the mixed solvent of DMTS and OTS (1:10 by vol.), the films started to dissolve, as shown in Figure 3.2 (d). Because of the large number of phenolic hydroxyl groups in ESCAP, it is not surprising that both the exposed and unexposed films became soluble in linear methyl siloxanes with the aid of DMTS. As shown in Figure 3.2 (d), the exposed film swelled but its dissolution rate was much slower than that of the unexposed film. This phenomenon can be explained by the increased film density of the exposed ESCAP. During the acidolysis reaction of ESCAP, *tert*-butyl ester groups decomposed and released gaseous 2-butene molecules and freed acrylic acid moieties. The carboxylic acids can hydrogen bond to each other or with the phenolic hydroxyl groups in the absence of *tert*-butyl groups. These strong hydrogen bonds can lead to higher film density of the exposed ESCAP compared to the unexposed film. This effect prevents fast diffusion of DMTS in the exposed polymer film and therefore results in only partial silylation in the exposed film and slower dissolution.

To study the ability of linear methyl siloxanes to pattern thin films, UV exposure was utilized. It was found that among all the linear methyl siloxanes, OTS has shown the best patterning results. A thin film of PBOCST with NI-Tf on a Si wafer was exposed under 365 nm UV light through a photomask and

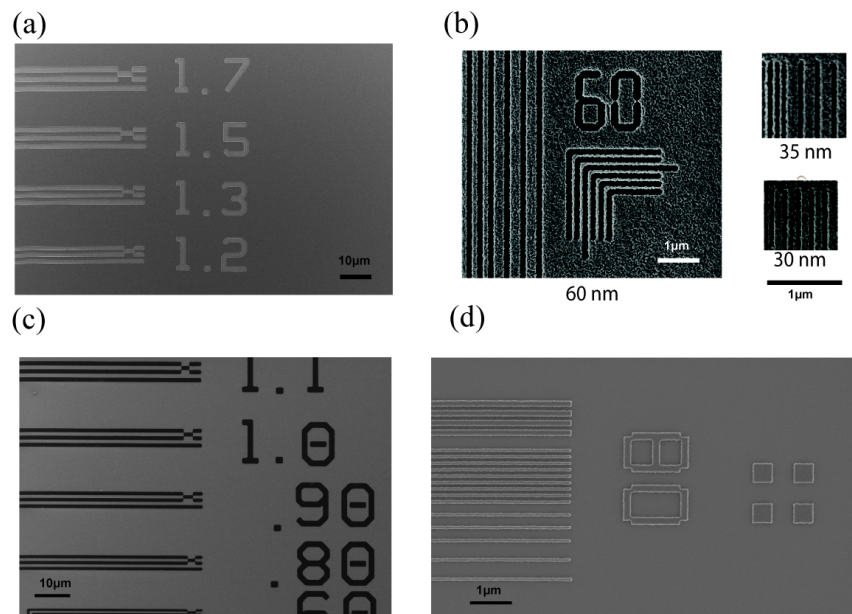


Figure 3.5. (a) PBOCST patterned using 365 nm light (dose: 50 mJ cm^{-2}) and developed in an OTS-DMTS mixture, (b) DHP-BOC patterned using e-beam (dose: $40 \text{ } \mu\text{C/cm}^2$) and developed in OTS-DMTS mixture, (c) ESCAP patterned using 365 nm light (dose: 50 mJ/cm^2) and developed in an OTS-DMTS mixture, (d) CHPB-BOC patterned using e-beam (dose: $32 \text{ } \mu\text{C/cm}^2$) and developed in OTS.

developed in linear methyl siloxane/DMTS mixed solvent and images were developed as shown in Figure 3.5 (a). As shown in Figure 3.5 (c), successful imaging was also achieved with ESCAP under 365 nm exposure. The thickness of the film after development was *ca.* 80% of the original ESCAP resist film thickness, which is in good accordance with the QCM results shown in Figure 3.2 (d).

In order to evaluate the ability of linear methyl siloxanes to reduce pattern collapse in high resolution images, the dissolution behavior and patterning capabilities of two molecular glass resists (DHP-BOC, CHPB-BOC^{22, 23}) were studied using electron beam (e-beam). Molecular glasses have drawn much attention recently because their smaller hydrodynamic volumes can enable high-resolution patterning compared to polymers under the 100 nm regime. As shown in Figure 3.5 (b), we were able to successfully pattern DHP-BOC with features as small as 30 nm by electron-beam exposure. As the thickness of the resist images was *ca.* 172.7 nm, the aspect ratio reaches as high as 5:1 without collapsing. We have also shown high-resolution patterning with CHPB-BOC and images with features as small as 80 nm were obtained as shown in Figure 3.5 (d). Because of its small molecular size, unexposed CHPB-BOC can dissolve easily in pure linear methyl siloxanes without any additive.

In order for linear methyl siloxanes to be applied to conventional solvent-based processes, it is important that they leave no residue after usage. X-ray photoelectron spectroscopic (XPS) studies (Appendix A) have been conducted and no residues were observed.

3.4 Conclusions

The increasing awareness of the environmental impact of many chemical

processing steps has led to the need for more environmentally friendly processes. In addition, in order to achieve high-resolution patterns, pattern collapse during the development process can become a severe problem as the feature size shrinks. In order to overcome both these issues, linear methyl siloxanes have been chosen as alternative solvents due to their low surface tension and environmental friendliness. In this work, we have shown a simple process to pattern thin films in linear methyl siloxanes. Two polymeric materials, ESCAP and PBOCST were patterned effectively in linear methyl siloxanes. We have also verified that linear methyl siloxanes are promising processing solvents by demonstrating high-resolution patterning with molecular glasses. We have shown patterns of CHPB-BOC with features as small as 80 nm. Because of their low surface tension, linear methyl siloxanes also have the potential to alleviate pattern collapse problems in high aspect ratio patterns and we have shown 30 nm features with approximately 5:1 aspect ratio with DHP-BOC.

REFERENCES

1. M. Poliakoff, J. M. Fitzpatrick, T. R. Farren and P. T. Anastas, *Science*, 2002, **297**, 807-810.
2. G. L. Weibel and C. K. Ober, *Microelectronic Engineering*, 2003, **65**, 145-152.
3. A. I. Cooper, *Journal of Materials Chemistry*, 2000, **10**, 207-234.
4. H. M. Woods, M. M. C. G. Silva, C. Nouvel, K. M. Shakesheff and S. M. Howdle, *Journal of Materials Chemistry*, 2004, **14**, 1663-1678.
5. L. Ionov and S. Diez, *Journal of the American Chemical Society*, 2009, **131**, 13315-13319.
6. H. Ito, R. Sooriyakumaran and E. A. Mash, *Journal of Photopolymer Science & Technology*, 1991, **4**, 319.
7. R. Sooriyakumaran, H. Ito and E. A. Mash, *Proceedings of SPIE*, 1991, p. 419.
8. Q. Lin, T. Steinhäusler, L. Simpson, M. Wilder, D. R. Medeiros, C. G. Willson, J. Havard and J. M. J. Fréchet, *Chemistry of Materials*, 1997, **9**, 1725.
9. J. M. Havard, D. Pasini, J. M. J. Fréchet, D. R. Medeiros, K. Patterson, S. Yamada and C. G. Willson, *Proceedings of SPIE*, 1998, p. 111.
10. J. M. Havard, Vladimirov. N, J. M. J. Fréchet, S. Yamada, C. G. Willson and J. D. Byers, *Macromolecules*, 1999, **32**, 86.
11. J. M. Havard, S.-Y. Shim, J. M. J. Fréchet, Q. Lin, D. R. Medeiros, C. G. Willson and J. D. Byers, *Chemistry of Materials*, 1999, **11**, 719.
12. Q. H. Lin, T. Steinhäusler, L. Simpson, M. Wilder, D. R. Medeiros, C. G. Willson, J. Havard and J. M. J. Fréchet, *Chemistry of Materials*, 1997, **9**, 1725-1730.
13. W. Noll, *Chemistry and Technology of Silicones*, Academic Press, 1968.
14. J. DeYoung, M. Wagner, C. Harbinson, M. Miles, A. E. Zweber and R. G. Carbonell, *Proceedings of SPIE*, 2006, **6153**, 615345-615341.

15. D. W. Hairston, *Chemical Engineering*, 1996, **103**, 69-&.
16. J. Sherman, B. Chin, P. D. T. Huibers, R. Garcia-Valls and T. A. Hatton, *Environmental Health Perspectives*, 1998, **106**, 253-271.
17. D. E. Williams, ACS symposium 2000.
18. R. Atkinson, *Environmental Science & Technology*, 1991, **25**, 863-866.
19. C. Y. Ouyang, J. K. Lee, M. Kryszak and C. K. Ober, *Proceedings of SPIE*, 2011, **7972**, 797200.
20. D. Brandhuber, H. Peterlik and N. Husing, *Journal of Materials Chemistry*, 2005, **15**, 3896-3902.
21. S. M. Lee, S. Matuszczak, J. M. J. Frechet, C. Lee and Y. Shachamdiamand, *Chemistry of Materials*, 1994, **6**, 1796-1802.
22. S. W. Chang, R. Ayothi, D. Bratton, D. Yang, N. Felix, H. B. Cao, H. Deng and C. K. Ober, *Journal of Materials Chemistry*, 2006, **16**, 1470-1474.
23. A. De Silva, J. K. Lee, X. Andre, N. M. Felix, H. B. Cao, H. Deng and C. K. Ober, *Chemistry of Materials*, 2008, **20**, 1606-1613.
24. W. D. Hinsberg, C. G. Willson and K. K. Kanazawa, *Journal of the Electrochemical Society*, 1986, **133**, 1448-1451.

APPENDIX A

X-ray Photoelectron Spectroscopic Study of Residual Solvents

Experimental

X-ray photoelectron spectroscopic (XPS) studies were used to detect the residues of linear methyl siloxanes after usage. In order to suppress the Si peak from the substrate (Si wafers), thick films of gold (~200nm) were sputtered on the Si wafers. Each sample was then dipped into hexamethyl siloxanes for various time lengths (5 to 100 seconds) and processed as shown in Table A.1.

Table A.1. Details of each sample

Sample Name	Immersion Time	Post-Immersion Cleaning
Sample A	0	None
Sample B	5 seconds	None
Sample C	5 seconds for 20 times	None
Sample D	5 seconds	CF ₄ plasma cleaning for 30 seconds

Sample C was immersed in hexamethyl siloxanes multiple times to get as much residues as possible in order to view the effects of residues using XPS. Sample D was cleaned using CF₄ to study the removability of residues.

Results and Discussion

Because Si can affect the etching step after development, the main purpose of this experiment is to study silicon-containing residues that remain on the surface after rinsing with linear methyl siloxanes. Au- and Si-Spectra of each sample are shown in Figure A.1-A.4.

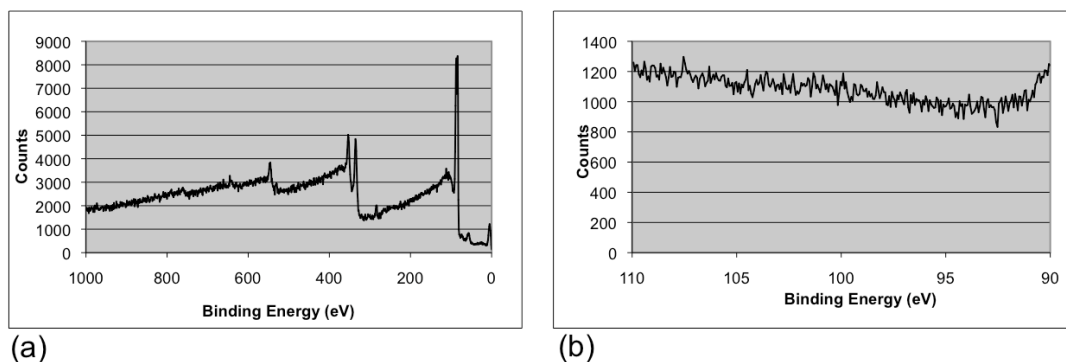


Figure A.1. (a) Au spectrum and (b) Si Spectrum of Sample A.

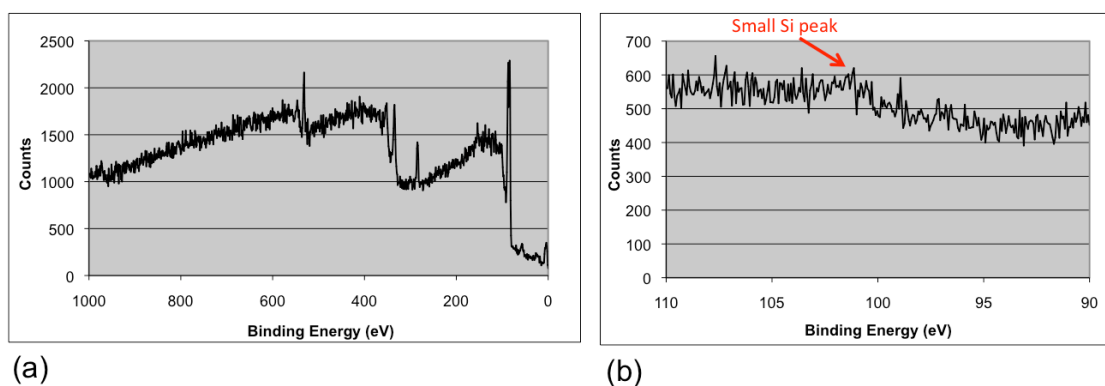


Figure A.2. (a) Au spectrum and (b) Si Spectrum of Sample B.

From Figure A.2 (a), the Au spectrum shows that there is a thin layer of material on top of the substrate when compared to Figure A.1 (a). A very weak Si peak may be seen in Figure A.2 (b) but it can also be attributed from the background noise. A stronger Si peak can be observed in Figure A.3 (b) but it still shows that the trace is negligible.

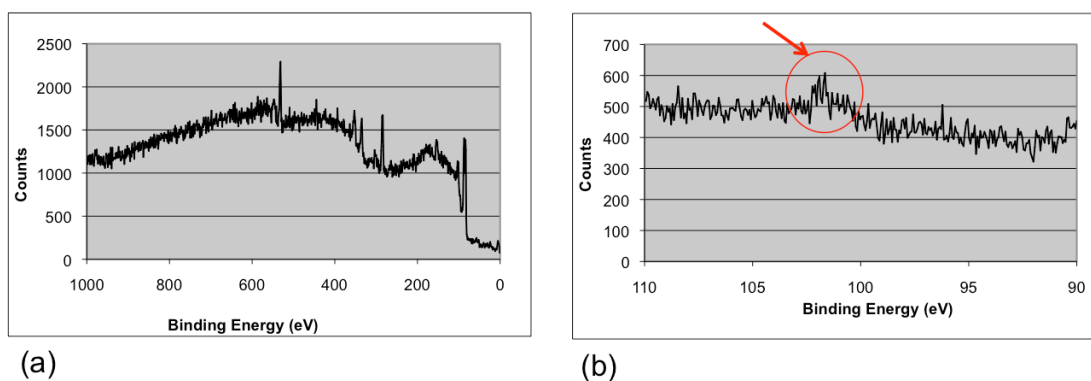


Figure A.3. (a) Au spectrum and (b) Si spectrum of Sample C

From Figure A.4, it can be shown that after a short CF_4 plasma cleaning, both the Au spectrum and the Si spectrum are almost identical (except for the F peak in Figure A.4 (a)) to the spectra of bare substrate (Figure A.1), which shows that it is very easy to remove the residues.

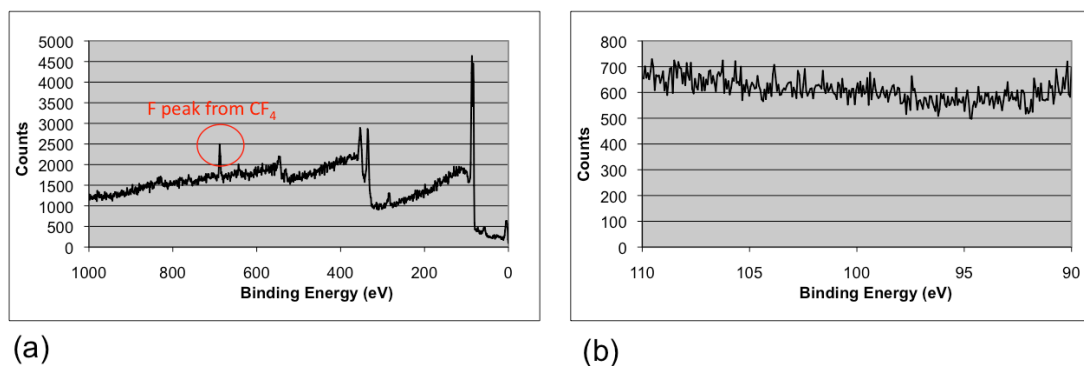


Figure A.4. (a) Au spectrum and (b) Si spectrum of Sample D

From Figure A.2 and Figure A.4, it can be concluded that the residue amount from linear methyl siloxanes is negligible as the Si peak is very weak. In addition, the residue can be easily removed by plasma cleaning as shown in Figure A.4 has spectra that are identical to Figure A.1.

CHAPTER 4

DISSOLUTION BEHAVIOR OF MOLECULAR GLASSES IN LINEAR METHYL SILOXANES

Abstract

Linear methyl siloxanes are a class of environmentally friendly solvents that can be used for many applications. However, there is little understanding about the solvating power and dissolution behavior of materials in these solvents. In order to understand the solvent characteristics of linear methyl siloxanes, three molecular glasses protected by acid-labile protecting groups have been synthesized and studied. The Hansen solubility parameters of each molecular glass were estimated and the dissolution behavior of molecular glasses in linear methyl siloxanes was studied. It was shown that the increase in polarity of these molecular glasses during deprotection could alter its solubility in these solvents. When the molecular glasses are protected by non-polar groups, they are soluble in linear methyl siloxanes because of their small sizes. As the non-polar group is removed, the solubility of molecular glasses in linear methyl siloxanes can drastically decrease and the molecule becomes insoluble. Using this solubility difference, we can further understand the patterning capability of linear methyl siloxanes by patterning thin films of these molecular glasses and high-resolution 36-nm features were demonstrated.

* This chapter was submitted to *Journal of Materials Chemistry C*

4.1 Introduction

The large amount of organic solvents used in many chemical processes has led to the need for more environmentally benign alternatives.^{1, 2} Many environmentally friendly solvents, such as water,^{3, 4} supercritical carbon dioxide (CO₂),⁵⁻¹² hydrofluoroethers^{13, 14} and linear methyl siloxanes¹⁵⁻¹⁷ have been considered for a variety of applications including cleaning, patterning, pharmaceutical and biological applications. Among them, linear methyl siloxanes are a class of silicon-based solvents that have shown several advantages over other environmentally friendly solvents due to their unique physical properties.

Since their initial application as heat-resistant polymers in the electrical industry in the 1930s, the versatility and unique properties of silicon-based materials were soon recognized and developed for many applications. Many different functional groups can be substituted for the methyl groups along the Si-O backbone and give silicones a combination of unique properties and different physical forms, making their use possible for diverse applications and fields. For example, they have been widely used in the aerospace industry due to their low and high temperature performance. Their long-term durability has made silicone sealants, adhesives and waterproof coatings in the construction industry. In addition, their outstanding biocompatibility and bio-durability have enabled them to be used frequently in health care products, pharmaceutical and medical applications. They have been shown to be excellent materials used in blood coagulation prevention, needle and syringe coatings, heart valves and aesthetic implants, to name a few.¹⁸

Among silicon-based materials, linear methyl siloxanes (LMS) are a class of non-polar solvents with low molecular weights. They are low in toxicity, not ozone-depleting, take little part in global warming,¹⁹ degrade to naturally occurring compounds^{17, 20} and can be recycled.²¹ Because of their volatile nature, they leave no

residue on a surface^{15, 17} which makes them promising processing solvents. Unlike supercritical CO₂, they do not require a high-pressure vessel and they are inexpensive. Their unique physical properties such as low surface tension and low viscosity (Table 4.1) are beneficial for cleaning surfaces and preventing pattern collapse for ultra-fine patterns.^{22,17}

Recently, there has been additional interest in patterning polymer thin films using non-polar solvents due to better pattern fidelity and patterning of polymers in linear methyl siloxanes has also been demonstrated. However, a silylation step is required to increase the solubility of polar polymers in linear methyl siloxanes.¹⁵ To improve their patterning results, is it important to understand the patterning capabilities and solvent characteristics of linear methyl siloxanes. Because of the non-polar nature of linear methyl siloxanes, non-polar materials are suitable candidates to be processed in these solvents because they are intrinsically soluble in these solvents.

Molecular glasses are small and amorphous molecules that have been used as high-resolution patterning materials.²³ Molecular glasses possess characteristic properties of small molecules such as well-defined structure, with beneficial aspects of polymers like high thermal stability and good film-forming property.²⁴ Unlike polymers, molecular glasses can be synthesized with well-defined control of molecular weight, composition and stereo-chemical factors. Because of their small sizes, non-polar molecular glasses can more readily dissolve in linear methyl siloxanes without any additives.¹⁵ In addition, altering functional groups on the core of molecular glasses can help detect subtle differences in solvent powers. We have therefore synthesized several phenolic molecular glasses with acid-labile functional groups and selected three to study the solvent power of linear methyl siloxanes. Using photolithography as a method to alter the polarity of the exposed molecular glasses, we were able to study the dissolution behavior of molecular glasses in linear methyl siloxanes. In order to

learn about the solvent power of different linear methyl siloxanes and the effect of molecular structures on the solubility of molecular glasses in linear methyl siloxanes, three linear methyl siloxanes with different molecular weights were chosen and studied with the three phenolic molecular glasses as shown in Figure 4.1.

4.2 Experimental

4.2.1 Materials

Three linear methyl siloxanes and (N,N-dimethylamino) trimethylsilane (DMTS) were purchased from Gelest and used without further purification. Trioctylamine (TOA), photoacid generators (PAGs), N-hydroxynaphthalimide triflate (NI-Tf), triphenylsulfonium perfluoro-1-butanefulfonate (TPS-Nf) and bis(4-tert-butylphenyl)iodonium perfluoro-1-butanefulfonate (Iod-Nf), were purchased from Sigma-Aldrich. C-4-Hydroxyphenyl calix[4]resorcinarene (CHPB), hexa-(3 or 4-hydroxyphenyl)benzene (HHPB), 1,3,5-tri(1,1-di(4-hydroxyphenyl)ethyl)benzene (CR15) and their fully *tert*-butoxycarbonylated (*t*-Boc)-protected molecular glass were prepared according to procedures reported in literature.²⁴

4.2.2 Lithographic Evaluation

5 wt% solutions of each molecular glass in propylene glycol methyl ether acetate (PGMEA) with NI-Tf or Iod-Nf (5 wt% with respect to molecular glass) were prepared. 0.2-0.25 wt% of TOA was added into the solutions of CR-15 and HHPB for better patterning performance. The solutions were then spin-coated onto Si wafers at 2000 rpm for 60s yielding ca. 100 nm thick films. The films were subsequently baked at 115 °C for 60s. Dose testing was performed using a GCA Autostep 200 DSW i-line Wafer Stepper ($\lambda=365$ nm, 500 mW cm²) with NI-Tf as a photoacid generator (PAG) and an ABM contact aligner ($\lambda=254$ nm, 6.54 mW cm²) with TPS-Nf as a PAG. High-resolution patterning was done using a JEOL JBX-9300FS e-beam lithography system operating at 100 kV with Iod-Nf or TPS-Nf as a PAG. Post-exposure bake (PEB) was

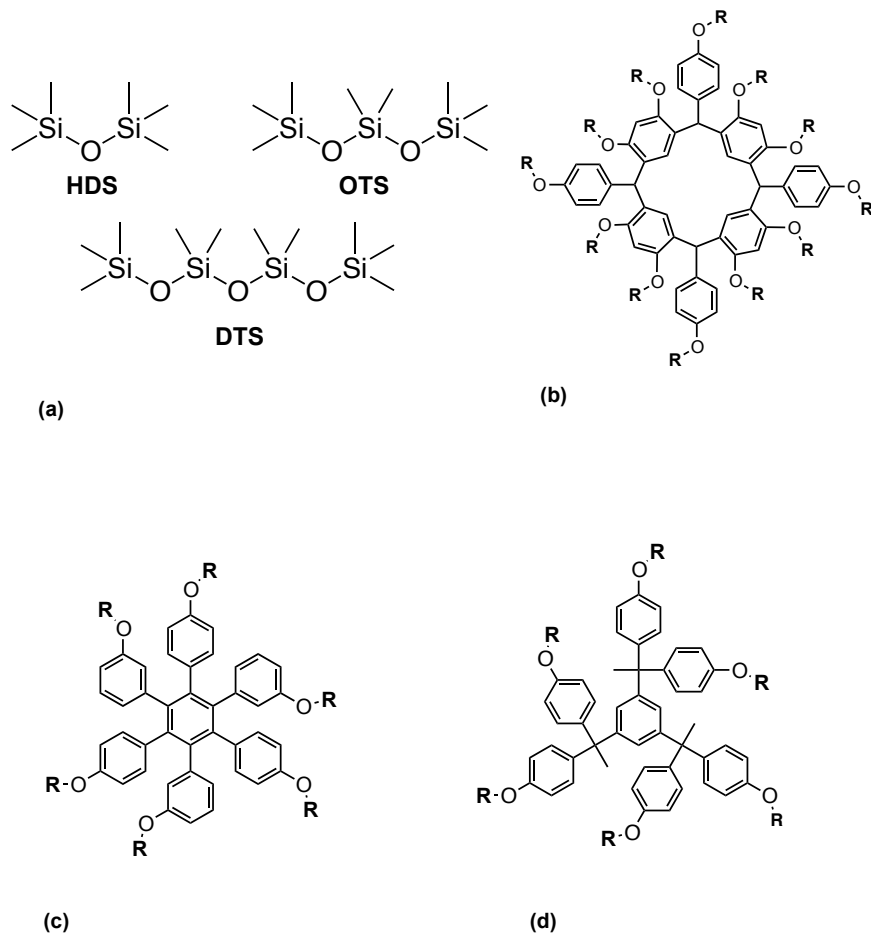


Figure 4.1. Chemical structures of (a) linear methyl siloxanes, (b) C-4-hydroxyphenyl calix[4]resorcinarene (CHPB), (c) hexa-(3 or 4-hydroxyphenyl)benzene (HHPB), and (d) 1,3,5-tri(1,1-di(4-hydroxyphenyl) ethyl)benzene (CR15) (R=H or tert-butoxycarbonyl).

performed at 115 °C for 60s. The exposed films were developed in each linear methyl siloxane at various time lengths and rinsed with linear methyl siloxanes before drying.

4.2.3 Metrology

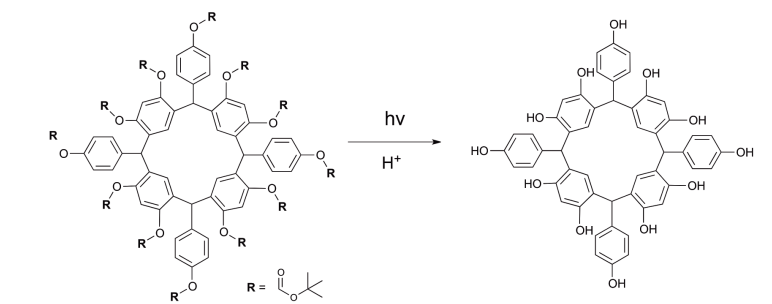
A Woollam Spectroscopic Ellipsometer was used to measure the film thickness of each molecular glass before and after pattern development. The developed images were examined using a Nikon Digital Sight D5-5M-L1 optical microscope and a Keck scanning electron microscope (SEM). Film dissolution studies were carried out by a quartz crystal microbalance (QCM) technique with a piezoelectric quartz crystal oscillator.²⁵ FT-IR was carried out using a Mattson Infinity FT-IR instrument.

4.3 Results and Discussion

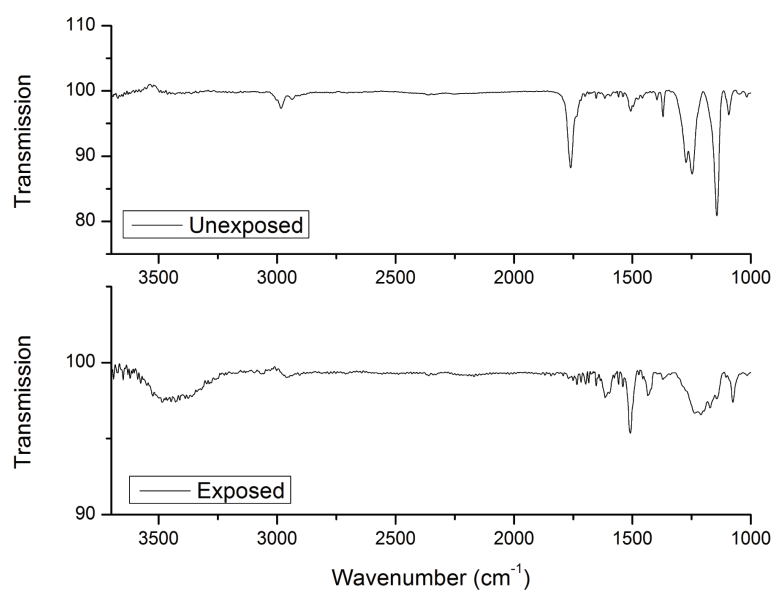
The chemical structures of linear methyl siloxanes are shown in Figure 4.1 and their physical properties presented in Table 4.1. Three molecular glasses (Figure 4.1) that have previously shown promising patterning capabilities²⁴ were synthesized to study these solvents. Upon exposure, all molecular glasses undergo structural changes from the light activated acidolysis of *tert*-butoxycarbonyl (*t*-boc) groups when acids are generated from the photoacid generator as shown in Figure 4.2(a) using CHPB as an example. The deprotection reaction can be monitored using FT-IR spectroscopy as shown in Figure 4.2(b). Figure 4.2(b) shows that when CHPB was exposed to light, the intensity of carbonyl groups ($\sim 1750\text{ cm}^{-1}$) decreased and the intensity of the OH peak (3500 cm^{-1}) increased, indicating deprotection of *t*-boc groups and generation of hydroxyl groups. The low intensity of the carbonyl peak also showed that almost all of the *t*-boc groups were effectively removed during exposure. This change of polarity of the molecular glass can therefore be used to study the solvent power of linear methyl siloxanes.

4.3.1 Hansen Solubility Parameters of Molecular Glasses

A common method to predict the solubility of a solute in a solvent is by using



(a)



(b)

Figure 4.2. (a) Chemical reactions of CHPB upon exposure, (b) FT-IR of CHPB before and after exposure.

the Hansen solubility parameters,²⁶ where the solubility is described by three different parameters related to the intermolecular forces. These forces include dispersion forces (δ_d), dipolar intermolecular forces (δ_p) and hydrogen bonds between molecules (δ_h). The three parameters can be used as co-ordinates to generate a three-dimensional Hansen space and the distance between each point in the Hansen space can determine the solubility of two substances. This distance can be represented as:

$$(R_a)^2 = 4(\delta_{d2} - \delta_{d1})^2 + (\delta_{p2} - \delta_{p1})^2 + (\delta_{h2} - \delta_{h1})^2 \quad (4.1)$$

and the closer two points are in the Hansen space, the more likely the two molecules are miscible. The Hansen solubility parameters of the three linear methyl siloxanes used in this study are shown in Table 4.2 and it can be seen that these solvents are very non-polar solvents as the Hansen parameters for both the polar and hydrogen-bonding forces are zero. Octamethyltrisiloxane has the weakest intermolecular forces among the three solvents while the other two solvents showed similar dispersion forces. Although the Hansen solubility parameters provide useful information about the solubility of a material in certain solvents, the lack of experimental Hansen parameter data can make the solubility prediction difficult for certain materials. In order to understand the solubility of these molecular glasses, a group-contribution model was therefore used to predict the Hansen solubility parameters of the molecular glasses used in this study.²⁷ This model is based solely on the molecular structure, where each molecule is described by two types of functional groups: first-order groups (UNIFAC groups) that represent the basic molecular structure and second-order groups that are based on the conjugation theory. From this model, the basic equation that gives the value of each parameter is:

Table 4.1. Physical properties of linear methyl siloxanes used in this study

Linear methyl siloxane	Molecular weight (g/mol)	Boiling point (°C)	Surface tension (mN/m)	Viscosity at 20°C (cSt)
Hexamethyldisiloxane (HDS)	162.38	99-100	15.9	0.65
Octamethyltrisiloxane (OTS)	236.53	152-3	17.4	1
Decamethyltetrasiloxane (DTS)	310.69	194-5	18.0	1.5

Table 4.2. Hansen solubility parameters of each linear methyl siloxane²⁶

Linear methyl siloxane	$\delta_d(\text{MPa}^{1/2})$	$\delta_p(\text{MPa}^{1/2})$	$\delta_h(\text{MPa}^{1/2})$
Hexamethyldisiloxane	12.4	0	0
Octamethyltrisiloxane	11.7	0	0
Decamethyltetrasiloxane	12.2	0	0

$$f(x) = \sum_i N_i C_i + W \sum_j M_j D_j \quad (4.2)$$

where C_i is the contribution of the first-order group of type i that occurs N_i times in the compound and D_j is the contribution of the second-order group of type j that occurs M_j times. $f(x)$ is a single equation of the parameter, x . The constant W is equal to 0 for compounds without second-order groups and is equal to 1 for compounds with second-order groups. The equations for estimating the Hansen parameters were developed and are represented as:

$$\delta_d = \left(\sum_i N_i C_i + W \sum_j M_j D_j + 17.3231 \right) \quad (4.3)$$

$$\delta_p = \left(\sum_i N_i C_i + W \sum_j M_j D_j + 7.3548 \right) \quad (4.4)$$

$$\delta_h = \left(\sum_i N_i C_i + W \sum_j M_j D_j + 7.9193 \right) \quad (4.5)$$

The Hansen parameters of each molecular glass were estimated and are shown in Table 4.3, detailed calculations are provided in Appendix B. In order to predict the solubility of different glasses in linear methyl siloxanes, we also calculated the distance between each molecular glass and octamethyltrisiloxane as a comparison since each linear methyl siloxane has similar values for the Hansen parameters. Hansen solubility parameters can also be plotted in a ternary plot (Teas graph), where each component is represented as a percentage of the total intermolecular forces (Teas parameters). All protected and deprotected molecular glasses as well as linear methyl siloxanes were plotted in Figure 4.3. Because linear methyl siloxanes do not have components for the dipolar and hydrogen-bonding forces, three of them are presented as one single point (LMS) in Figure 4.3. As shown in Figure 4.3 and Table 4.3, the biggest difference between the protected and deprotected molecular glasses are the hydrogen-bonding forces. Because of the strong hydrogen bonds in the deprotected

Table 4.3. Estimated Hansen solubility parameters of each molecular glass

Molecular glass	δ_d (MPa ^{1/2})	δ_p (MPa ^{1/2})	δ_h (MPa ^{1/2})	R_a (MPa ^{1/2})
CHPB	38.2	19.1	95.9	111.2
CHPB-boc	28.3	83.6	0.40	89.9
HHPB	32.9	9.30	47.2	64.1
HHPB-boc	27.9	41.5	9.10	53.5
CR-15	31.6	7.17	42.8	58.8
CR-15-boc	26.6	39.4	10.9	50.6

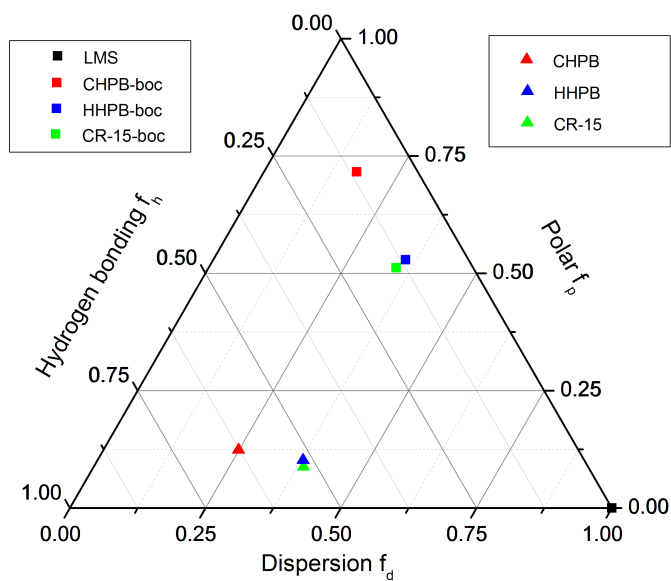


Figure 4.3. Hansen solubility parameter map of each molecular glass relative to linear methyl siloxanes.

molecular glasses, a stronger solvent is required to dissolve them. Since linear methyl siloxanes are non-polar solvents, this difference in intermolecular forces of the different areas can lead to a solubility difference between the protected and deprotected molecular glasses. From Table 4.3, we can see that the R_a of each deprotected molecular glass is larger than the R_a of each protected molecular glass, which shows that the protected form is more soluble in octamethyltrisiloxane than the deprotected form. By comparing the R_a 's of each molecular glass, CHPB-based molecular glasses possess the lowest solubility in linear methyl siloxanes while CR-15 type molecular glasses have the highest solubility. From Figure 4.3, we can also see that CR-15 and HHPB are very close to each other on the graph, which shows that they should have similar solubility in linear methyl siloxanes.

4.3.2 Dissolution Behavior of Molecular Glasses

QCM was carried out to understand the dissolution kinetics of molecular glasses in linear methyl siloxanes as shown in Figure 4.4. It can be observed that both deprotected CHPB and deprotected CR-15 showed no solubility in linear methyl siloxanes but the protected HHPB dissolved slowly in linear methyl siloxanes at a longer time compared to its deprotected counterpart. As predicted by the Hansen solubility parameters, all deprotected molecular glasses were less soluble than their protected form and CHPB did show the slowest dissolution rate compared to the other two molecular glasses. Although from Table 4.3, deprotected HHPB should be less soluble in the solvent compared to deprotected CR-15, the opposite was observed. This can be explained by its lowest molecular weight among the three molecular glasses. In contrast to the deprotected molecular glasses, all the *t*-boc protected molecular glasses dissolved in linear methyl siloxanes. From the dissolution kinetics of CR-15 and CHPB (Figure 4.4 (a) and 4(b)), a sharp change of slope of the protected molecular glasses was observed. There was also a decrease in dissolution rate of

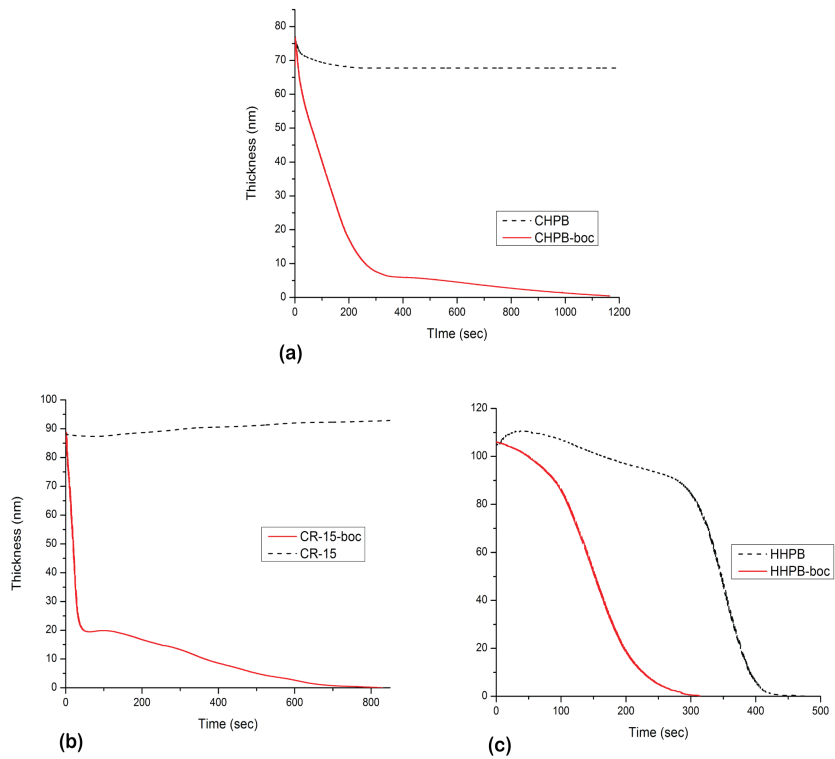
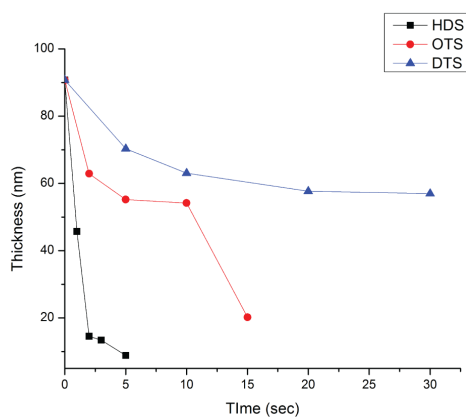


Figure 4.4. QCM study of (a) CHPB in hexamethyldisiloxane, (b) CR-15 in octamethyltrisiloxane, (c) HHPB in octamethyltrisiloxane.

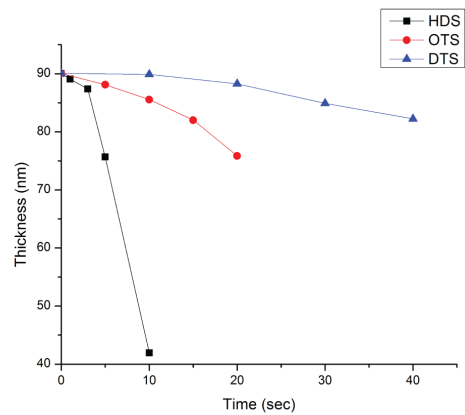
protected HHPB near the end of the dissolution process. This can be related to the fast dissolution of the molecular glasses in the solvent at initial contact, as more and more molecules dissolve into the solvents, the high concentration of solutes in the solvent decreases the solvent power and the dissolution rate decreases before complete dissolution. On the other hand, for the deprotected HHPB (Figure 4.4 (c)), the opposite behavior was seen, an increase in dissolution rate was shown at the final stage of dissolution. Because the deprotected HHPB is more polar than the unexposed molecular glasses, even though the molecule is soluble in the solvent, the solvent may be too weak to solvate the molecules at the initial stage of dissolution, as the solvent diffused into the film, the interactions of the solvent with the molecular glass can induce a small gel layer before it completely dissolves the molecular glass.

Comparing with the estimated solubility parameters and the parameter map in Table 4.3 and Figure 4.3, the solubility difference shown in Figure 4.4 between the protected and deprotected molecular glasses can be attributed to the strong hydrogen bonding between the deprotected molecular glasses. Also, as discussed earlier, indicating by the dissolution behavior of HHPB, it shows that the solubility of molecular glasses in linear methyl siloxanes is also affected by the molecular weight of the material. It is therefore important to balance the polarity and size of the molecule to provide adequate solubility when dissolving a molecule in linear methyl siloxanes.

In order to investigate the solvent power of different linear methyl siloxanes, we also studied the dissolution rate of each molecular glass in different linear methyl siloxanes. As CR-15 and CHPB showed similar dissolution kinetics, we only compared the dissolution rate of *t*-boc protected CR-15 and HHPB in different linear methyl siloxanes as shown in Figure 4.5. The dissolution rate decreases as the



(a)



(b)

Figure 4.5. Dissolution rate of *t*-boc protected (a) CR-15, (b) HHPB in three linear methyl siloxanes.

molecular weight of the linear methyl siloxane increases because it is easier for smaller solvent molecules to surround the solute and dissolve it. As shown in Table 4.3, HHPB-boc had a larger R_a compared to CR-15-boc, which indicates that it should be less soluble in linear methyl siloxanes than CR-15-boc. Figure 4.5 shows that the dissolution rate of HHPB-boc was slower than CR-15-boc, which was consistent with the estimated Hansen solubility parameters. Also, the glass transition temperature of HHPB-boc was reported to be higher than CR-15-boc,⁹ which means that there are stronger intermolecular forces presented between HHPB-boc molecules and it requires a longer time for the solvent to diffuse into the film and break the stronger intermolecular forces and hence the slower dissolution rate, which was also observed in the dissolution kinetics in Figure 4.4(c).

4.3.3 Patterning of Molecular Glasses in Linear Methyl Siloxanes

From the dissolution study of molecular glasses, it was seen that their solubility in linear methyl siloxanes can be altered by the change of polarity. Because of the insolubility of deprotected CR-15 and CHPB in linear methyl siloxanes, we can use linear methyl siloxanes to dissolve the unexposed part and pattern thin films of molecular glasses. Although deprotected HHPB still showed some solubility in these solvents, from Figure 4.4, it was shown that the dissolution rate of deprotected HHPB was much slower compared to protected HHPB and we can use this difference in dissolution rate to pattern HHPB.

In order to pattern thin films, it is important to have a high solubility contrast between the exposed and unexposed film. FT-IR spectroscopy was carried out to study the chemical contrast and dissolution contrast of molecular glasses in linear methyl siloxanes. The contrast curves of CHPB are shown in Figure 4.6. Since the dissolution rate decreases as the molecular glass becomes more polar with the generation of hydroxyl groups, we monitored the changes of the hydroxyl peak intensity (3500 cm^{-1})

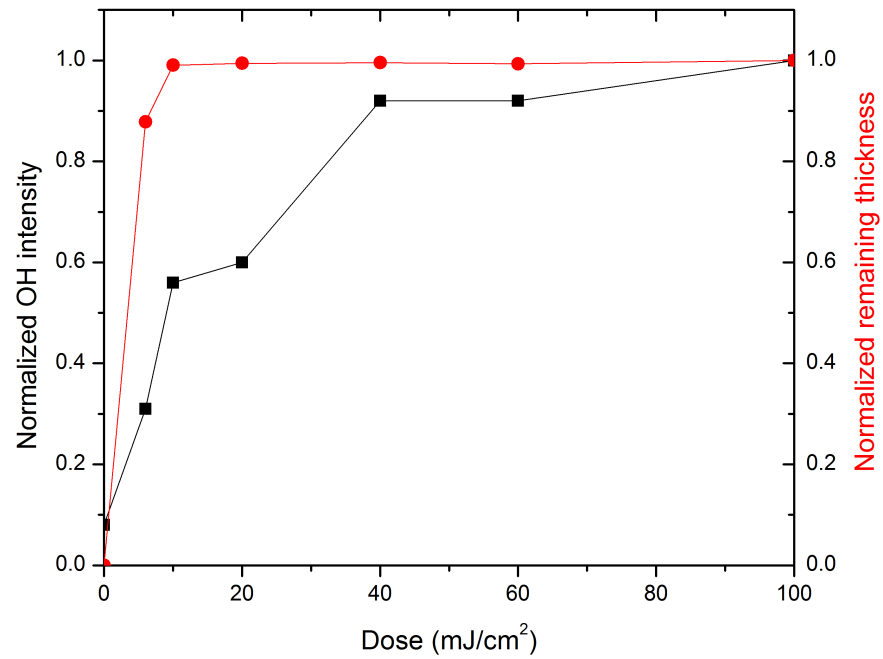


Figure 4.6. Chemical and dissolution contrast curves of CHPB in octamethyltrisiloxane.

to plot the chemical contrast curve. The film was exposed using 254-nm UV light at different doses, as seen in Figure 4.6, the hydroxyl groups can be generated at relatively low doses and the solubility of CHPB drastically changed with the deprotection of *t*-boc groups. The high dissolution contrast as shown in Figure 4.6 indicates that only a few protecting groups need to be removed to render the molecular glass insoluble which enables thin film patterning of these molecular glasses in linear methyl siloxanes.

To further understand the patterning capability of linear methyl siloxanes, e-beam lithography was utilized to generate high-resolution patterns. As shown in Figure 4.7, high-resolution patterns of each molecular glass developed in linear methyl siloxanes were successfully demonstrated. Because of the small sizes of molecular glasses, they have the potential to enable high-resolution patterning and both CR-15 and HHPB were able to generate patterns as small as 36 nm and 37 nm in linear methyl siloxanes.

4.4 Conclusions

In order to understand the solvent power of linear methyl siloxanes, the dissolution behavior of molecular glasses with acid-labile protecting groups in these solvents were studied. A group-contribution model was used to estimate the solubility of each molecular glass in linear methyl siloxanes and CR-15 was shown to be the most soluble molecular glass while CHPB showed the highest R_a among the three molecular glasses. As predicted by the Hansen solubility parameters, all *t*-boc protected molecular glasses showed high solubility in linear methyl siloxanes due to their non-polar nature. Both deprotected CHPB and CR-15 showed no solubility in linear methyl siloxanes, but deprotected HHPB showed some solubility. It can be concluded that the solubility of molecular glasses is determined by both its polarity and size. The high dissolution contrast between the exposed and unexposed molecular

glasses has also enable the possibility of patterning them in linear methyl siloxanes. High-contrast, high-resolution patterns with features as small as 36 nm were achieved.

REFERENCES

1. M. Poliakoff, J. M. Fitzpatrick, T. R. Farren and P. T. Anastas, *Science*, 2002, **297**, 807-810.
2. J. Sherman, B. Chin, P. D. T. Huibers, R. Garcia-Valls and T. A. Hatton, *Environmental Health Perspectives*, 1998, **106**, 253-271.
3. X. Chen, R. E. Palmer and A. P. G. Robinson, *Nanotechnology*, 2008, **19**.
4. J. M. Havard, S. Y. Shim, J. M. J. Frechet, Q. H. Lin, D. R. Medeiros, C. G. Willson and J. D. Byers, *Chemistry of Materials*, 1999, **11**, 719-725.
5. M. Tanaka, A. Rastogi, G. N. Toepferwein, R. A. Riggelman, N. M. Felix, J. J. de Pablo and C. K. Ober, *Chemistry of Materials*, 2009, **21**, 3125-3135.
6. N. Sundararajan, S. Yang, K. Ogino, S. Valiyaveetil, J. G. Wang, X. Y. Zhou, C. K. Ober, S. K. Obendorf and R. D. Allen, *Chemistry of Materials*, 2000, **12**, 41-48.
7. N. M. Felix, K. Tsuchiya and C. K. Ober, *Advanced Materials*, 2006, **18**, 442-446.
8. N. M. Felix, A. De Silva and C. K. Ober, *Advanced Materials*, 2008, **20**, 1303.
9. N. M. Felix, A. De Silva, C. M. Y. Luk and C. K. Ober, *Journal of Materials Chemistry*, 2007, **17**, 4598-4604.
10. N. Felix and C. K. Ober, *Chemistry of Materials*, 2008, **20**, 2932-2936.
11. G. L. Weibel and C. K. Ober, *Microelectronic Engineering*, 2003, **65**, 145-152.
12. A. I. Cooper, *J. Mater. Chem.*, 2000, **10**, 207-234.
13. J. K. Lee, H. H. Fong, A. A. Zakhidov, G. E. McCluskey, P. G. Taylor, M. Santiago-Berrios, H. D. Abruna, A. B. Holmes, G. G. Malliaras and C. K. Ober, *Macromolecules*, 2010, **43**, 1195-1198.
14. A. A. Zakhidov, J. K. Lee, J. A. DeFranco, H. H. Fong, P. G. Taylor, M. Chatzichristidi, C. K. Ober and G. G. Malliaras, *Chemical Science*, 2011, **2**,

1178-1182.

15. C. Y. Ouyang, J. K. Lee, M. E. Krysak, J. Sha and C. K. Ober, *Journal of Materials Chemistry*, 2012, **22**, 5746-5750.
16. J. F. Hobson, R. Atkinson and W. P. L. Carter, *Volatile Methylsiloxanes*, Springer-Verlag, 1997.
17. D. E. Williams, ACS symposium 2000.
18. H. Alexander, J. B. Brunski, S. L. Cooper, L. L. Hench, R. W. Hergenrother, A. S. Hoffman, J. Kohn, R. Langer, N. A. Peppas, B. D. Ratner, S. W. Shalaby, S. A. Visser and I. V. Yannas, in *Biomaterials science: An introduction to materials in medicine*, Academic Press, Inc.; Academic Press Ltd., 1996, pp. 37-130.
19. D. W. Hairston, *Chemical Engineering*, 1996, **103**, 69-&.
20. D. Graiver, K. W. Farminer and R. Narayan, *Journal of Polymers and the Environment*, 2003, **11**, 129-136.
21. W. J. Chatterton, in *IEEE International Symposium on Electrical Insulation*, 2000, pp. 412-416.
22. T. Tanaka, M. Morigami and N. Atoda, *Japanese Journal of Applied Physics Part 1-Regular Papers Short Notes & Review Papers*, 1993, **32**, 6059-6064.
23. S. W. Chang, R. Ayothi, D. Bratton, D. Yang, N. Felix, H. B. Cao, H. Deng and C. K. Ober, *Journal of Materials Chemistry*, 2006, **16**, 1470-1474.
24. A. De Silva, J. K. Lee, X. Andre, N. M. Felix, H. B. Cao, H. Deng and C. K. Ober, *Chemistry of Materials*, 2008, **20**, 1606-1613.
25. W. D. Hinsberg, C. G. Willson and K. K. Kanazawa, *Journal of the Electrochemical Society*, 1986, **133**, 1448-1451.
26. C. M. Hansen, *Hansen Solubility Parameters: A User's Handbook*, CRC Press, 2007.

27. E. Stefanis and C. Panayiotou, *International Journal of Thermophysics*, 2008, **29**, 568-585.

APPENDIX B

Calculations of Hansen Solubility Parameters for Molecular Glasses

The Hansen solubility parameters of each molecular glass can be estimated using the group-contribution method. The equations for the estimation of Hansen solubility parameters¹³¹ are the following:

$$\delta_d = \left(\sum_i N_i C_i + W \sum_j M_j D_j + 17.3231 \right) \quad (\text{B1})$$

$$\delta_p = \left(\sum_i N_i C_i + W \sum_j M_j D_j + 7.3548 \right) \quad (\text{B2})$$

$$\delta_h = \left(\sum_i N_i C_i + W \sum_j M_j D_j + 7.9193 \right) \quad (\text{B3})$$

where C_i is the contribution of the first-order group of type i that occurs N_i times in the compound and D_j is the contribution of the second-order group of type j that occurs M_j times. The constant W is 1 for molecules with second-order groups and 0 for molecules without second-order groups. The contribution of each group can be found in literature.²⁶ The detailed calculations for protected and deprotected CHPB are presented here.

CHPB(R=H)

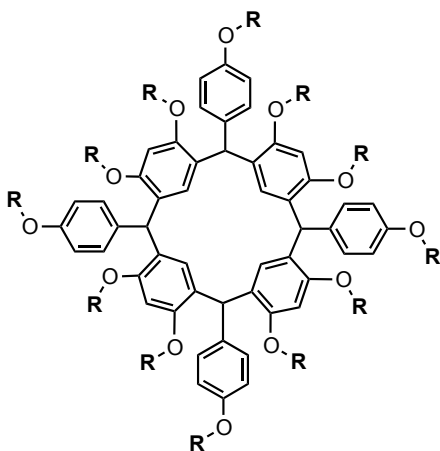


Table B.1. First-order group approximation for the prediction of the dispersion partial solubility parameter

1 st -order groups	Occurrence, N_i	Contributions, C_i	$N_i C_i$
ACOH	12	0.5288	6.3456
AC	12	0.8446	10.1352
ACH	24	0.1105	2.6520
>CH	4	0.6450	2.5800
Constant, C			17.3231
$\sum_i N_i C_i + C$			39.0359

Table B.2. Second-order group approximation for the prediction of the dispersion partial solubility parameter

2 nd -order groups	Occurrence, M_j	Contributions, D_j	$M_j D_j$
>C<OH	12	-0.0680	-0.816
$\sum_j M_j D_j$			-0.816

$$\delta_d = 38.2199 \text{ MPa}^{1/2}$$

Table B.3. First-order group approximation for the prediction of the polar partial solubility parameter

1 st -order groups	Occurrence, N_i	Contributions, C_i	$N_i C_i$
ACOH	12	1.1010	13.212
AC	12	0.6187	7.4244
ACH	24	-0.5305	-12.732
>CH	4	0.6491	2.5964
Constant, C			7.3548
$\sum_i N_i C_i + C$			17.8556

Table B.4. Second-order group approximation for the prediction of the polar partial solubility parameter

2 nd -order groups	Occurrence, M _j	Contributions, D _j	M _j D _j
>C<OH	12	0.1075	1.2900
$\sum_j M_j D_j$			1.2900

$$\delta_p = 19.1456 \text{ MPa}^{1/2}$$

Table B.5. First-order group approximation for the prediction of the hydrogen-bonding partial solubility parameter

1 st -order groups	Occurrence, N _i	Contributions, C _i	N _i C _i
ACOH	12	6.9580	83.496
AC	12	0.0084	0.1008
ACH	24	-0.4305	-10.332
>CH	4	-0.2018	-0.8072
Constant, C			7.9193
$\sum_i N_i C_i + C$			80.3769

Table B.6. Second-order group approximation for the prediction of the hydrogen-bonding partial solubility parameter

2 nd -order groups	Occurrence, M _j	Contributions, D _j	M _j D _j
>C<OH	12	1.2931	15.5172
$\sum_j M_j D_j$			15.5172

$$\delta_h = 95.8941 \text{ MPa}^{1/2}$$

R_a of CHPB and octamethylsiloxane can be calculated as:

$$(R_a)^2 = 4(\delta_{d2} - \delta_{d1})^2 + (\delta_{p2} - \delta_{p1})^2 + (\delta_{h2} - \delta_{h1})^2 \quad (\text{B4})$$

which is 111.2 MPa^{1/2}

CHPB-boc (R=tert-butoxycarbonyl)

Table B.7. First-order group approximation for the prediction of the dispersion partial solubility parameter

1 st -order groups	Occurrence, N _i	Contributions, C _i	N _i C _i
AC	24	0.8446	20.2704
ACH	24	0.1105	2.6520
-CH ₃	36	-0.9714	-34.9704
COO	12	0.2039	2.4468
>C<	12	1.2686	15.2232
>CH	4	0.6450	2.5800
O	12	0.0472	0.5664
Constant, C			17.3231
$\sum_i N_i C_i + C$			26.0915

Table B.8. Second-order group approximation for the prediction of the dispersion partial solubility parameter

2 nd -order groups	Occurrence, M _j	Contributions, D _j	M _j D _j
(CH ₃) ₃ -C-	12	-0.0738	-0.8856
AC-O-C	12	0.2568	3.0816
$\sum_j M_j D_j$			2.1960

$\delta_d = 28.2875 \text{ MPa}^{1/2}$

Table B.9. First-order group approximation for the prediction of the polar partial solubility parameter

1 st -order groups	Occurrence, N_i	Contributions, C_i	$N_i C_i$
AC	24	0.6187	14.8488
ACH	24	-0.5303	-12.7272
-CH ₃	36	-1.6448	-59.2128
COO	12	3.4637	41.5644
>C<	12	2.0838	25.0056
O	12	3.3432	40.1184
>CH	4	0.6491	2.5964
Constant, C			7.3548
$\sum_i N_i C_i + C$			59.5484

Table B.10. Second-order group approximation for the prediction of the polar partial solubility parameter

2 nd -order groups	Occurrence, M_j	Contributions, D_j	$M_j D_j$
(CH ₃) ₃ -C-	12	1.1881	14.2572
AC-O-C	12	0.8153	9.7836
$\sum_j M_j D_j$			24.0408

$$\delta_p = 83.5892 \text{ MPa}^{1/2}$$

For the hydrogen-bonding partial solubility parameter, the estimation for low δ_h was used:

$$\delta_h = \left(\sum_i N_i C_i + W \sum_j M_j D_j + 1.3720 \right) \quad (\text{B5})$$

Table B.11. First-order group approximation for the prediction of the hydrogen-bonding partial solubility parameter

1 st -order groups	Occurrence, N _i	Contributions, C _i	N _i C _i
ACH	24	0.13532	3.24768
AC	12	-0.17405	-2.0886
-CH ₃	36	0.29901	10.76436
COO	12	0.37204	4.46448
ACCH<	12	-1.44666	-17.35992
Constant, C			1.3720
δ _h			0.4000

R_a for CHPB-boc and octamethyltrisiloxane is 89.93 MPa^{1/2}

CHAPTER 5

THE ROLE OF ADDITIVES AND SOLVENTS IN PATTERNING INORGANIC METAL OXIDE NANOPARTICLES

Abstract

Inorganic metal oxide nanoparticles have drawn much attention recently due to their unique properties that are advantageous for various applications. The ability to directly pattern metal oxides through these nanoparticles has also made them a new class of patterning materials. We have synthesized inorganic metal oxide nanoparticles based on hafnium oxide (HfO_2) and zirconium oxide (ZrO_2) with organic ligands. The high sensitivity of hafnium and zirconium at the EUV (13.5 nm) wavelength has also made them promising next-generation patterning materials. As there is increasing interest in negative-tone development (NTD) due to its better performance, we have selected different solvents to study the patterning performance of these materials. The effect of different additives in the film has also been studied. It was shown that the solvent choice was an important factor for the patterning performance and 4-methyl-2-pentanol provided the best result due to its moderate solvent power for the nanoparticles and the least film thickness loss was observed. A non-ionic PAG was shown to be the best photoactive compound for patterning these nanoparticles and it also had the best film quality. High-resolution patterns down to 21.5 nm and contact hole printing down to 60 nm using EUV wavelength were achieved with ZrO_2 -MAA.

* Part of this chapter was adapted from Christine Y. Ouyang, Yeon Sook Chung, Li Li, Mark Neisser, Kyoungyong Cho, Emmanuel P. Giannelis, Christopher K. Ober, "Non-aqueous negative-tone development of inorganic metal oxide nanoparticles for next generation lithography," *Proceedings of SPIE*, 2013, 8682, 86820R

5.1 Introduction

Inorganic nanoparticles have become the interest of much research due to their unique physical, chemical,^{1, 2} biological,³⁻⁵ photoelectrochemical,⁶ optical,⁷ mechanical,⁸ electrical,⁹ magnetic⁸ properties that differ from the bulk materials. Inorganic metal oxide nanoparticles have drawn much attention due to the distinct characteristics of transition metal oxides, which make them one of the most diverse class of materials,¹⁰ They have been widely used for applications such as gas sensing¹¹⁻¹³ in biomedical components,¹⁴⁻¹⁶ solar cells,^{17, 18} holographic gratings,¹⁹ or batteries.^{20, 21} The ability to directly fabricate metal oxide patterns for various features has also led to much interest in patterning metal oxide nanoparticles.²²⁻²⁸

Lithography is the most widely used process to pattern thin films, in which a photosensitive material is deposited on a substrate and exposed to light through a mask. Photochemical reactions can occur in the exposed area of the material and change its solubility in a developing solvent which selectively dissolves either the exposed (Positive-tone development) or the unexposed (Negative-tone development) material. Traditionally, organic polymers with photo-switchable functional groups are used as patterning materials through positive-development (PTD) in an aqueous-base developer. As the smallest achievable features (or resolution) can be limited by materials, processes and light sources being used,²⁹ the continuing drive to reduce feature size has led to the need to tailor certain processes for specific feature types and develop materials for next-generation lithography using EUV and e-beam as light sources. Recently, there has been growing interest in negative-tone development (NTD) for certain feature types due to its better patterning performance and process window compared to positive-tone development (PTD).³⁰ The reason for its better performance can be related to the ease of mask design and better optical contrast provided by a bright field mask for NTD.^{31, 32} NTD has shown better performance

when printing contact holes and narrow trenches, which are generally difficult to achieve for the PTD process.³¹⁻³⁴ Traditional solvent-based NTD uses cross-linkable materials to change their solubility after exposure; however, many issues such as swelling and bridging related to the process can limit resolution.³⁵⁻³⁷ In order to study the NTD process without the issues encountered in traditional NTD methods, most work has been focused on the use of a chemically amplified system which changes the solubility of the material after exposure. This leads to higher chemical contrast and higher development contrast and promising results have been shown.^{33, 38} However, although chemically amplified systems have shown good patterning results with NTD,^{33, 39} there remain several problems,⁴⁰ largely because most chemically amplified materials are optimized as positive-tone materials using an aqueous base developer. As the polymer deprotects, thickness shrinkage can occur, which is generally not an issue for positive-tone development; however, when it is developed in a negative-tone developer, the thickness shrinkage can affect the subsequent etching step when the pattern is transferred to the substrate. As organic materials have poor etch resistance, the thickness shrinkage can lead to poor pattern transfer. In addition, because the negative-tone developer dissolves the unexposed and hydrophobic polymer while the exposed and hydrophilic polymer remains, the surface energy mismatch between the polymer and substrate can be quite big in the presence of the negative-tone developer and can therefore result in adhesion problems. Also, by using a chemically amplified system, many issues related to chemical amplification still remain, such as acid diffusion and image blur that can affect roughness and resolution.

In addition to chemically amplified polymeric materials, small molecular materials have also been a topic of recent interest due to their smaller sizes that can enable high-resolution patterning. Molecular glasses have been widely studied as potential candidates for environmentally friendly solvent-based development and

high-resolution patterning has been successfully demonstrated.^{38, 41-44} Other small cross-linkable molecular materials such as calixarene- and epoxide-based molecules have also been studied using e-beam lithography and they have shown high sensitivity and high resolution.^{45, 46} Although organic patterning materials have been the main workhorses for current technology, certain issues still need to be addressed for the next-generation lithography (e-beam, EUV). As the feature size decreases, the high aspect ratio patterns generated can lead to pattern collapse and limit the ultimate resolution.⁴⁷ Besides using low surface tension fluids to reduce the capillary forces on the resist sidewalls,³⁸ changing the materials property such as hardness^{2, 7} and etch resistance can also improve the lithographic result. Inorganic materials have become attractive candidates for next-generation lithography because of their unique properties and high-resolution patternability. Hydrogen silsesquioxane (HSQ) and its derivatives have shown high-resolution patterns down to 6-nm isolated lines and 10-nm dense lines using e-beam lithography.^{1, 3, 5, 48} Materials based on hafnium and zirconium oxide sulfates have also been developed and high-resolution patterns down to 12 nm have been shown using EUV lithography.^{49, 50} Although these inorganic materials have shown promising high-resolution patterns, their sensitivities are rather poor and require more improvement to be considered for manufacturing.

Because of the low intensity of current EUV sources, the next-generation patterning materials need to demonstrate high sensitivity and optimum absorbance. At the EUV wavelength, the composition of patterning materials will strongly affect the performance. It is therefore challenging and important to balance the transparency and absorption of a material for EUV lithography. Previously, we have synthesized inorganic metal oxide nanoparticles based on HfO_2 and ZrO_2 with organic ligands and have shown high sensitivity and dual-tone patterning capability with EUV lithography.^{25-28, 51} The metal oxide core provides not only adequate absorbance at this

wavelength but also high etch resistance which eliminates the needs for thick films as thick patterns always suffer from pattern collapse. Although high-resolution negative-tone patterning has been demonstrated with these nanoparticles, there is still little understanding of the development process and the effect of different developing solvents for the NTD performance. As more understanding is required for improving the patterning performance, we studied the effect of different additives and different negative-tone developing solvents on the patterning results for these inorganic nanoparticles.

5.2 Experimental

5.2.1 Materials

All chemicals were purchased from Sigma-Aldrich and used without further purification.

5.2.2 Nanoparticle Synthesis

Hafnium oxide nanoparticles stabilized with methacrylic acid ligands were prepared by a controlled hydrolysis reaction. Hafnium isopropoxide was dissolved in excess of methacrylic acids at 65°C followed by slow addition of a water/methacrylic acid mixture. It was reacted for 21 hours and the product was precipitated in water. It was then centrifuged at 8000g, followed by two washings in acetone. The final precipitate was dried under vacuum overnight to reveal a white powder. The same approach was used to prepare zirconium oxide nanoparticles.

5.2.3 Nanoparticle Characterization

A TA Instruments Q500 Thermogravimetric Analyzer (TGA) was used to obtain the organic content of the nanoparticles. The particle size was measured using a Malven Zetasizer Nano-ZS instrument. FT-IR was carried out using a Mattson Infinity FT-IR instrument.

5.2.4 Lithographic Evaluation

1-5 wt % of photoactive compound (photoacid generator or photoradical initiator) with 5-10 wt% of the nanoparticles were dissolved in PGMEA. Methacrylic acid was added into the solution to keep the organic constant (ca. 36 wt % for HfO₂-MAA and 50 wt% for ZrO₂-MAA). The solution was then spin-coated onto a silicon wafer at 2000 rpm for 60s and baked at 110°C for 60s. Dose testing was performed using an ABM contact aligner ($\lambda=254$ nm, 6.4 mW cm⁻²). High-resolution patterning was done using a JEOL JBX-9300FS e-beam lithography system operating at 100 kV. EUV exposures were carried out at Lawrence Berkeley National Laboratory using the SEMATECH BMET. The exposed films were developed in an organic solvent yielding negative-tone patterns. Etch studies were carried out using an Oxford 81 or a PT72 etcher.

5.2.5 Metrology

A Woollam Spectroscopic Ellipsometer was used to measure the film thickness before and after development. The developed images were examined using a Nikon Digital Sight D5-5M-L1 optical microscope and a Keck scanning electron microscope (SEM). Film dissolution studies were carried out by a quartz crystal microbalance (QCM) technique with a piezoelectric quartz crystal oscillator. A surface science instrument SSX-100 X-ray photoelectron spectroscopy (XPS) instrument was used to study the atomic composition of nanoparticles before and after etching.

5.3 Results and Discussion

5.3.1 Zirconium Oxide Nanoparticle Characterization

The schematic of the nanoparticles platform is shown in Figure 5.1. The organic content of the ZrO₂-MAA nanoparticles were measured using TGA and was calculated to be 41.7 % as indicated in Figure 5.2 (a). Dynamic light scattering (DLS) was carried out to measure the particle size; as shown in Figure 5.2 (b), the particle size is ca. 2-3 nm. Compared to previous results of HfO₂-MAA nanoparticles,²⁸ the

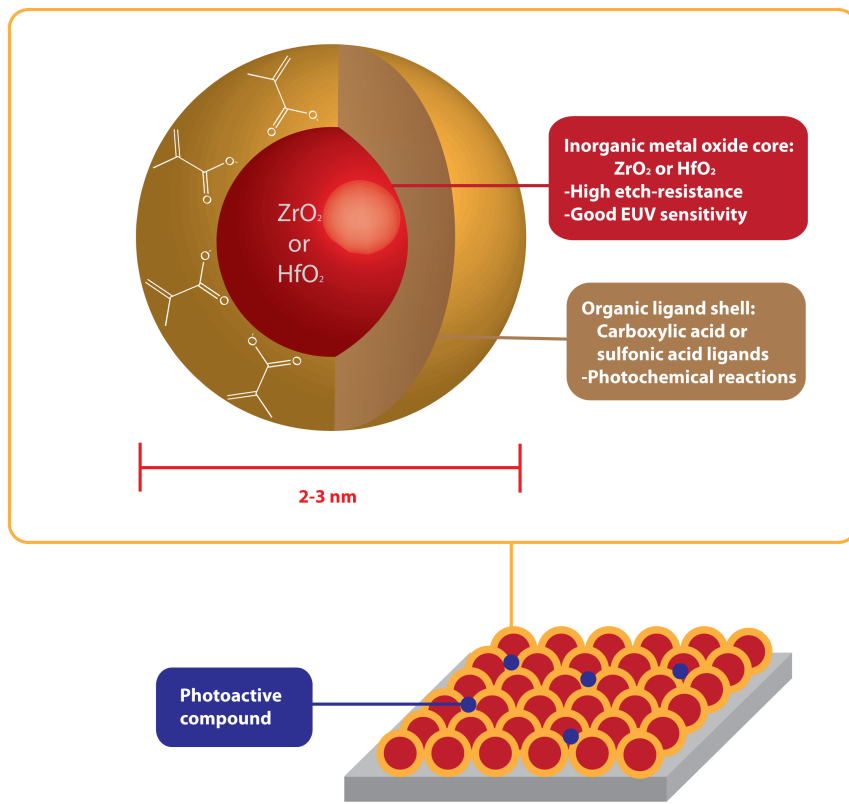


Figure 5.1. Nanoparticle resist platform.

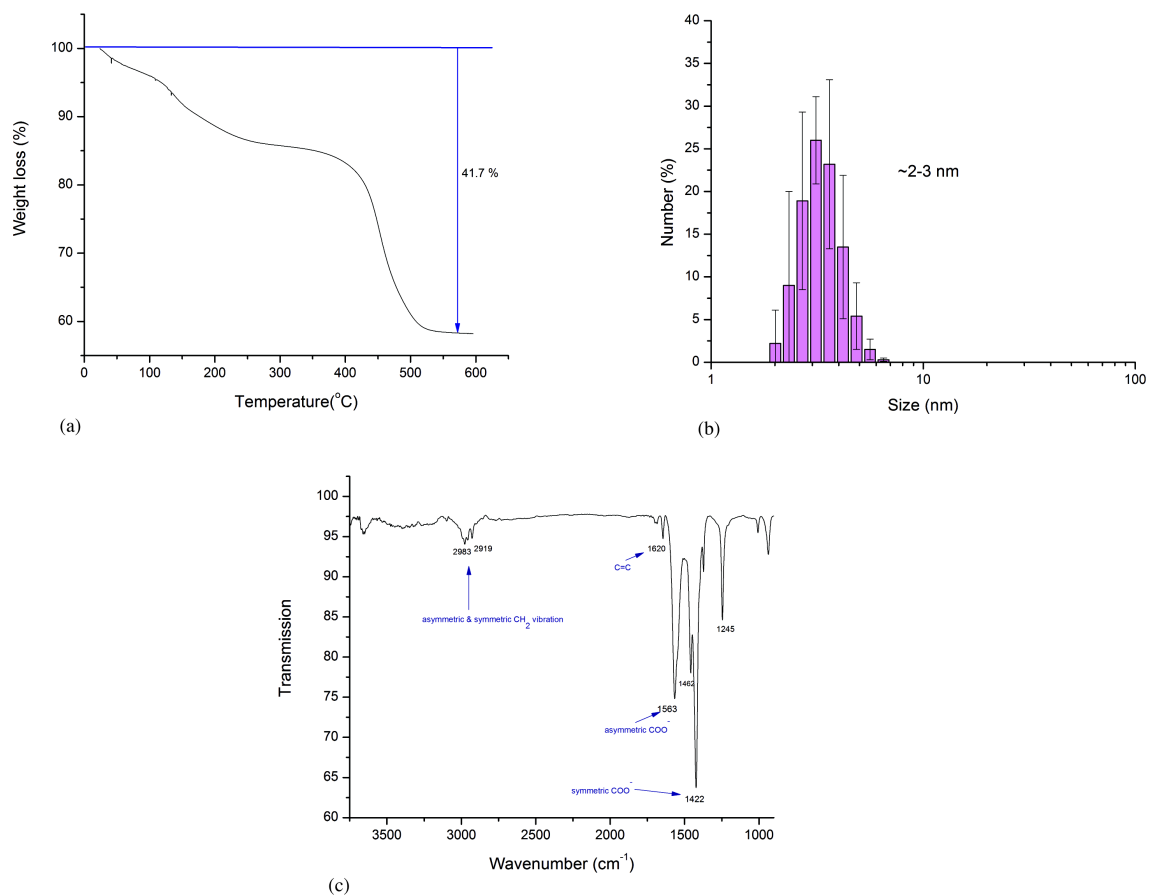


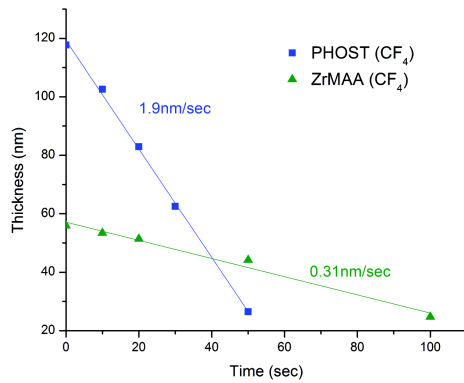
Figure 5.2. (a) TGA data of ZrO₂-MAA nanoparticles, (b) Size distribution of ZrO₂-MAA, (c) FT-IR of ZrMAA.

size of ZrO₂-MAA is smaller and the organic content is higher. In order to confirm ligand attachment, FT-IR spectroscopy was carried out to investigate the absorption peaks of different functional groups as shown in Figure 5.2 (c). Two COO⁻ binding peaks were observed at 1563 cm⁻¹ (asymmetric stretching) and 1422 cm⁻¹ (symmetric stretching); as the symmetric stretching showed a stronger peak compared to the asymmetric stretching, it showed that the MAA ligands are bidentate.

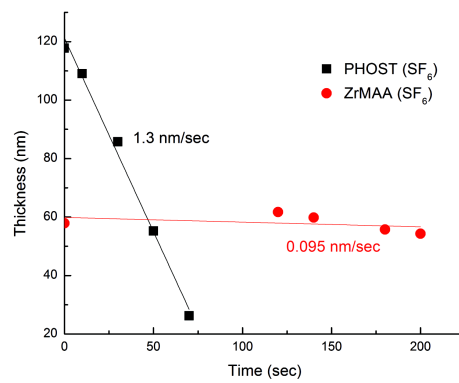
5.3.2 Etch Resistance Study

One of the advantages of using an inorganic platform is the high etch-resistance provided by its metal oxide core. Negative-tone development of chemically amplified resists leads to film shrinkage during exposure which affects the etching step and pattern transfer due to their poor etch resistance. In addition, pattern collapse, which occurs for high aspect ratio patterns, can be prevented if a thinner film is used. By using thin films of a high etch-resistant inorganic resist, pattern collapse can be eliminated while achieving good pattern transfer. Previous studies have shown the high etch resistance of HfO₂-MAA resist, and here we also studied the etch resistance of ZrO₂-MAA using CF₄ and SF₆/O₂ as etch gases. Poly(4-hydroxystyrene) (PHOST), a standard DUV photoresist was used as a comparison for the etch resistance. In order to focus on the increase of etch resistance from the metal oxide core, a 30-second oxygen plasma cleaning was applied before the etch study to remove the organics of the resist in order to see the effect of the metal oxide core. As seen in Figure 5.3, ZrO₂-MAA showed 6 times better etch resistance compared to PHOST using CF₄ as the etch gas and 14 times better etch resistance when SF₆/O₂ was used. This shows that using an inorganic core does provide higher etch resistance and eliminate the need for thick films and can mitigate pattern collapse problems which can be a problem for organic resists such as those currently used for aqueous base development.

5.3.2.1 Effect of Oxygen Plasma Cleaning Time



(a)



(b)

Figure 5.3. Etch rate comparison of ZrO₂-MAA and PHOST (a) CF₄ etching, (b) SF₆/O₂ etching.

In order to examine the effect of oxygen plasma cleaning time on the etch resistance, we studied the etch rate of ZrO₂-MAA using SF₆/O₂ with different oxygen plasma cleaning time. From Figure 5.4, it can be observed that as the cleaning time increases, the etch resistance increases, which can be related to the removal of organics during the cleaning process. X-ray photoelectron spectroscopy (XPS) was carried out to study the change of the organic/inorganic ratio with increasing oxygen plasma cleaning time. As shown in Table 5.1, the inorganic/organic ratio increases as the cleaning time increases, which in turn increases the etch resistance of the resist. Although Figure 5.4 shows that ZrO₂-MAA possesses high etch resistance even without any oxygen plasma cleaning, when the oxygen plasma cleaning is not adequate, the subsequent pattern transfer can be affected as discussed in 5.3.2.2. The XPS study shows that after oxygen plasma cleaning and 30s SF₆/O₂ etching, the organic content slightly increased which indicates some organic layer may be formed during the etching process and redeposited on the surface and affect the subsequent pattern transfer as discussed in the next section.

5.3.2.2 Pattern Transfer

For CF₄ etching, 30s plasma cleaning was sufficient to remove the organics and provide good pattern transfer as shown in Figure 5.5 (a). For SF₆/O₂ etching, as discussed in the previous section, when the oxygen plasma cleaning is 30s, the remaining organics may react with the etch gas and form an organic layer on top which leads to undercut images in Figure 5.5 (b). As we increased the cleaning time to 7 minutes, from both the top-down image and the cross-sectional image, a clean surface was observed and good pattern transfer was shown in Figure 5.5 (c). This shows that for SF₆/O₂ etching, the amount of remaining organics in the resist film can affect the pattern transfer result, and with a 7-minute long cleaning, there was no dramatic decrease in etch resistance or detrimental pattern transfer problems.

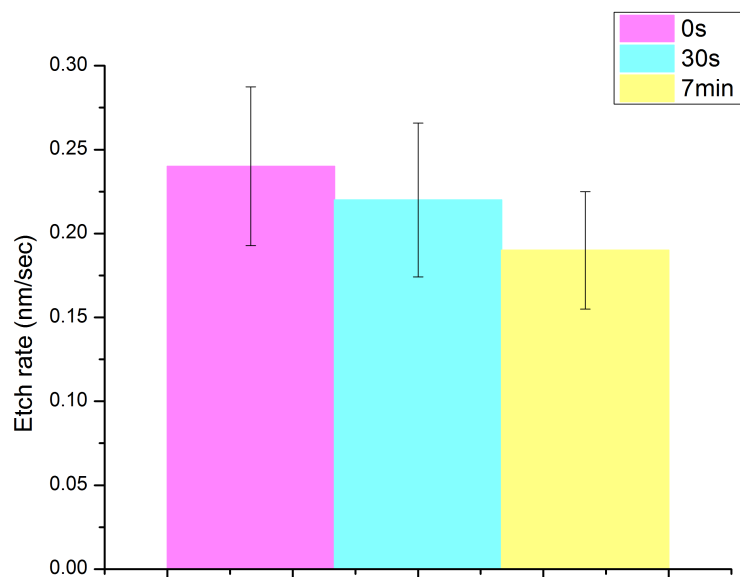
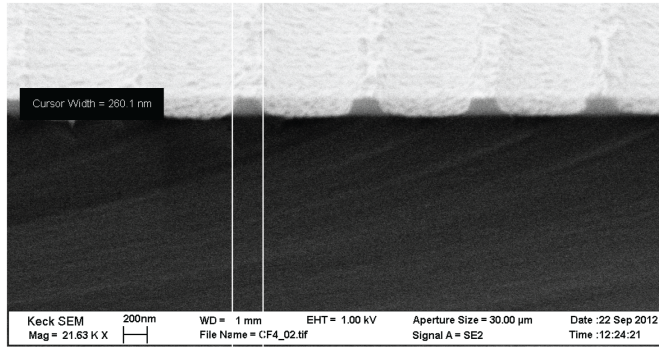


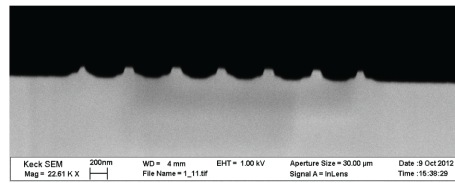
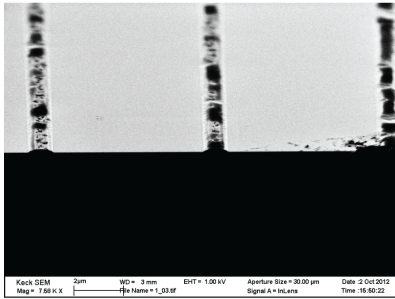
Figure 5.4. Etch rate comparison with different oxygen plasma cleaning time for ZrO₂-MAA.

Table 5.1. Organic and inorganic content of ZrO₂-MAA with different oxygen plasma cleaning time

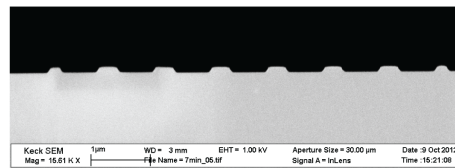
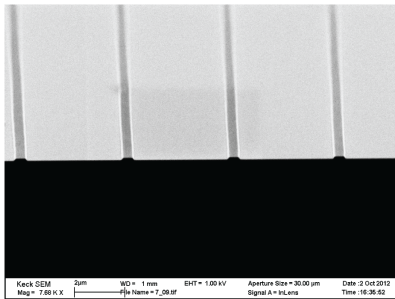
Oxygen plasma cleaning time	Inorganic	Organic
0s	49%	51%
30s	72%	28%
7min	82%	18%



(a)



(b)



(c)

Figure 5.5. Pattern transfer of ZrO_2 -MAA (a) CF_4 etching, (b) SF_6/O_2 etching with 30s O_2 cleaning, (c) SF_6/O_2 etching with 7 min O_2 cleaning.

5.3.3 Solvent-Based Negative-Tone Development

5.3.3.1 Patterning Mechanism

The resist film is composed of the nanoparticles, MAA, and a photoactive compound (photoacid generator or photoradical initiator). The chemical structures of the photoactive compounds used in this study are shown in Figure 5.6. Two types of photoactive compounds were used for patterning ZrO₂-MAA, one is a photoradical initiator and the other is a photoacid generator (PAG). The photoradical initiator chosen was dimethoxy phenyl acetophenone (DPAP) due to its high absorption at the DUV wavelength (254 nm). Three PAGs were used in this study, N-hydroxynaphthalimide (NI-Tf) is a non-ionic PAG while the other two, triphenylsulfonium triflate (TPS-tf) and triphenylsulfonium perfluoro-1-butane sulfonate (TPS-nf) are ionic PAGs. The photochemical reactions of these photoactive compounds are shown in Figure 5.7; for the ionic PAGs, only the reaction for TPS-tf was shown because the only difference between TPS-nf and TPS-tf is the perfluorinated chain length in the acid generated. When exposed to light, DPAP can generate a photoradical for cross-linking which can rearrange and form a benzoic acid. On the other hand, the photoacid generators generate a sulfonic acid upon exposure. As shown in Figure 5.8, ZrO₂-MAA nanoparticles can be negatively developed in an organic alcohol solvent using both types of photoactive compounds. The patterning mechanism is shown in Figure 5.9 with NI-Tf as the photoactive compound. When the resist film is exposed to light, because sulfonate is a stronger binding ligand compared to methacrylic acid (MAA),³⁹ the sulfonates generated from NI-Tf can exchange with the methacrylic acid (MAA) ligands and change the solubility in the developer. There may also be some loss of organic ligands during the exposure step that further reduces the solubility. As there is no dramatic change in film thickness after exposure, problems related to thickness shrinkage can be eliminated. In addition, as there is no

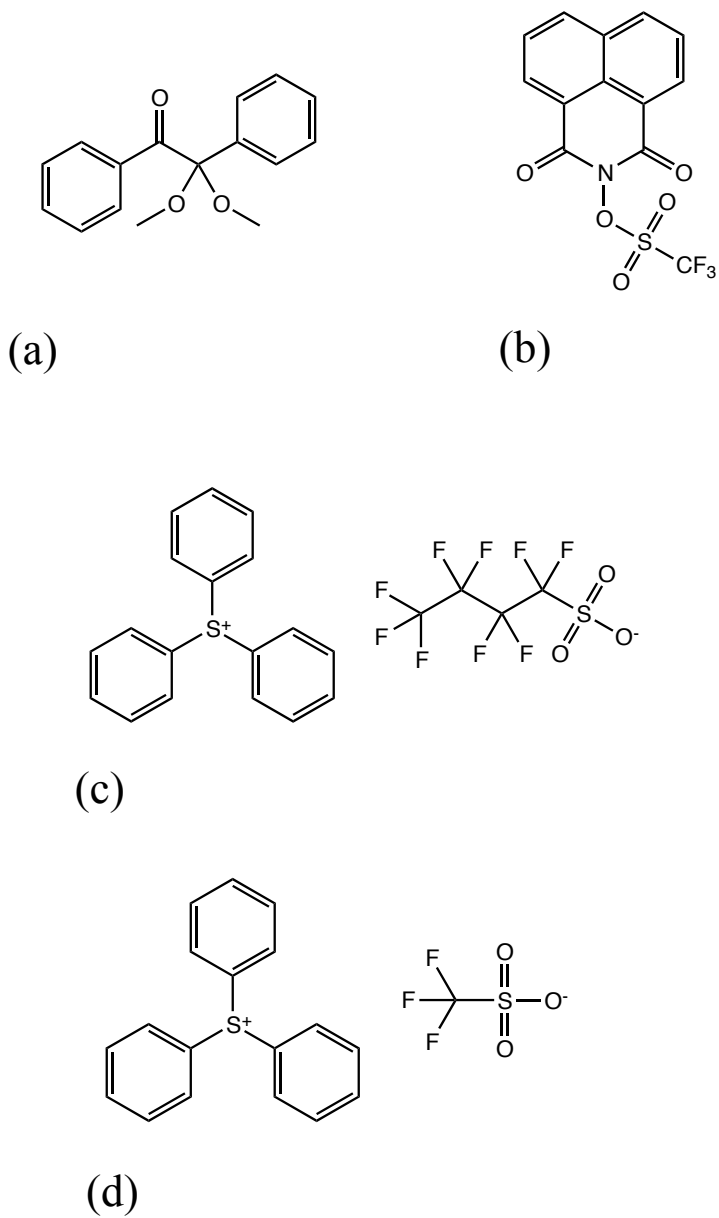
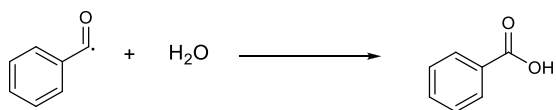
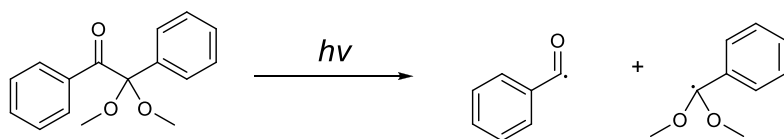
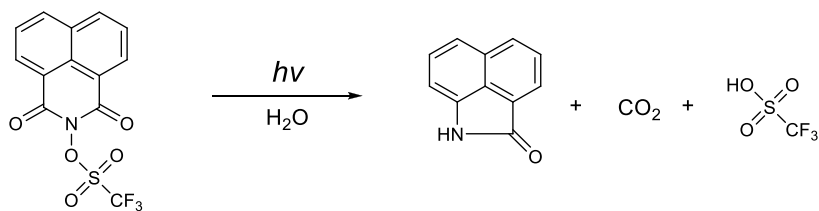


Figure 5.6. Chemical structures of photoactive compounds used in this study (a) dimethoxy phenyl acetophenone (DPAP), (b) N-hydroxynaphthalimide (NI-Tf), (c) triphenylsulfonium perfluoro-1-butane sulfonate (TPS-nf), (d) triphenylsulfonium triflate (TPS-tf).

(a)



(b)



(c)

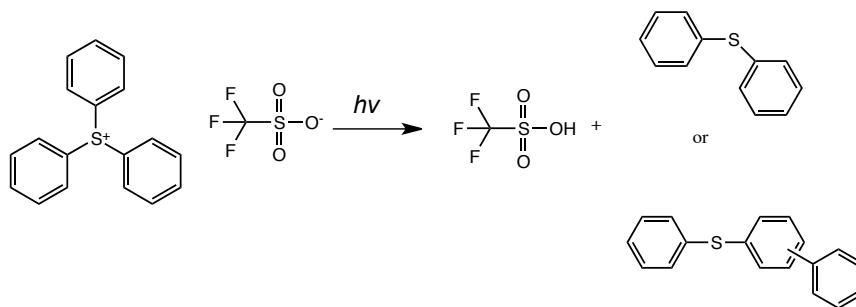
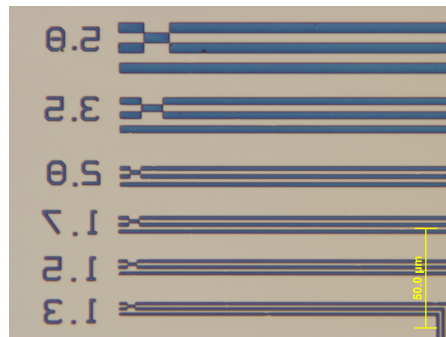
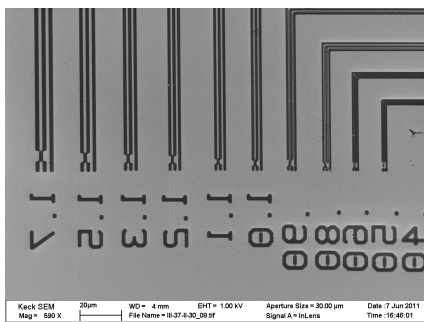


Figure 5.7. Photochemical reactions of (a) DPAP, (b) NI-Tf, (c) TPS-tf upon exposure.



(a)

(b)

Figure 5.8. DUV (254-nm) negative-tone patterns of ZrO_2 -MAA with (a) DPAP (dose: 200 mJ/cm^2 , 50 wt% MAA), (b) NI-Tf (dose: 150 mJ/cm^2 , 50 wt % MAA).

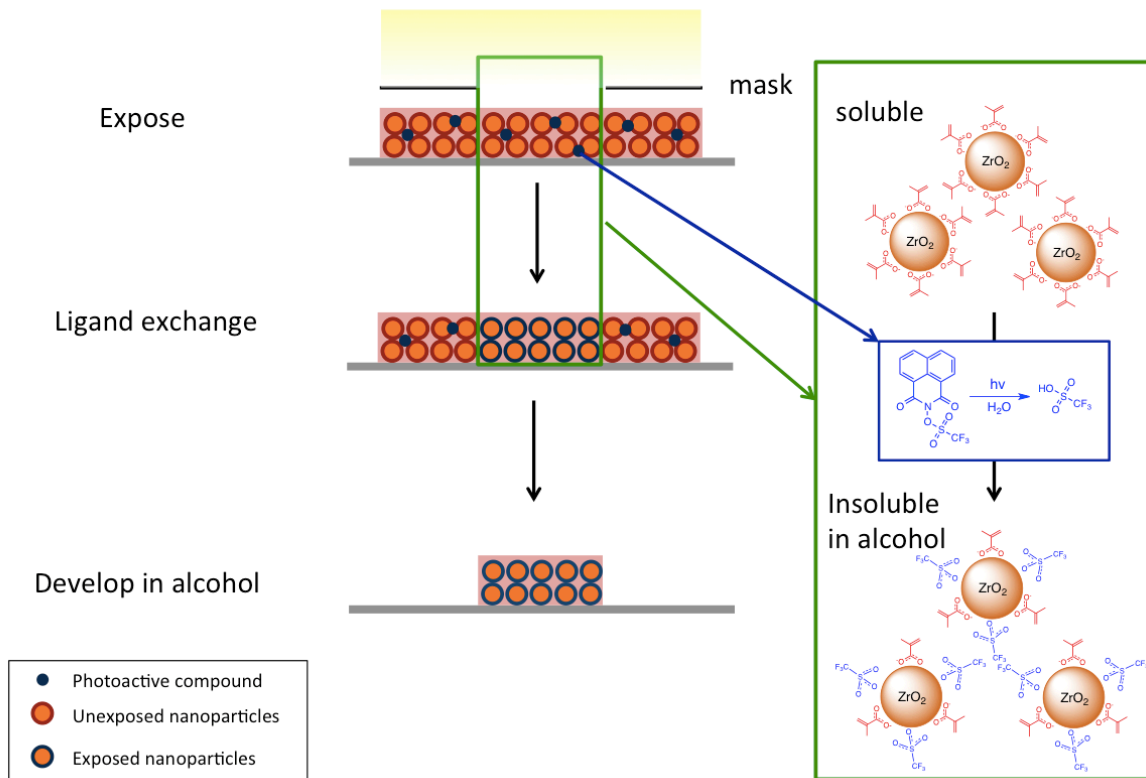


Figure 5.9. Proposed negative-tone patterning mechanism.

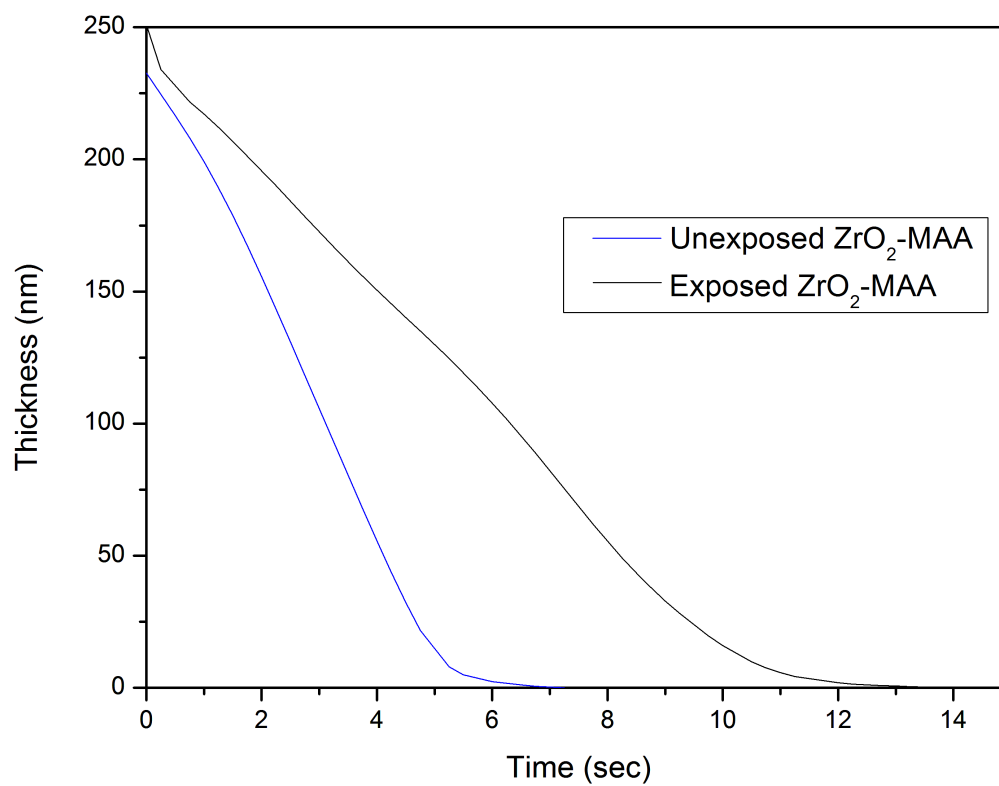


Figure 5.10. QCM of unexposed and exposed ZrO₂-MAA in 4-methyl-2-pentanol.

cross-linking reaction, issues such as resist swelling were also not observed as shown in Figure 5.10.

In order to keep the organic content constant for consistent patterning results, different amounts of methacrylic acid were added into the resist film and the results were compared. We tested samples with 40, 45, 50 and 55 wt % MAA and among them, it was found that the developed contrast for 40 and 45 wt% MAA was too low and 50 wt% MAA showed the best patterning result. In the following sections, we discuss the effect of different additives and developing solvents on patterning these inorganic nanoparticles.

5.3.3.2 Effect of Different Additives on Patterning Inorganic Nanoparticles

As shown by previous study, high-resolution patterning has been demonstrated with both HfO₂-MAA and ZrO₂-MAA using 4-methyl-2-pentanol as the developing solvent. Therefore, 4-methyl-2-pentanol was used as the developing solvent in the following sections to understand the effect of different additives on patterning inorganic metal oxide nanoparticles.

5.3.3.2.1 Effect of Photoactive Compounds

As the photoactive compounds control the photochemical reactions, the patterning results can be very different with various amounts of photoactive compounds. Two types of photoactive compounds were used, one is a photoradical initiator and the other is a photoacid generator with their photochemical reactions shown in Figure 5.7. In the following sections, both photoactive compounds and their effects on patterning are discussed.

Photoradical Initiator

0.5 wt %-2 wt % of DPAP was added into the resist solution to study its effect on patterning. The patterning results are shown in Figure 5.11 and it was observed that as the DPAP concentration increased, micro-bridging of resist lines occurred. This can

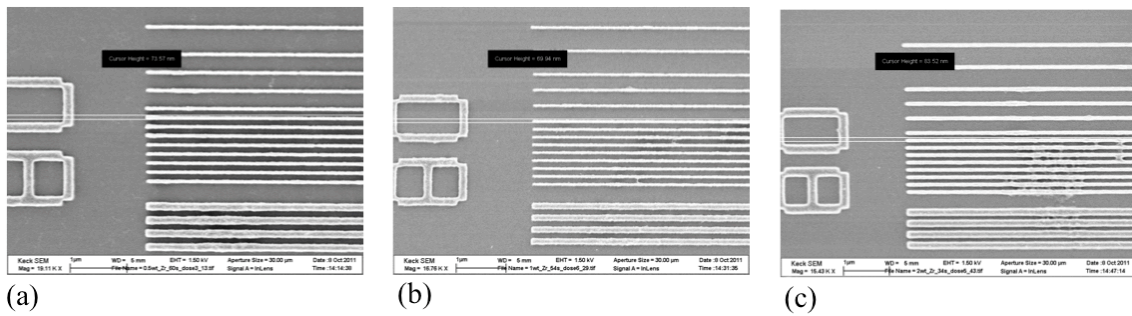


Figure 5.11. E-beam patterns of ZrO_2 -MAA with different amounts of DPAP (a) 0.5 wt % (dose: $20\mu C/cm^2$), (b) 1 wt % (dose: $20\mu C/cm^2$), (c) 2 wt % (dose: $18\mu C/cm^2$).

be related to the diffusion of generated benzoic acids into unexposed areas or the increased cross-linking of the MAA from the high amount of photoradicals generated.

To further study the patterning performance, we investigated the pattern profile using cross-sectional SEM as shown in Figure 5.12. Figure 5.12 shows that ZrO₂-MAA produced the best patterning result with 1 wt % of DPAP, which had the best cross-sectional profile.

Photoacid Generators

Three photoacid generators (PAGs) were used in this study: (i) N-hydroxynaphthalimide (NI-Tf), (ii) triphenylsulfonium perfluoro-1-butane sulfonate (TPS-nf) and (iii) triphenylsulfonium triflate (TPS-tf). NI-Tf is a non-ionic PAG while TPS-nf and TPS-tf are ionic PAGs. The dissolution rates of unexposed ZrO₂-MAA with different PAGs were studied and shown in Figure 5.13 (a). Among the three PAGs used, the non-ionic NI-Tf PAG showed the highest solubility in 4-methyl-2-pentanol compared to the ionic PAGs. The patterning results of ZrO₂-MAA with three different PAGs are shown in Figure 5.13, and it was seen that NI-Tf showed the best patterning results and both ionic PAGs showed some micro-bridging and residual materials in the background which can be attributed to the poor solubility of ionic PAGs in 4-methyl-2-pentanol compared to non-ionic PAG, as indicated by the QCM results. In order to further study the resolution of ZrO₂-MAA that can be achieved using a PAG as the photoactive compound, we used NI-Tf since it showed the best patterning performance compared to the ionic PAGs. We also compared the patterning result with using DPAP as the photoactive compound as shown in Figure 5.14. It can be observed that NI-Tf showed a much higher resolution, down to 32 nm compared to using DPAP as the photoactive compound, which was only able to achieve feature sizes down to 60 nm. The effect of PAG amounts on the dissolution rate of unexposed ZrO₂-MAA was also studied and shown in Figure 5.15. It can be seen that the

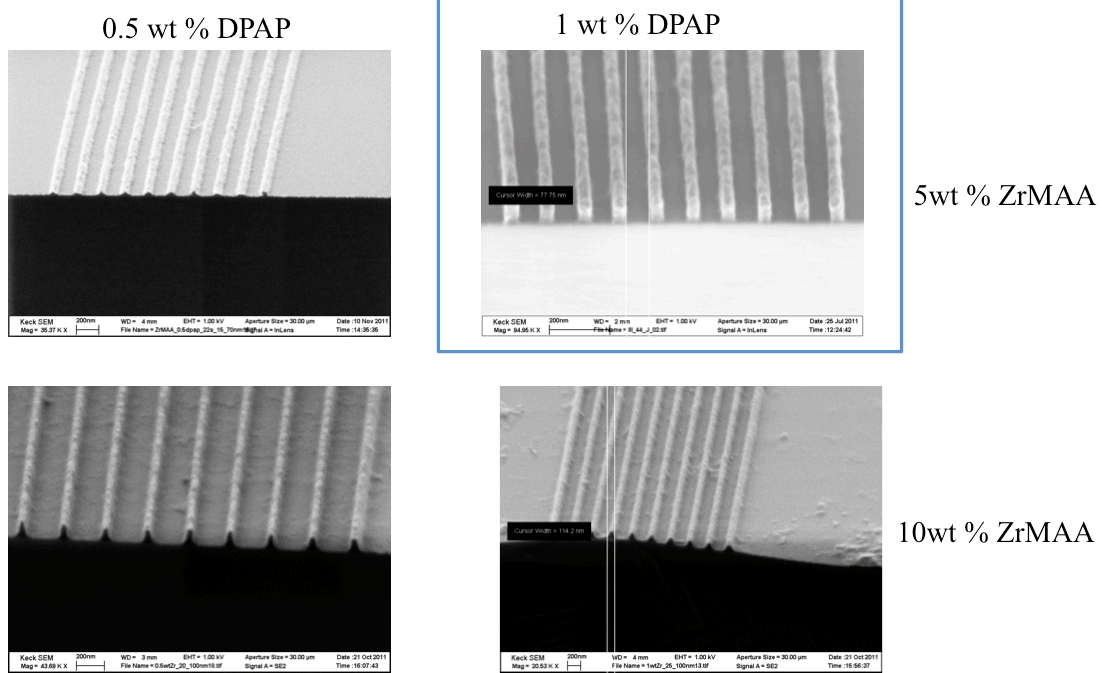
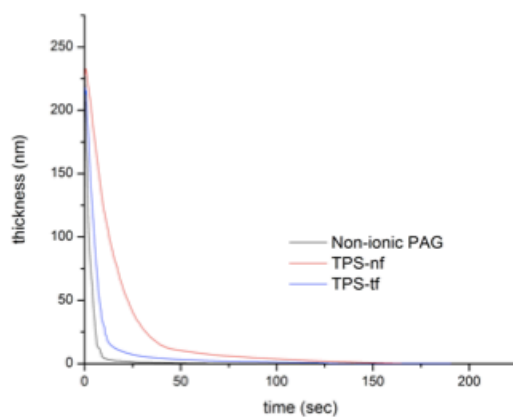
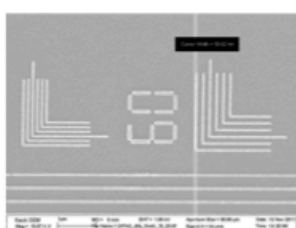


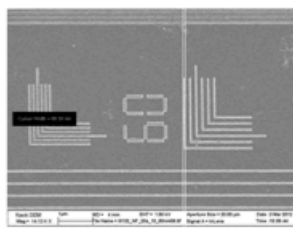
Figure 5.12. Cross-sectional SEM images of ZrO₂-MAA with different DPAP amounts.



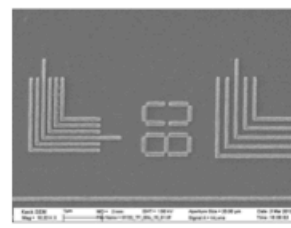
(a)



(b)

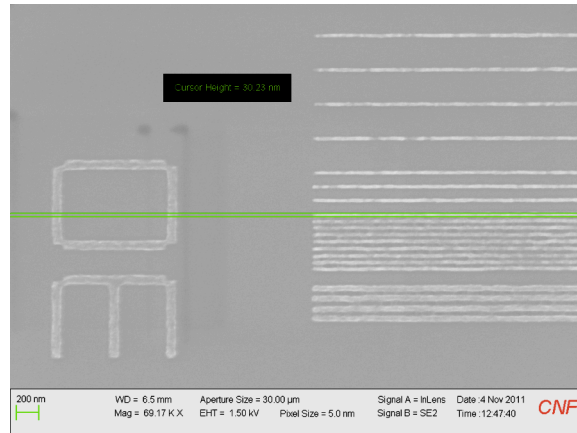


(c)

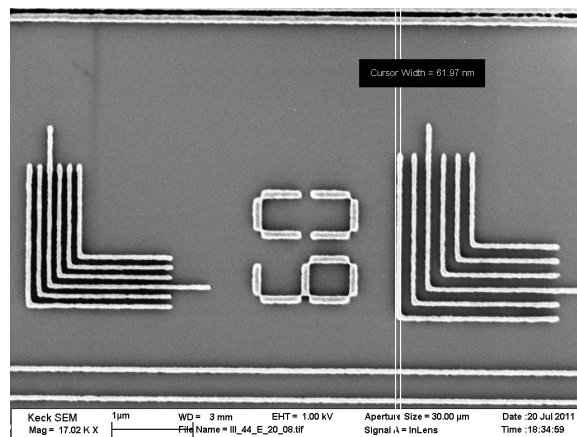


(d)

Figure 5.13. (a) QCM of unexposed ZrO_2 -MAA with 1 wt% of each PAG in 4-methyl-2-pentanol; e-beam patterns of ZrO_2 -MAA with 1 wt% of (b) NI-Tf (dose: $15\mu C/cm^2$), (c) TPS-tf (dose: $10\mu C/cm^2$), (d) TPS-nf ($15\mu C/cm^2$).



(a)



(b)

Figure 5.14. E-beam patterning of ZrO_2 -MAA with 1 wt% of (a) NI-Tf, (b) DPAP (dose: $15\mu C/cm^2$).

dissolution rate was dramatically increased with adding just 1 wt % of PAG into the resist film and increased with increasing PAG content, though the differences were small. Although higher PAG amount has shown better dissolution rate without damaging the film quality, higher PAG increases the sensitivity too much and led to overexposure and poor patterning results.

Film Quality

Besides the patterning performance, one important factor that should be considered is the effect of additives on the film quality. The effect of additives on film quality was examined and shown in Figure 5.16 and Figure 5.17. Different weight percentages of DPAP and MAA were added into the resist film for comparison in Figure 5.16. It can be seen that higher percentages of DPAP and MAA deteriorated the film quality and it is therefore important to keep the amount of additives as low as possible for better film quality. On the other hand, the amount of NI-Tf added into the resist film did not seem to have any detrimental effect on film quality as shown in Figure 5.17. As NI-Tf showed the best patterning performance and better film quality, it was therefore chosen as the photoactive compound to study the effect of different NTD solvents on patterning these nanoparticles.

5.3.3.2.2. Effect of Cross-Linkable Additives

In order to look at the role of free methacrylic acid or cross-linkable additives in the resist formulation, we also studied the effect of the addition of multifunctional acrylates. The structure of the penta-/hexafunctional acrylate is shown in Figure 5.18 (a) and the e-beam patterning results are shown in Figure 5.18 (b) and (c) with different amounts of acrylates added. As we added multifunctional acrylates, the sensitivity of the resist was increased but micro-bridging was observed, this can be resulted from the cross-linking of these acrylates. Because of the multifunctional cross-linking groups, the networked materials have a higher molecular weight

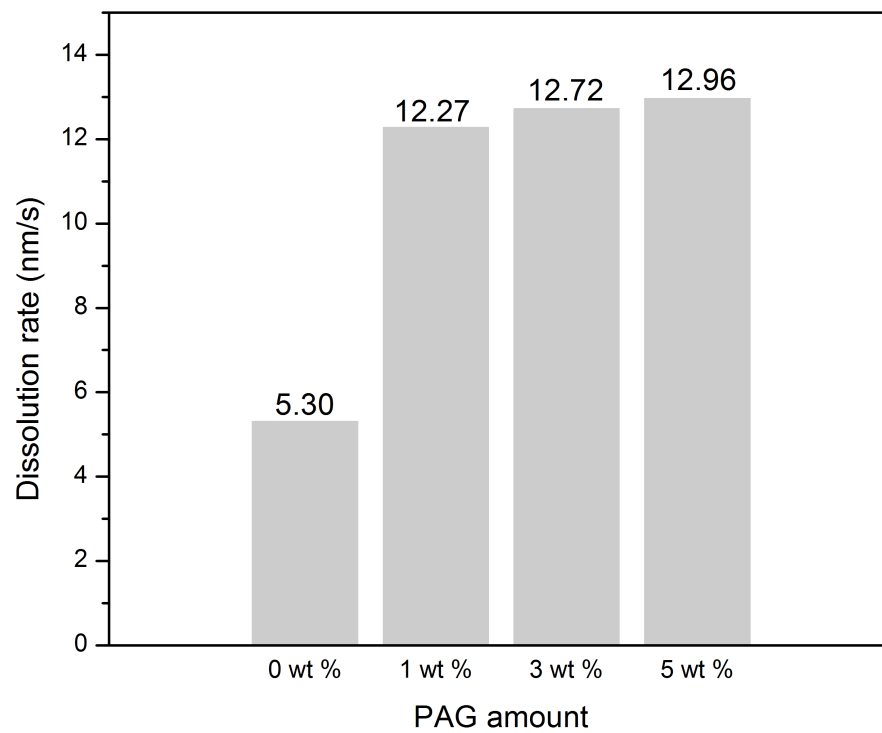
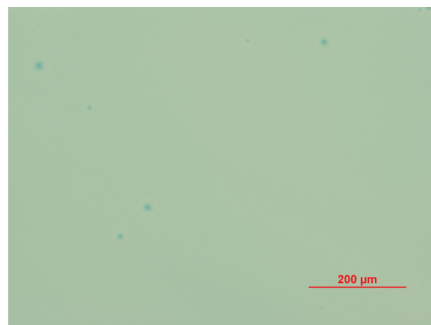
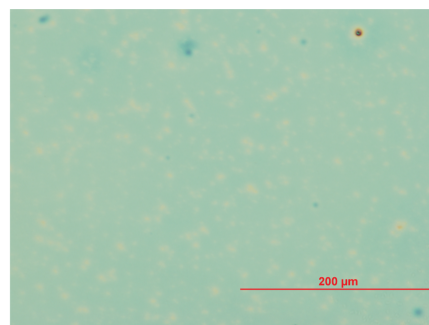


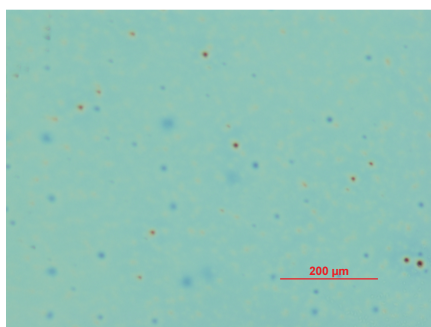
Figure 5.15. Effect of PAG content on dissolution rate in 4-methyl-2-pentanol.



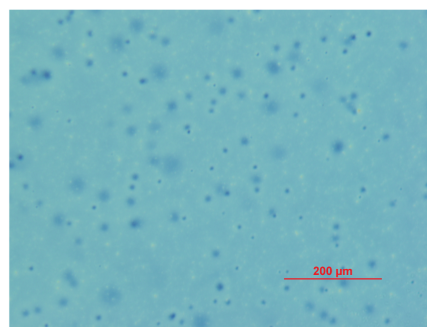
1 wt % DPAP



2 wt % DPAP



16 wt % MAA



20 wt % MAA

Figure 5.16. (top) HfO₂-MAA with different weight percentages of DPAP (bottom) HfO₂-MAA with 1 wt % of DPAP and different amounts of MAA.

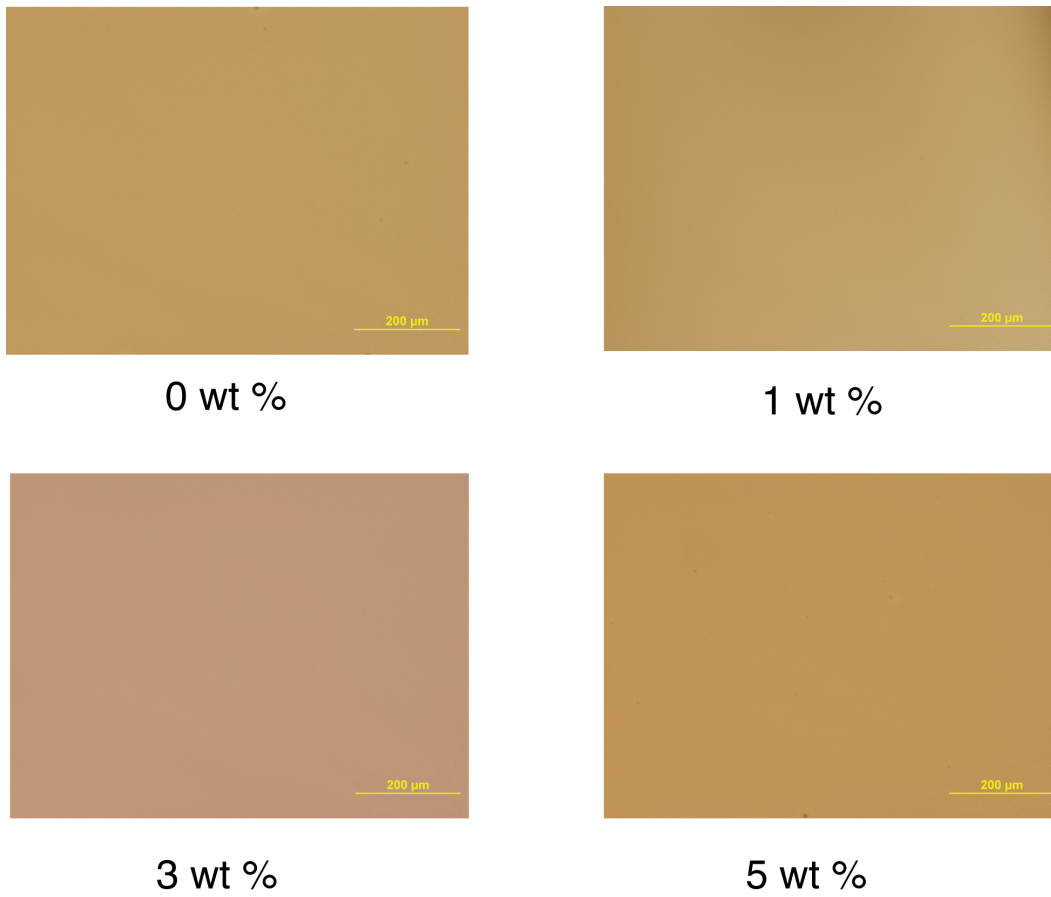
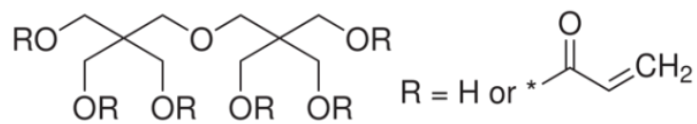
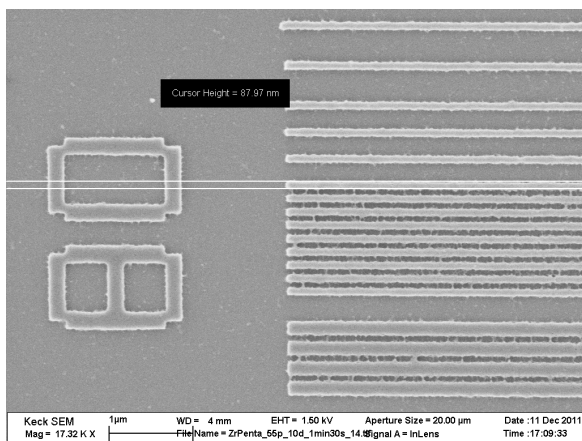


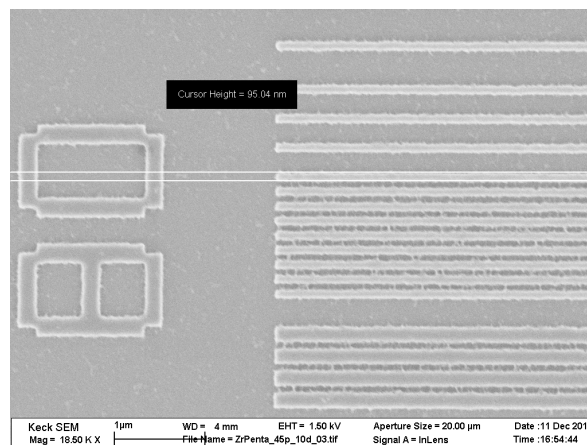
Figure 5.17. ZrO_2 -MAA with different amounts of PAG (NI-Tf) showing that increasing PAG content has no detrimental effect on film quality.



(a)



(b)



(c)

Figure 5.18. (a) Chemical structure of dipentaerythritol penta-/hexa-acrylate; E-beam patterning of ZrO_2 -MAA with 1 wt% NI-Tf and (b) 55 % of multifunctional acrylate, (c) 45 % of multifunctional acrylate (dose: $10\mu\text{C}/\text{cm}^2$).

compared to cross-linked methacrylic acid that leads to more serious micro-bridging. It is therefore undesirable to use these highly cross-linkable additives in our resist formulations.

5.3.3.3. Effect of Different Developing Solvents

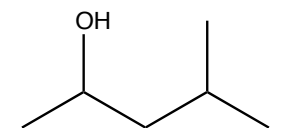
Although previous results have shown high-resolution patterning of ZrO₂-MAA and HfO₂-MAA with 4-methyl-2-pentanol, the most commonly used NTD solvents are acetate- or ketone- based solvents. In addition, most NTD studies focus on the use of chemically amplified organic polymers⁵² and there are few reported studies of the dissolution behavior of inorganic patterning materials in different NTD solvents. Besides better performance provided by a bright-field mask used in NTD, NTD solvents also have lower surface tension compared to aqueous base developers as shown in Table 5.2, which can mitigate pattern collapse problems seen in high aspect ratio patterns. As the NTD performance can be affected by the developing solvents,^{30, 53, 54} studying the behavior of inorganic nanoparticle resists in different developing solvents can provide more understanding of the development mechanism and provides information for performance enhancement. Five conventional NTD solvents were chosen for the study, o-xylene, propylene glycol methyl ether acetate (PGMEA), n-butyl acetate, 2-butanone and 2-heptanone with their chemical structures shown in Figure 5.19.

Dissolution Rate Study of NTD Solvents

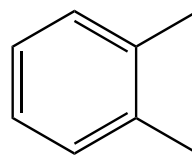
The dissolution rate of unexposed (R_{\max}) and exposed (R_{\min}) ZrO₂-MAA in each solvent was measured and presented in Table 5.3. The nanoparticles were highly soluble in acetate- and ketone-based solvents which can be related to the higher polarity of these solvents. On the other hand, the unexposed nanoparticles showed moderate dissolution in 4-methyl-2-pentanol and o-xylene. Because of the high solubility of unexposed ZrO₂-MAA in acetate- and ketone-based developers, QCM

Table 5.2. Surface tension of the NTD solvents

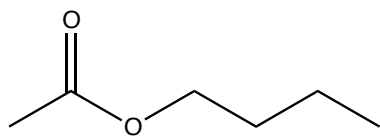
Solvent	Surface tension (dynes/cm)
4-methyl-2-pentanol	23.0
PGMEA	26.9
2-heptanone	24.9
o-xylene	30.1
2-butanone	23.9
n-butyl acetate	25.3



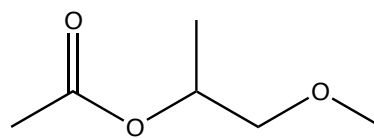
4-methyl-2-pentanol



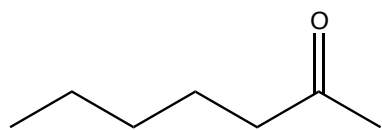
o-xylene



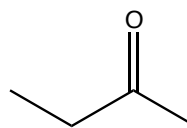
n-butyl acetate



PGMEA



2-heptanone



2-butanone

Figure 5.19. Developing solvents used in this study.

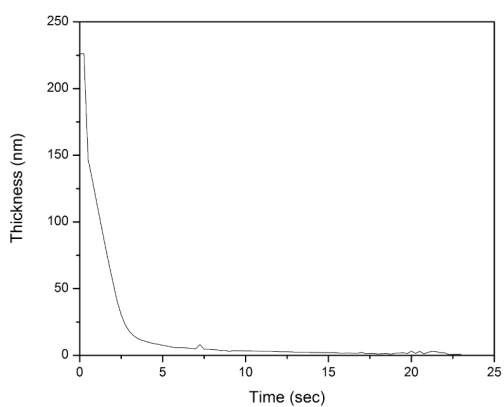
could not be used to monitor the film thickness changes at such fast rates. However, we were able to study the dissolution kinetics of ZrO₂-MAA in 4-methyl-2-pentanol and o-xylene as shown in Figure 5.20. In that figure, unexposed ZrO₂-MAA showed a much faster dissolution rate in 4-methyl-2-pentanol compared to o-xylene that can be attributed to the higher polarity of 4-methyl-2-pentanol and both showed uniform dissolution rates. Table 5.3 shows that exposed nanoparticles were less soluble compared to unexposed nanoparticles which can enable negative-tone patterning. R_{\max}/R_{\min} , which is generally a good indicator of the development contrast, was also calculated for each solvent and presented in Table 5.3. 2-butanone and n-butyl acetate showed the worst R_{\max}/R_{\min} values in the table which can lead to poor patterning results. The dissolution rate study shows that both the polarity and size of the developers play important roles, in general, both exposed and unexposed ZrO₂-MAA shows higher solubility in more polar solvents. For unexposed nanoparticles, the higher the solvent polarity, the higher the dissolution rate is. However, although some polarity is required to dissolve the nanoparticles, too high of a polarity can lead to very high dissolution of both exposed and unexposed nanoparticles, which is undesirable for high development contrast. For the exposed nanoparticles, besides the polarity of developing solvents, the solvent size and favored interactions with the nanoparticles can also affect the dissolution rate. Although PGMEA is more polar than n-butyl acetate, a higher dissolution rate was observed for n-butyl acetate due to its smaller size. Also, despite having a higher polarity than PGMEA and n-butyl acetate, 2-heptanone showed the slowest dissolution rate for exposed ZrO₂-MAA among the three, which can be related to some favored interactions of acetate solvents with the nanoparticles.

E-beam patterning results with different NTD solvents

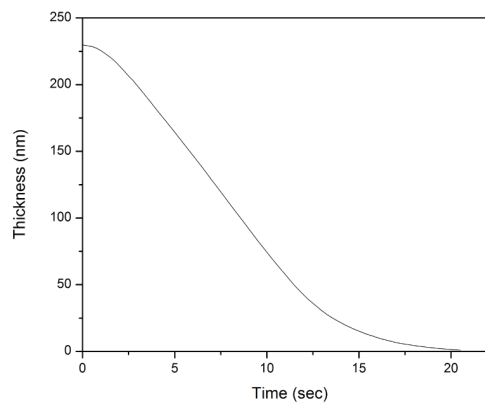
To examine the patterning capability of different NTD solvents, the optimized

Table 5.3. Dissolution rate of unexposed (R_{\max}) and exposed (R_{\min}) ZrO_2 -MAA in different developing solvents

Solvent	R_{\max} (nm/s)	R_{\min} (nm/s)	R_{\max}/R_{\min}
4-methyl-2-pentanol	11.35	0.085	133.53
o-xylene	10.09	0.062	162.74
PGMEA	> 60	0.74	> 81.08
2-heptanone	> 60	0.38	> 157.89
2-butanone	> 60	4.73	> 12.68
n-butyl acetate	> 60	2.15	> 27.91



(a)



(b)

Figure 5.20. QCM of unexposed ZrO₂-MAA in (a) 4-methyl-2-pentanol, (b) o-xylene.

CD Developer	100nm	80nm	60nm	50nm	45nm	35nm
4-methyl-2-pentanol (25 μ C/cm ²)						
o-xylene (30 μ C/cm ²)						
PGMEA (60 μ C/cm ²)						
2-butanone (60 μ C/cm ²)						
2-heptanone (60 μ C/cm ²)						
N-butyl acetate (60 μ C/cm ²)						

Figure 5.21. E-beam Patterning results of ZrO₂-MAA with 1 wt % PAG in different NTD developers.

resist formulations from 5.3.3.2 was used. As shown in Figure 5.21, 4-methyl-2-pentanol showed the best development contrast compared to all the NTD solvents. O-xylene showed high contrast patterns even though some bridging was observed at higher resolution patterns. For the acetate- and ketone-based developers, it was seen that PGMEA and 2-heptanone showed the best patterning results with 1 wt % PAG (NI-Tf). Higher doses were required for acetate- and ketone- based solvents due to the high solubility of nanoparticles in these solvents, more ligand exchanges were required to have dramatic decreases in solubility. As discussed in the preceding section, the poor development contrast of 2-butanone and n-butyl acetate can be related to the high dissolution rate of exposed ZrO_2 -MAA in these solvents and the poor R_{max}/R_{min} values in Table 5.3. In order to investigate the effect of PAG amount on the patterning results, the amount of PAG was increased to 5 wt % as shown in Figure 5.22. For 4-methyl-2-pentanol, similar patterning results were seen, but the contrast decreased, which can be attributed to the increased dissolution of exposed area from the higher PAG amount. Figure 5.22 shows that the patterning results were improved for o-xylene, ketone-, and acetate-based solvents, but higher doses were required for acetate- and ketone-based solvents. As discussed previously, higher PAG content can lead to higher dissolution rate, which means that the balance between exposed and unexposed PAG in the resist film can be important when determining the solubility of the exposed area in the developing solvent and the patterning results. Higher amounts of unexposed PAG remaining in the film can lead to dissolution of both exposed and unexposed area and deteriorated the patterns. As higher doses were required for printing the lines with the correct sizes for acetate- and ketone-based solvents when 5 wt% PAG was used, more MAA ligands can be exchanged and led to higher contrasts compared to 1 wt % PAG. For o-xylene, a lower dose was used for 5 wt % PAG and bridging was observed when higher doses were used, the higher

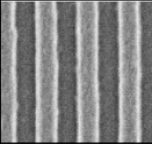
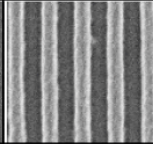
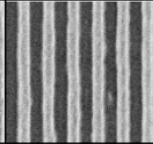
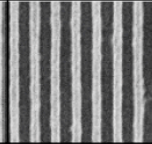
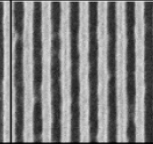
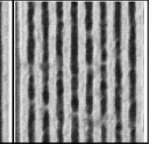
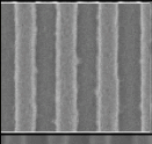
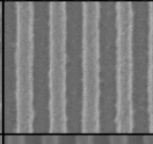
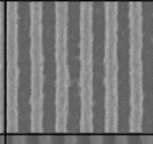
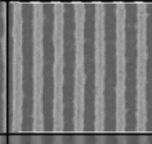
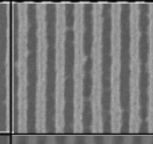
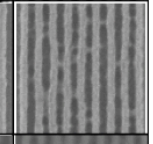
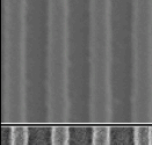
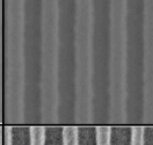
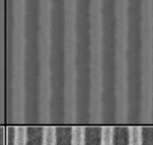
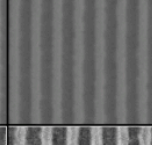
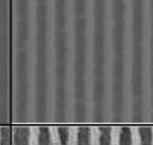
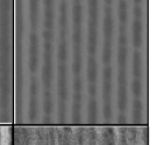
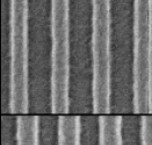
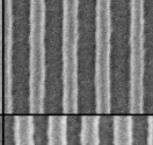
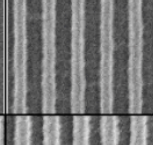
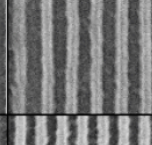
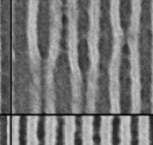
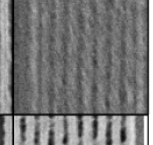
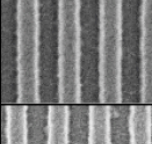
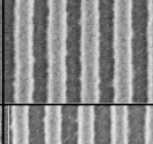
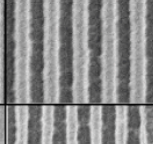
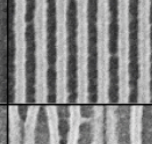
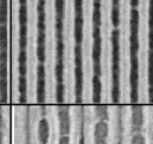
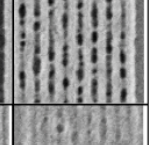
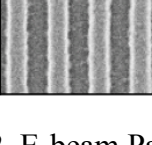
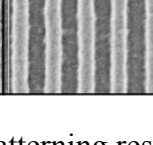
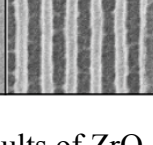
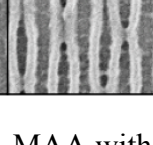
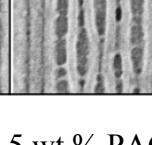
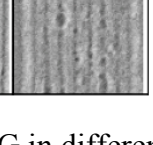
CD \ Developer	100nm	80nm	60nm	50nm	45nm	35nm
4-methyl-2-pentanol (20 μ C/cm ²)						
o-xylene (15 μ C/cm ²)						
PGMEA (90 μ C/cm ²)						
2-butanone (120 μ C/cm ²)						
2-heptanone (120 μ C/cm ²)						
n-butyl acetate (80 μ C/cm ²)						

Figure 5.22. E-beam Patterning results of ZrO₂-MAA with 5 wt % PAG in different NTD developers.

amount of PAG in the unexposed area were able to reduce the roughness and increase the resolution.

EUV Patterning

The high sensitivity of hafnia and zirconia have made them promising patterning materials for EUV wavelength.^{26, 27} As demonstrated above, the best acetate- and ketone-based solvents are PGMEA and 2-heptanone, respectively. The contrast curves of both solvents with 4-methyl-2-pentanol as comparison are shown in Figure 5.23. All three solvents have shown high development contrasts, with 4-methyl-2-pentanol showing the highest contrast and highest sensitivity. Therefore, EUV patterning of ZrO₂-MAA in 4-methyl-2-pentanol was demonstrated in Figure 5.24 and Figure 5.24 (a) shows high-resolution 21.5 nm line/space patterns of ZrO₂-MAA. One main reason for the growing interest in negative-tone development is because of its better performance in printing contact holes. This can be attributed to the better optical contrast provided by a bright-field mask compared to a dark-field mask. In order to study the contact hole printing ability of the nanoparticle photoresist, we also exposed ZrO₂-MAA using EUV lithography with a bright-field mask. ZrO₂-MAA showed high sensitivity (3.0 mJ/cm²) for printing contact holes in Figure 5.24 (b) and we were able to print down to 72-nm contact holes. The higher sensitivity can be due to the bright field mask used for contact hole printing. These results showed the versatility of these materials in terms of patterning different feature types.

5.4 Conclusions

The continuing drive for reduced feature sizes has led to the need for new materials and processes for next-generation lithography. We have synthesized inorganic metal oxide nanoparticles based on HfO₂ and ZrO₂ with organic ligands that have high sensitivity at the EUV wavelength. The effect of different photoactive compounds and additives on patterning was studied. It was shown that a non-ionic

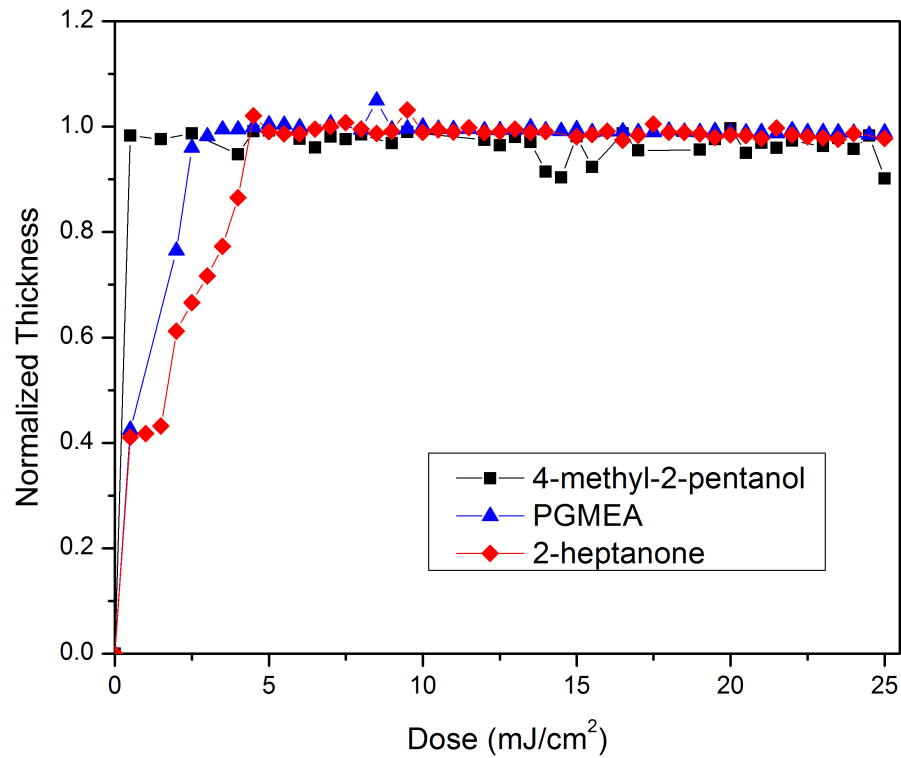
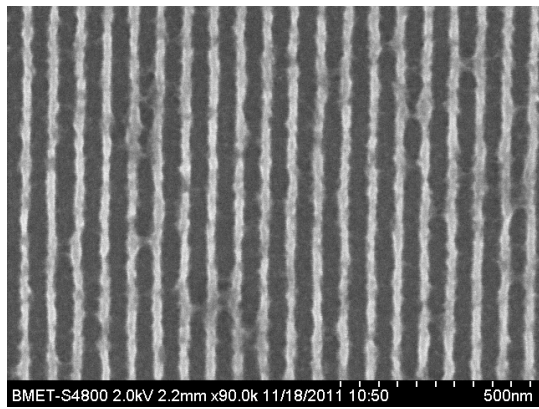
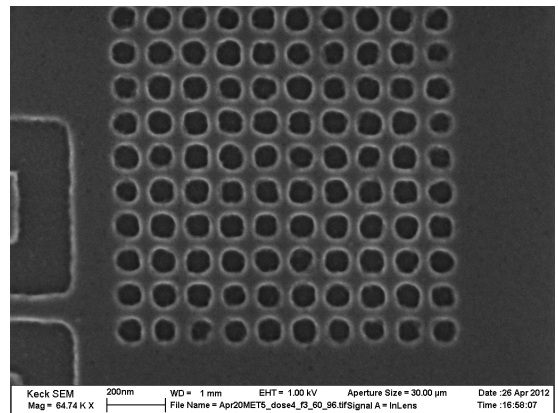


Figure 5.23. Contrast curves of different developers for ZrO₂-MAA at EUV wavelength.



(a)



(b)

Figure 5.24. EUV patterning of ZrO_2 -MAA (a) 21.5 nm line/space (7 wt% PAG, dose: 4.2 mJ/cm^2 , LER:5.6 nm) and (b) 72.1 nm contact holes (5 wt % PAG, dose: 3 mJ/cm^2 , LER: 6.5 nm).

PAG provided the best patterning performance. Different negative-tone developers and their patterning capabilities were also investigated and 4-methyl-2-pentanol and o-xylene provided the best development performance because of their moderate solvating power for these nanoparticles compared to acetate- and ketone-based developers. This shows that both solvent choice and additives are important in patterning inorganic nanoparticles. The polarity of the developer needs to be sufficient to provide enough dissolution of the unexposed nanoparticles while maintaining minimum thickness loss for the exposed nanoparticles to achieve the best patterning results. As the solubility of nanoparticles in the developers can also be affected by the amount of additives in the film, it is important to select the right additive content for each developer. These studies provide invaluable information to improve patterning results of inorganic nanoparticles. As these nanoparticles have high sensitivity for EUV, we were able to achieve line/space patterns down to 21.5 nm and contact hole patterns down to 72 nm with ZrO₂-MAA using EUV lithography. The high sensitivity and versatility of these materials have made them promising next-generation resists.

REFERENCES

1. M. J. Hajipour, K. M. Fromm, A. A. Ashkarran, D. Jimenez de Aberasturi, I. Ruiz de Larramendi, T. Rojo, V. Serpooshan, W. J. Parak and M. Mahmoudi, *Trends in Biotechnology*, 2012, **30**, 499-511.
2. J. Salla, K. K. Pandey and K. Srinivas, *Polymer Degradation and Stability*, 2012, **97**, 592-596.
3. I. Lopes, R. Ribeiro, F. E. Antunes, T. A. P. Rocha-Santos, M. G. Rasteiro, A. M. V. M. Soares, F. Goncalves and R. Pereira, *Ecotoxicology*, 2012, **21**, 637-648.
4. C. Chafer-Pericas, A. Maquieira and R. Puchades, *Trac-Trends in Analytical Chemistry*, 2012, **31**, 144-156.
5. A. Quarta, A. Curcio, H. Kakwere and T. Pellegrino, *Nanoscale*, 2012, **4**, 3319-3334.
6. D. G. Shchukin and R. A. Caruso, *Advanced Functional Materials*, 2003, **13**, 789-794.
7. X. Bai, A. Pucci, V. T. Freitas, R. A. S. Ferreira and N. Pinna, *Advanced Functional Materials*, 2012, **22**, 4275-4283.
8. K. Chrissafis and D. Bikiaris, *Thermochimica Acta*, 2011, **523**, 1-24.
9. C. Jolley, V. Pool, Y. Idzerda and T. Douglas, *Chemistry of Materials*, 2011, **23**, 3921-3929.
10. B. Raveau, *Journal of the European Ceramic Society*, 2005, **25**, 1965-1969.
11. K. Soulantica, L. Erades, M. Sauvan, F. Senocq, A. Maisonnat and B. Chaudret, *Advanced Functional Materials*, 2003, **13**, 553-557.
12. F. Sun, W. Cai, Y. Li, L. Jia and F. Lu, *Advanced Materials*, 2005, **17**, 2872-2877.
13. Y. Wang, X. Jiang and Y. Xia, *Journal of the American Chemical Society*,

- 2003, **125**, 16176-16177.
14. H.-T. Song, J.-s. Choi, Y.-M. Huh, S. Kim, Y.-w. Jun, J.-S. Suh and J. Cheon, *Journal of the American Chemical Society*, 2005, **127**, 9992-9993.
 15. Y.-W. Jun, J.-H. Lee and J. Cheon, *Angewandte Chemie International Edition*, 2008, **47**, 5135.
 16. X. Michalet, F. F. Pinaud, L. A. Bentolila, J. M. Tsay, S. Doose, J. J. Li, G. Sundaresan, A. M. Wu, S. S. Gambhir and S. Weiss, *Science*, 2005, **307**, 538-544.
 17. Q. Zhang, T. P. Chou, B. Russo, S. A. Jenekhe and G. Cao, *Angewandte Chemie International Edition*, 2008, **120**, -2440.
 18. Q. Zhang, T. P. Chou, B. Russo, S. A. Jenekhe and G. Cao, 2008, - **18**, - 1660.
 19. G. Garnweitner, L. M. Goldenberg, O. V. Sakhno, M. Antonietti, M. Niederberger and J. Stumpe, *Angewandte Chemie International Edition*, 2007, **3**, 1632.
 20. B. Koo, H. Xiong, M. D. Slater, V. B. Prakapenka, M. Balasubramanian, P. Podsiadlo, C. S. Johnson, T. Rajh and E. V. Shevchenko, *Angewandte Chemie International Edition*, 2012, **12**, 2435.
 21. G. H. Jeong, H.-B. Bae, D. Choi, Y. H. Kim, S. Yoon and S.-W. Kim, *Journal of Physical Chemistry C*, 2012, **116**, 23851-23857.
 22. G. Ramakrishnan, D. Saman Safari, L. Su Hui, M. S. M. Saifullah, C. Wee Tit, H. H. L. Andrew, Y. Jin Jie, T. Eng San, H. Chaobin and L. Hong Yee, *Nanotechnology*, 2012, **23**, 315304.
 23. L. Ding, W. Zhou, H. Chu, Z. Jin, Y. Zhang and Y. Li, *Chemistry of Materials*, 2006, **18**, 4109-4114.
 24. R. Ganesan, J. Dumond, M. S. M. Saifullah, S. H. Lim, H. Hussain and H. Y. Low, *ACS Nano*, 2012, **6**, 1494-1502.

25. M. Krysak, M. Trikeriotis, E. Schwartz, N. Lafferty, P. Xie, B. Smith, P. Zimmerman, W. Montgomery, E. Giannelis and C. K. Ober, *Proceedings of SPIE*, 2011, **7972**, 79721C/79721-79721C/79726.
26. M. Trikeriotis, W. J. Bae, E. Schwartz, M. Krysak, N. Lafferty, P. Xie, B. Smith, P. A. Zimmerman, C. K. Ober and E. P. Giannelis, *Proceedings of SPIE*, 2010, **7639**, 76390E/76391-76390E/76310.
27. M. Trikeriotis, M. Krysak, Y. S. Chung, C. Ouyang, B. Cardineau, R. Brainard, C. K. Ober, E. P. Giannelis and K. Cho, *Journal of Photopolymer Science and Technology*, 2012, **25**, 583-586.
28. M. Trikeriotis, M. Krysak, Y. S. Chung, C. Ouyang, B. Cardineau, R. Brainard, C. K. Ober, E. P. Giannelis and K. Cho, *Proceedings of SPIE*, 2012, **8322**, 83220U/83221-83220U/83226.
29. H. Ito, in *Microlithography- Molecular Imprinting*, Springer Berlin Heidelberg, 2005, pp. 37-245.
30. L. Van Look, J. Bekaert, V. Truffert, V. Wiaux, F. Lazzarino, M. Maenhoudt, G. Vandenberghe, M. Reybrouck and S. Tarutani, *Proceedings of SPIE*, 2010, **7640**, 764011-764011-764012.
31. T. A. Brunner and C. A. Fonseca, *Proceedings of SPIE*, 2001, 30-36.
32. C. A. Mack and J. E. Connors, *Proceedings of SPIE*, 1992, 328-338.
33. Y. C. Bae, S.-H. Lee, R. Bell, L. Joesten and G. G. Barclay, *Proceedings of SPIE*, 2011, 797207.
34. S. A. Robertson, M. Reilly, J. J. Biafore, M. D. Smith and Y. Bae, *Proceedings of SPIE*, 2011, 79720Y.
35. L. F. Thompson, C. G. Wilson and M. J. Bowden, *Introduction to Microlithography*, American Chemical Society, 1983.
36. E. D. Feit and L. E. Stillwagon, *Polymer Engineering & Science*, 1980, **20**,

- 1058-1063.
37. H. Shiraishi, Y. Taniguchi, S. Horigome and S. Nonogaki, *Polymer Engineering & Science*, 1980, **20**, 1054-1057.
 38. C. Y. Ouyang, J.-K. Lee, M. E. Krysak, J. Sha and C. K. Ober, *Journal of Materials Chemistry*, 2012, **22**, 5746-5750.
 39. B. Cardineau, M. Krysak, M. Trikeriotis, E. Giannelis, C. K. Ober, K. Cho and R. Brainard, *Proceedings of SPIE*, 2012, 83220V.
 40. R. Gronheid, C. Fonseca, M. J. Leeson, J. R. Adams, J. R. Strahan, C. G. Willson and B. W. Smith, *Proceedings of SPIE*, 2009, **7273**, 727332-727332-727338.
 41. S. W. Chang, R. Ayothi, D. Bratton, D. Yang, N. Felix, H. B. Cao, H. Deng and C. K. Ober, *Journal of Materials Chemistry*, 2006, **16**, 1470-1474.
 42. A. De Silva, J. K. Lee, X. Andre, N. M. Felix, H. B. Cao, H. Deng and C. K. Ober, *Chemistry of Materials*, 2008, **20**, 1606-1613.
 43. N. M. Felix, A. De Silva and C. K. Ober, *Advanced Materials*, 2008, **20**, 1303.
 44. C. Y. Ouyang, J.-K. Lee, J. Sha and C. K. Ober, *Proceedings of SPIE*, 2010, 7639.
 45. R. A. Lawson, J. Cheng, D. E. Noga, T. R. Younkin, L. M. Tolbert and C. L. Henderson, *Proceedings of SPIE*, 2010, 76390O.
 46. R. A. Lawson, D. E. Noga, J. Cheng, L. M. Tolbert and C. L. Henderson, *Proceedings of SPIE*, 2010, 76392F.
 47. T. Tanaka, M. Morigami and N. Atoda, *Japanese Journal of Applied Physics*, 1993, **32**, pp.6059-6064.
 48. A. E. Grigorescu, M. C. van der Krogt, C. W. Hagen and P. Kruit, *Microelectronic Engineering*, 2007, **84**, 822-824.
 49. J. Stowers and D. A. Keszler, *Microelectronic Engineering*, 2009, **86**, 730-733.

50. J. K. Stowers, A. Telecky, M. Kocsis, B. L. Clark, D. A. Keszler, A. Grenville, C. N. Anderson and P. P. Naulleau, *Proceedings of SPIE*, 2011, 796915-796915.
51. M. Trikeriotis, R. Rodriguez, M. F. Zettel, A. Bakandritsos, W. J. Bae, P. A. Zimmerman, C. K. Ober and E. P. Giannelis, *Proceedings of SPIE*, 2009, **7273**, 72732A/72731-72732A/72736.
52. S.-H. Lee, J. K. Park, T. Cardolaccia, J. Sun, C. Andes, K. O'Connell and G. G. Barclay, *Proceedings of SPIE*, 2012, **8325**, 83250Q-83250Q-83212.
53. J. Versluijs, V. Truffert, G. Murdoch, P. De Bisschop, D. Trivkovic, V. Wiaux, E. Kunnen, L. Souriau, S. Demuyneck and M. Ercken, *Proceedings of SPIE*, 2012, **8326**, 83260W-83260W-83210.
54. S.-H. Yang, E. S. Kim, S. Moon, S. Lee, S.-W. Choi and J. Choi, *Proceedings of SPIE*, 2012, **8325**, 832504-832504-832514.

APPENDIX C

EUV Exposure Data for ZrO₂-MAA

Exposure Data and LER Trade-Off for ZrO₂-MAA (Negative-Tone)

Table C.1 summarizes the EUV exposure data of ZrO₂-MAA, 4-methyl-2-pentanol was used as the developer and negative-tone patterns are shown.

Table C.1. Exposure data for ZrO₂-MAA (EUV lithography)

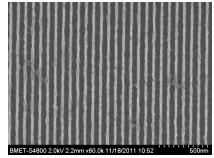
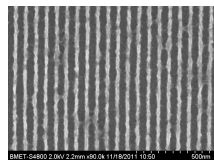
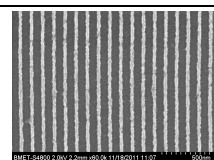
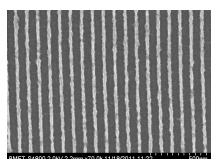
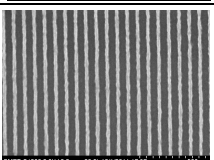
SEM	Dose (mJ/cm ²)	CD (nm)	LER (nm)	PAG/MAA (wt %)
	4.2	26.1	3.8	3/55
	4.2	21.5	5.6	3/55
	16.5	32.1	5.9	5/55
	4.9	25.5	5.1	5/55
	16.5	54.5	3.1	7/55

Table C.2 shows the LER trade-off for ZrO₂-MAA with different pitch sizes, as the feature size decreases, the LER increases. As the current LER target is <1.2 nm, further optimization of the resist formulations is needed to reduce LER.

Table C.2. LER trade-off for ZrO₂-MAA (EUV lithography)

L/S Half-pitch (nm)	LER (nm)
50	3.1
40	3.8
36	5.2

Exposure Data for ZrO₂-MAA (Positive-Tone)

ZrO₂-MAA can also be patterned as a positive-tone resist when a post-exposure bake (120s) is applied and an aqueous base developer is used. The proposed patterning mechanism is shown in Figure C.1, after exposure, a PEB step can bake off the loosely bound methacrylic acid ligands and reduce the solubility of the unexposed nanoparticles in an aqueous base developer while the exposed part is soluble in base due to the exchange of ligands. Only non-ionic PAGs can generate positive-tone images here because possible ligand exchange reactions may occur during the spin-coating step and lead to poor solubility difference in base between the exposed and unexposed nanoparticles. Table C.3 is a summary of the preliminary EUV exposure data for ZrO₂-MAA, further optimization is required to improve resolution and contrast.

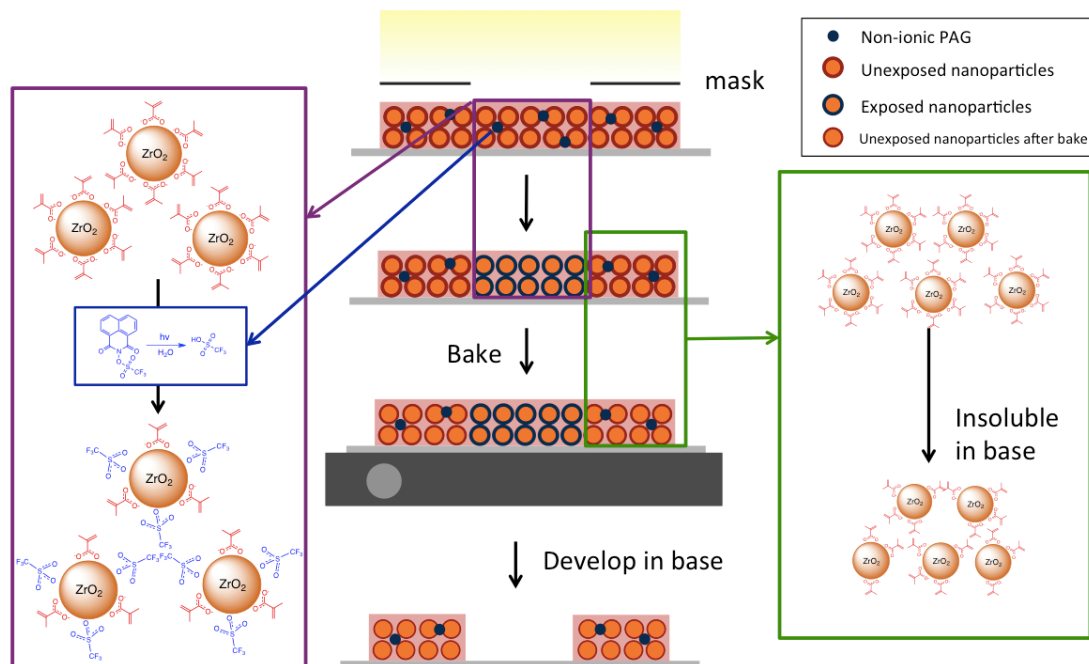
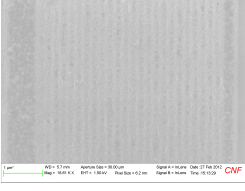
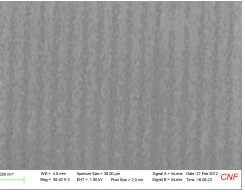
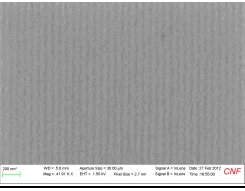
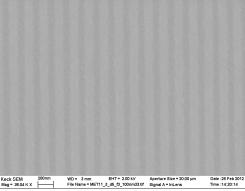
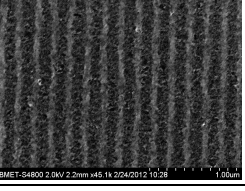


Figure C.1. Proposed positive-tone patterning mechanism with a non-ionic PAG.

Table C.3. Exposure data for ZrO₂-MAA, developer: 0.28 N TMAH (EUV lithography)

SEM	Dose (mJ/cm ²)	PEB (°C)	CD (nm)	PAG (wt %)
	13.5	130	100	5
	13.5	160	60	5
	13.5	175	40	5
	2.5	160	100	3
	0.5	130	100	7